Assessment of radiological and chemical risk due to natural radionuclides and heavy metals in water, soil and food

A thesis presented for the degree of

Doctor of Philosophy

by

Beant Kaur

(Reg. No. 901812014)

Under the guidance of

Dr. Sunil Devi
Department of Physics and Material Science
Thapar Institute of Engineering & Technology,
Patiala, India

and

Dr. Rohit Mehra
Department of Physics
Dr BR Ambedkar National Institute of Technology,
Jalandhar, India

Department of Physics and Material Science

Thapar Institute of Engineering & Technology Patiala (India)

2024

Declaration

It is to certify that the work presented in this thesis entitled 'Assessment of radiological and chemical risk due to natural radionuclides and heavy metals in water, soil and food' in the fulfilment of the requirements for the award of the degree of Doctor of Philosophy is an authentic record of my own research work under the supervision of Dr. Sunil Devi, Associate Professor at Thapar Institute of Engineering and Technology, Patiala, India and Dr. Rohit Mehra, Professor in the Department of Physics at Dr B R Ambedkar National Institute of Technology, Jalandhar, India. The matter presented in this thesis has not been submitted elsewhere in a part or fully to any other university or institute for the award of any other degree.

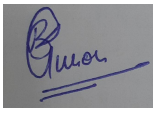

Date: 11-9-2024

Beant Kaur

It is certified that the above statement made by the candidate is correct to best of our knowledge.

Dr. Sunil Devi
Department of Physics and Materials Science
Thapar Institute of Engineering & Technology
Patiala, India

Dr. Rohit Mehra
Department of Physics
Dr. B R Ambedkar National Institute of Technology, Jalandhar, India

Acknowledgements

This thesis is the culmination of years of hard work and dedication and it would not have been possible without the unwavering support of many individuals who have walked alongside me on this journey directly or indirectly.

First and foremost, I would like to express my deepest gratitude to my late grandfather, S. Bhag Singh. Just a week before he passed away on April 21, 2014, he told my parents, "Let her study as long as she wants." His words have resonated with me ever since, serving as a guiding light throughout my academic pursuits.

I am immensely grateful to my parents, S. Parminder Singh and Mrs. Rajwant Kaur, whose unconditional love and financial support have been the bedrock of my education. I extend my heartfelt thanks to my grandmother, Sdn. Pritam Kaur, Taya Ji, S. Balbir Singh and Tayi Ji, Mrs. Ravneet Kaur, and S. Gurmail Singh for their constant encouragement and support. Your faith in me has always been a source of inspiration. A big shoutout to my younger brother, Dilpreet Singh, for keeping me sane with his antics and reminding me that sibling rivalry is just another form of love with an extra sarcasm.

I owe a special debt of gratitude to my supervisors, Dr. Sunil Devi and Dr. Rohit Mehra whose wisdom and guidance have been instrumental throughout these years. I am also thankful to Department of Physics and Material Science, TIET, Patiala.

My sincere thanks go to Jaspreet Kaur Ghuman, Rayees Ahmad Yatoo and Sarmad Rashid, whose friendship and support brightened even the dullest days during my academic tenure. I am deeply grateful to Rahul and Nitish for not only offering support but also adding much-needed humor to the situations.

I am deeply thankful to my Fufar Ji and Bhua Ji, Adv. Surinder Singh Sohi and Mrs. Narinder Kaur Sohi, for their steadfast motivation during my most challenging times and their generous hospitality during my stay at their home in Patiala. Your kindness and encouragement have meant the world to me. A special mention goes to Mehtab Singh Sohi for organizing wonderful gatherings and introducing me to new places in town and to Harjot Kaur Sohi for her physiotherapy sessions when I needed them the most.

I am forever indebted to Prof. Jaipal Singh, who has been more than just an academic mentor-a fatherly figure and guiding light throughout this journey. Your wisdom and support have been invaluable. I am grateful to Dr. Sukhdev (Department of Mathematics) for helping me with statistical concepts and answering my queries time and again.

I would like to thank Shoaib Noor, Kundan and Neeraj for their guidance during my early years in this field. Your mentorship has been instrumental in shaping my academic path.

I extend my heartfelt gratitude to Pranjal Chaturvedi for his guidance with programming and for our enriching conversations that spanned from science to sitcoms. I will cherish the time that I spent with my labmates Sangeeta, Jayant and Amritpal.

I also wish to express my gratitude to Sansar Chand, Sarabjot Kaur, Arti and Abhishek from NIT, Jalandhar for their invaluable assistance with instrumentation,

which significantly contributed to the success of my research.

Finally, I want to express my most profound appreciation to my fiance, Mr. Ratinderpal Singh Randhawa, for his unwavering support and encouragement. Your presence has been a constant source of comfort and strength.

To each of you, I extend my heartfelt thanks. This thesis would not have been possible without your love, support and encouragement.

"Contemplate and reflect upon knowledge, and you will become a benefactor to others." - Nanak

Abstract

With the growing global concern regarding environmental pollution, it is essential to comprehend its effects with timely monitoring. The objective of this study is to measure the concentrations of natural radionuclides such as ^{238}U, ^{232}Th and ^{40}K in addition to heavy metals in the water and food to analyze the potential health risks to the population of Mansa district, located within the cancer belt of Punjab which is distinguished for its association with cotton cultivation, earning it the moniker 'area of white gold'. The fertiliser usage is high in the study area. The study utilizes comprehensive assessment techniques that encompasses probabilistic approach as well as deterministic approach for water contamination to evaluate the corresponding health risks. Moreover, biokinetic modelling of uranium resulting from ingestion of uranium contaminated water is performed to assess the retention of uranium in the human body. The natural radiolonuclides are measured for both soil and food. The heavy metals analysis is also carried out for wheat samples. The research findings indicate a high level of uranium and cadmium contamination of groundwater in Mansa district, Punjab (India), raising concerns regarding safety of its utilisation for domestic purposes. Although the wheat samples have cadmium concentration above permissible limits set by Kent but the values are below Indian permissible limits. The activity of natural radionuclides ^{226}Ra, ^{232}Th and ^{40}K in soil samples are within permissible limits whereas the activity of ^{40}K in wheat samples is above permissible limit. This thesis offers significant insights into the health challenges encountered by the population of Mansa due to regular use of groundwater. By identifying key areas of concern, the study seeks to bolster initiatives aimed at enhancing environmental and health safety for the population.

Contents

List of Figures

List of Tables

Chapter 1

Introduction

The history of radiation physics, concept of radioactivity, basic terms of the subject and literature survey are discussed in this chapter. Foremost, a brief history of the radiation physics is discussed. Further, fundamental concepts of radiation physics are discussed. The primordial nuclei and their geochemistry are discussed in section 1.1. The details about the provenance of radiation are given in section 1.2. Heavy metals are described in section 1.3. Environmental monitoring and related agencies are discussed in section 1.4. The basic notations and terms are described in section 1.5. The exposure pathways and health risks are described in section 1.6, followed by a literature survey in section 1.7. The study area, motivation for the work and objectives of the current study are discussed in section 1.8.

The radiation physics has come a long way since radioactivity was fortuitously discovered by Henri Becquerel, who saw the darkening of a photographic plate caused by uranium salt. This phenomenon garnered the attention of Marie and her husband Pierre Curie. In April of 1897, Marie Curie delivered a comprehensive report to the esteemed Paris Academy of Science, detailing her extensive research on the emissions of radiation from different substances. The aforementioned property was seen exclusively in compounds containing uranium or thorium. In a subsequent publication by Curie and Curie in 1898 [1], she designated the appellation 'radioactive' to a recently identified material that had been extracted from the mineral pitchblende, named as polonium, and subsequently followed by the discovery of radium. The half of Nobel Prize (physics) in 1903 was jointly shared by Marie and Pierre Curie, and the other half was awarded to Henri Becquerel for their ground-breaking research. Ernest Rutherford is credited for the identification and nomenclature of the alpha and beta particles [2]. Furthermore, he made a significant finding in 1899 by detecting a gaseous radioactive emanation of ^{220}Rn from thorium compounds where he used the term 'emanation' to describe the emission from parent nuclei [3]. In 1934, Irene Curie and Frederick Joliot made the groundbreaking discovery of artificial radioactivity, unfolding a new phase in the applicability of radioisotopes in various fields, which include radiometric dating, health and usage in nuclear power plants.

The arrangement of all atomic nuclei according to their respective binding energies in

relation to their neutron and proton number is known as the 'nuclear chart'. The ratio of neutrons to protons is equal to one for lighter isotopes. As we progress towards heavier nuclei, the number of protons increases, necessitating the incorporation of more neutrons within the nucleus to counteract the repulsive Coulomb force. The nuclei that are not stable are situated away from the region known as the valley of stability, as shown in figure 1.1 [4]. The phenomenon of the spontaneous nuclear transformation of radionuclides with the release of particles such as α or β, usually accompanied by the emission of γ radiations due to the instability of a nucleus is called radioactivity, and the nuclides are referred to as radionuclides. The notation for the process is as below -

$$(A, Z)X \rightarrow (A1, Z1)Y + (A2, Z2)Particle \tag{1.1}$$

where A and Z have their usual meaning, and X and Y refer to parent and daughter nuclei, respectively. The particle can be α or β.

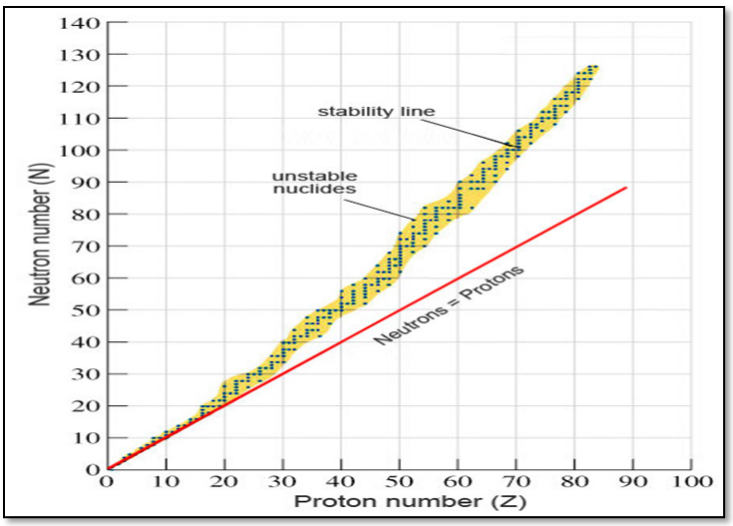

Figure 1.1: Nuclear chart showing stability line [4].

The primordial radionuclides predominantly belong to heavy elements with an atomic number exceeding 80 except ^{40}K, ^{87}Rb, ^{176}Lu and ^{147}Sm. Some of the naturally occurring radionuclides are uranium, thorium, and ^{40}K, along with their daughter nuclei from long-lived decay chains. ^{238}U and ^{235}U has a half-life of 4.5×10^9 and 0.7×10^9 years, respectively. ^{232}Th has a half-life of 14.1×10^9 years, where half-life is the duration required for the initial atoms to disintegrate to its half value. The atoms in the radioactive materials are unstable and therefore, achieve stability by emitting the charged particles. The number of atoms of the radionuclide decays exponentially with time, and once formed they contribute differently to the total radioactive burden depending upon their half-lives. The radionuclides undergo two unique types of decay processes, namely series decay and single decay. Potassium undergoes a single decay process, while uranium and thorium exhibit a series decay process. The classification of each series is based on the divisibility of the mass numbers of its individual parts by 4, as demonstrated in the equation below-

$$A = 4p + q \tag{1.2}$$

where A is the mass number, p represents the greatest whole integer that is divisible to A, and q represents the remainder [5].

1.1 Primordial radionuclides

Primordial radionuclides possess extended half-lives that have endured since the beginning of the earth. Uranium, thorium and ^{40}K are some of the primordial radionuclides. The distribution of these primordial radionuclides in the environment is influenced by several variables, such as the physiological characteristics of the biota, the chemical properties of the nuclides and the physical parameters of the environment.

1.1.1 Uranium

In 1789, uranium, the heaviest naturally occurring element with Z = 92, was discovered by the German scientist Martin Klaproth from the samples of pitchblende. Its density is 19.1 times of the water. Naturally, uranium on earth is distributed as 99.28% of ^{238}U, 0.72% of ^{235}U, and trace amounts of about 0.0058 % of ^{234}U [6]. The concentration of ^{238}U varies between 1-4 parts per million (ppm) in the earth's crust as well as in soil and rocks [7]. Uranium is commonly found in significant quantity in minerals, either as a primary or secondary constituent. However, the number of primary uranium ore minerals are uraninite, davidite and pitchblende [8]. Uranium exhibits two distinct decay series, namely the uranium-radium series (4n + 2) for ^{238}U and the actinium series (4n + 3) for ^{235}U leading to a stable nucleus, ^{206}Pb for ^{238}U, ^{207}Pb for ^{235}U, respectively. The primary risks associated with ^{238}U are its chemical and radiological toxicity produced due to the decay of its daughter nuclei, particularly alpha emitters, such as ^{210}Po, ^{226}Ra, and ^{222}Rn. The ^{238}U decay chain is shown in figure 1.2. ^{238}U does not emit gamma rays itself, therefore, it is estimated by measuring the gamma ray emissions emanating from its radioactive progeny. So, in gamma spectroscopy, ^{214}Bi with a peak of 1765 keV is used to measure the concentration of uranium.

The geochemical behaviour of uranium involves its occurrence in several oxidation states in aqueous solutions, namely U(III), U(IV), U(V), and U(VI). It exhibits a large atomic radius of 0.97 Å and demonstrates high chemical reactivity. Uranium compounds in the hexavalent oxidation state U(VI), as uranyl cation UO_2^{2+}, tend to be more soluble in aqueous solutions, whereas the tetravalent oxidation state U(IV) as UO_2 is insoluble [9]. Under oxidizing conditions, the groundwater present within fissures has a significant quantity of dissolved oxygen. The presence of oxygen enables the transformation of uranium into hexavalent species, which exhibit enhanced mobility, therefore, making it prone to leaching into water. In a reducing environment, uranium undergoes a reduction process, resulting in the formation of its tetravalent U(IV) state [10]. Hence, it may be deduced that groundwater located at deeper levels would demonstrate a reduced concentration of uranium as a result of the predominance of reducing conditions and decreased solubility of uranium. In groundwater, U(VI) prevails in low pH circumstances. However, at higher pH values, U(VI) may form carbonate and hydroxide compounds. The quantities of uranium present in groundwater are notably influenced by two key chemical factors: carbonate complexation and oxidising conditions. Abiotic variables such as redox

potential, pH, organic matter of soil and phosphorus levels as well as biotic factors such as microbes, have a crucial role in influencing the bioavailability of uranium in soil [11]. The presence of phosphorus within the soil can significantly impact the mobility of uranium. In regions with higher phosphate concentration, it has been found that uranyl phosphate solids formed by U(IV) exhibit higher insolubility compared to U(VI) solids [12].

1.1.2 Thorium

Thorium, Z = 90 was first identified in 1828 by Jons Jakob Berzelius, a chemist from Norway. It is found in abundance in the earth's crust compared to uranium. The thorium content in the continental top crust and soils is around 9-10 ppm by weight, which is approximately four times higher than the uranium amount [13]. It is commonly found in the Th(IV) oxidation state and exhibits little solubility except in environments with pH value exceeding 3 [14]. The only long-lived isotope of thorium is ^{232}Th, and its decay chain is called 4n series due to mass numbers being the integral multiples of 4. The ^{232}Th cascade is shown in figure 1.3 [15]. The concentration of thorium (^{232}Th) in samples is measured with 2615 keV peak of ^{208}Tl using gamma spectroscopy. In all three natural decay chains (^{235,238}U, ^{232}Th), there exist thorium isotopes with short lifespans. Specifically, these isotopes are as follows: ^{234}Th with a half-life of 24.1 days and ^{230}Th with a half-life of 7.54 x 10^4 years in the ^{238}U decay chain; ^{228}Th with a half-life of 1.9 years in the ^{232}Th decay

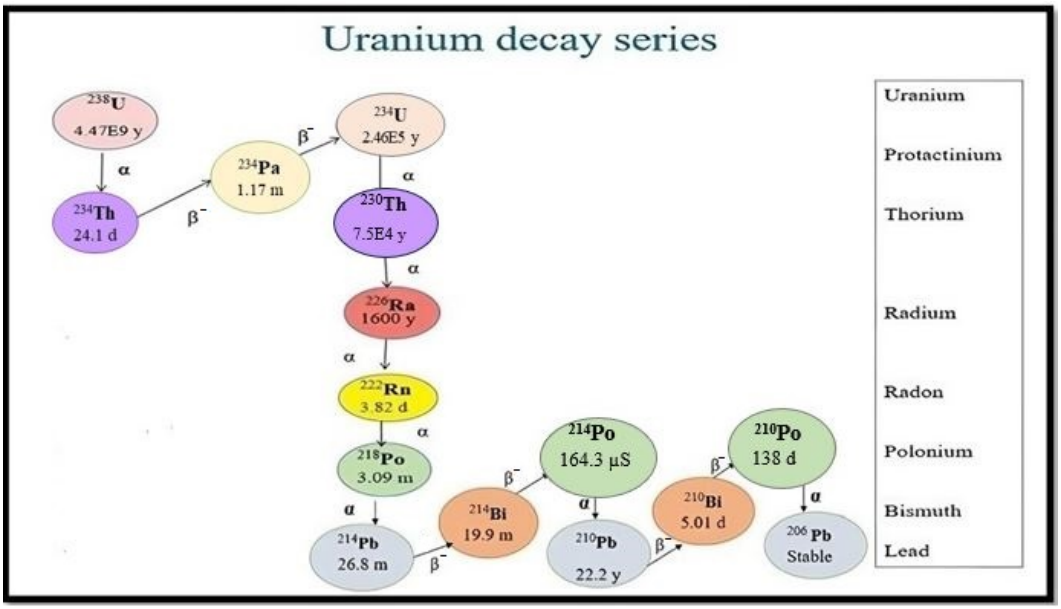

Figure 1.2: ^{238}U decay series [15].

chain; and ^{231}Th with a half-life of 1.06 days in the ^{235}U decay chain. Monazite sands are the primary commercial source of thorium. The thorium oxide concentration in monazite sands ranges from approximately 3% to 10%. Thorium is also found in the thorite mineral, which is composed of thorium silicate, as well as thorianite [16].

As thorium is present just in one oxidation state of Th(IV), the significance of its reduction processes is negligible. Due to sorption and precipitation processes, along

with the low dissolution rate of minerals containing thorium, the concentration of thorium in the majority of terrestrial waters is typically low [17]. The leaching of thorium-rich terranes by ground and surface water is often greater when elevated levels of phosphates, sulphates, carbonates, nitrates, phosphates, and fluorides are present [18]. The variability of thorium concentration in groundwater is typically greater with low salinity, hardness, and pH in addition to high organic content [19]. The presence of thorium in soil may occur in several chemical forms, which are contingent upon soil characteristics including pH levels along with the amount of organic matter in the region. [16]. In the pH range observed in soils (5-8), it is possible for some fractions of soluble thorium to undergo hydrolysis. This hydrolysis process leads to the creation of a positively charged hydroxide gel. Additionally, water molecules are released as a result of this reaction, ultimately resulting in the synthesis of thorium oxide, ThO_2 [20].

The most substantial reserves of thorium are predominantly located in coastal areas [19]. India possesses several monazite placer deposits along its coastline, with thorium concentrations ranging from 8% to 10.5% by weight. These deposits, located in Chatrapur (Orissa), Ullal (Karnataka), Kandivalasa (Andhra Pradesh), Kanyakumari (Tamil Nadu), and Chavara (Kerala), contributes to elevated background radiation levels in these areas [21-25]. The elevated concentration of thorium is also found in Yangjiang (China) and Ramsar (Iran) [26-27].

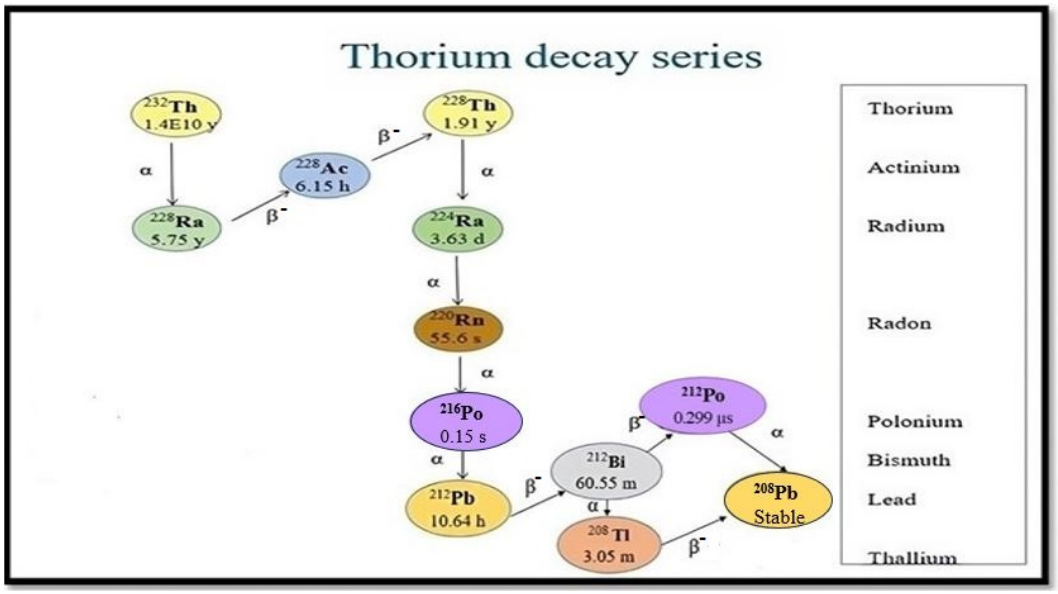

Figure 1.3: Decay chain of ^{232}Th [15].

1.1.3 Potassium

Potassium in its natural state is composed of three isotopes: ^{39,40,41}K present in the mass percentages of 93.08%, 0.0118%, and 6.91%, respectively [28]. Among these three isotopes, it is noteworthy that ^{40}K is inherently radioactive, with a half-life of 1.28×10^9 years. It is a singly occurring radionuclide which is defined as direct decay of a radioactive nuclide into a stable nuclide. In the earth's crust, potassium

can be found in quantities as low as 0.1% in limestones and as high as 4% in certain granites [4]. The concentration of ^{40}K is determined by 1460.8 keV peak using gamma spectroscopy.

1.2 Provenance of Radiation

1.2.1 Natural provenance

1.2.1.1 Cosmogenic sources

The earth is continuously bombarded with high-energy rays from the sun, stars in addition to galactic and intergalactic plasma. Solar events like coronal mass ejections, sunspots and solar flares also emanate radiation. Approximately 10 million kg of extra-terrestrial dust particles collide with the earth every year, carrying radioactivity up to 27 Bq kg^{-1} [29]. This radioactivity is generally attributed to lighter nuclides, however, the presence of heavier elements like thorium, uranium has also been identified in meteorites [30]. The spallation process takes place in the upper atmosphere at thresholds of around 50 MeV where cosmic rays come in contact with stable elements such as nitrogen, oxygen resulting in the formation of radionuclides, further adhering to aerosols and deposition on earth's surface [31-32]. The variations in the elevation of terrain, in addition to the magnetic field of the earth, affect the radiation dose received by humans. ^{137}Cs,^{14}C, ^{10}Be, ^{3}H are examples of the cosmic radiation [33]. The figure 1.4 shows the different sources of radiation [34].

1.2.1.2 Terrestrial sources

Primordial sources are found in the earth's crust since the beginning. In the early history of earth, uranium oxides were present on earth as grains. Due to variations in density from other lower-density particles, uranium oxide grains had a tendency to sink or settle in the earth's crust with time in alkalic rocks [33]. Due to the relatively low density of these oxides, they tend to accumulate in the earth's crust rather than in the denser mantle or core regions [35].

Igneous rocks - As mentioned above, density differentiation took place as magma underwent cooling and crystallisation in the process of forming igneous rocks. Uranium and thorium, due to their substantial size and high density, had a tendency to accumulate in particular regions of the cooling magma. The alkaline rocks are highly conducive to uranium and thorium accumulation [36]. They are present in larger amounts in granite due to incomplete melting along with crystal fractionation of magma concentrating them in the liquid phase, therefore, further assimilating them into silica-rich products [37-38]. The minerals pyrochlore, monazite, along with allanite possess a significant level of radioactivity. However, their disposition in igneous rocks leads to localised regions with elevated levels of radioactivity. Northeastern Washington, Nevada, Idaho, Alaska (USA), Sinai (Egypt), Shingbhum (India), and Longhuashan, Changjiang, Zhuguangshan (China) are places with high uranium content in granite [39-44]. The quantity of potassium in igneous rocks often corresponds to the percentage of silica [9]. The potassium is found in certain types of granites, specifically those with low calcium content, as well as syenites and can reach concentrations that surpass the activity of 1.85 Bq g^{-1} [29]. Volcanic

rocks exhibit slightly elevated levels of radioactivity compared to plutonic rocks with similar compositions. Additionally, it has been noted that acid rocks often possess greater concentrations of radioactive components in comparison to intermediate or basic rocks [9]. The mean concentrations of primordial nuclei in the earth's crust are listed in table 1.1.

Metamorphic rocks - Different chemical processes, pressure and heat result in the formation of metamorphic rocks from protoliths. There is a huge fluctuation in uranium levels of metamorphic rocks as few top-quality metamorphic rocks have a low content of uranium while their inferior counterparts have high content [45]. Similarly, thorium levels also vary in metamorphic rocks but are mostly concentrated in the liquid phase [46]. Metamorphic rocks have diminishing thorium concentration as metamorphism progresses from the greenschist to the granulite facies [20]. Additionally, it has been discovered that metamorphic rocks have a greater concentration of thorium compared to igneous rocks [19].

Sedimentary rocks - Uranium present in sedimentary deposits can be classified into three categories: (a) uranium that is naturally occurring within clastic sediments, (b) uranium that is deposited concurrently with the sediments, and (c) uranium that is deposited epigenetically after the cessation of sedimentation [9]. Uranium enters sedimentary rocks via the process of leaching from low-grade sources, followed by its transportation by water and accumulation by physio-chemical processes, whereas thorium is resistant to weathering due to its host rocks (zircon, monazite) [47]. Black shale has elevated levels of thorium but in other rocks, uranium levels are higher as the uranium (VI) has more mobility and has a great affinity towards organic materials [48]. The potassium concentration in sedimentary rocks is primarily influenced by the proportions of feldspar, micas, and clay mineral-aggregate deposits [9].

Table 1.1: The mean concentrations of naturally occurring radionuclides inside the earth's crust in µg g^{-1} [9, 20, 49].

Nuclide	Igneous rocks				Sedimentary rocks				Sea Water
	Ultra basic	Basaltic	Granite		Syenites	Shales	Sand-stones	Carbo-nates	
			High-Ca	Low-Ca					
^{238}U	0.001	1	3	3	3	3.7	0.45	2.2	0.003
^{232}Th	0.004	4	8.5	17	13	12	1.7	1.7	5×10^{-7}
^{40}K	0.0047	0.98	2.97	4.96	5.66	3.14	1.26	0.32	-

1.2.2 Artificial sources

Humans have been susceptible to disseminated natural radioactivity from early times, and with invent of artificial radionuclides, the intensity of specific activities has increased, which further increases the radiation exposure [50]. The first nuclear explosion named Trinity, had emancipated a huge amount of plutonium into the atmosphere. The nuclear weapons can cause severe contamination of the environment. Similarly, nuclear power plant disasters like Kyshtym and Chernobyl in Soviet Union, Three Mile Island in USA, and Fukushima in Japan also released large amounts of radionuclides. Other artificial sources of radiation are used in medical diagnosis,

production of fertilizers, mining and processing, oil and gas industry, thermal power plants.

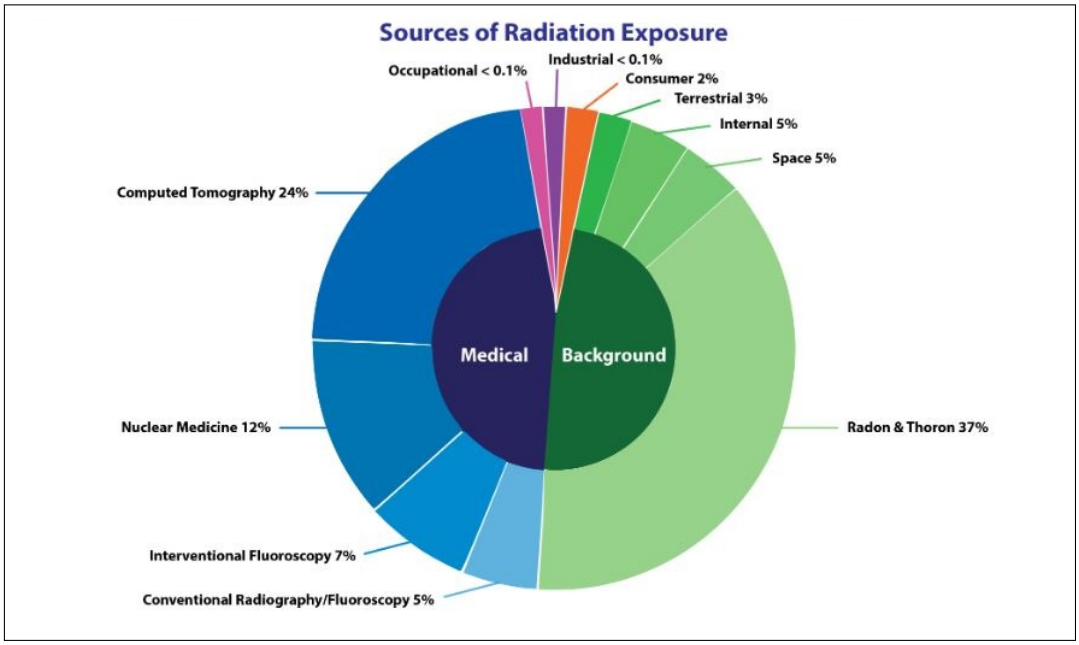

Figure 1.4: Sources of radiation [34].

1.3 Heavy metals

Heavy metals generally fall in the category of transition elements and metalloids in the periodic table and they pose a potential threat to human health even at minimal concentrations. They are elements that possess a density exceeding 5 g cm^{-3} [51]. Nevertheless, the chemical characteristics of heavy metals have greater consequences than their density. There are more than 50 elements that can be categorised as heavy metals, and among them, 17 are considered to be highly toxic [51]. These include nickel, arsenic, cobalt, mercury, cadmium, vanadium, chromium, selenium, lead etc. The environmental contamination resulting from these metals has increasingly emerged as a pressing ecological issue and a global public health challenge in recent years. There has been a substantial rise in human exposure, attributed to the rapid expansion of their use across agricultural, industrial and technological domains [52]. While heavy metals are inherently found within the earth's crust, the primary cause of ecological damage and human exposure are activities such as smelting, mining, manufacturing as well as the application of metal-containing chemicals in agriculture [53-56]. Heavy metals are most abundant in soil and aquatic environments, and to a lesser extent in the atmosphere as particles or vapours.

1.4 Environmental Monitoring

Humans are an integral component of the natural environment and are subjected to pollutant exposure due to several factors such as geology, dietary patterns, and occupation, etc [57]. The interaction of human cells with the macro-environment

determines human health. For survival, human beings need essential inorganic minerals, chemicals and organic nutrients but within certain limits. When these limits are defied, the human body becomes more prone to diseases. So, there is a need to monitor exposure continuously to lower the risk. Environmental monitoring is the systematic approach of making a methodical observation, measurement, collection and evaluation of pollutant levels in the air, water, sediment, soil and food within a certain geographical area.

The primary objectives of monitoring are recognizing contamination sources with pollutant levels in the environment and reckoning the variation in pollutant levels in the environment. Environmental monitoring provides essential insights into various pollutants, facilitating the assessment of environmental quality in accordance with established guidelines. This process also evaluates the associated health risks. Furthermore, it offers data on current levels of contamination, which can serve as a reference point for future assessments. So, a scientific approach to understand pollutants in soil, water and food is necessary.

1.4.1 Environmental Agencies

International agencies - World Health Organisation (WHO), an agency of the United Nations, established in 1948, is committed to the comprehensive assessment of the existing scientific literature and analysing its implications for the development of health safety limits. The purpose of these recommendations is to educate personnel on creating policies and to establish suitable objectives for a diverse array of policy alternatives pertaining to health management in various regions around the globe. The WHO has established a tolerable threshold of 30 μg L^{-1} for uranium contamination in water [58]. The permissible limits for heavy metals recommended by WHO for cadmium, zinc, chromium and iron are 0.003 mg L^{-1}, 5 mg L^{-1}, 0.05 mg L^{-1} and 0.3 mg L^{-1}, respectively [59-60]. The United States Environment Protection Agency (USEPA) is an autonomous executive agency of the United States that is responsible for addressing a wide range of environmental protection concerns. The United Nations Scientific Committee on the Effects of Atomic Radiation (UNSCEAR) was established in 1955, following the resolution adopted by the United Nations General Assembly. A total of twenty-one states are assigned the responsibility of appointing scientists to serve as committee members. This committee convenes official meetings on a yearly basis and presents a report to the General Assembly. It releases significant public reports periodically regarding the origins and impacts of ionising radiation. The International Commission on Radiation Protection (ICRP) is an advisory body that provides guidelines to regulatory and advisory agencies at international, national, and regional levels regarding the fundamental concepts that form the basis for effective radiation protection [61]. The activity concentration of ^{226}Ra must be below 35 Bq kg^{-1} , whereas for ^{232}Th it must be below 30 Bq kg^{-1} for food samples and soil samples. The activity concentration of ^{40}K must not exceed 420 Bq kg^{-1} for food samples as well as soil samples according to UNCEAR [57].

National agency of India - The Department of Atomic Energy (DAE) was established in August 1954. The environmental monitoring programme implemented by the DAE encompasses several key components like programmes focusing on monitoring environmental radioactivity throughout the country and developing appropriate

instrumentation, radiation protection measures for the nuclear fuel cycle in addition to analysing pollutants in different environmental genres. Atomic Energy Regulatory Board (AERB) aims to safeguard against potential hazards posed by the utilisation of ionising radiation and nuclear energy within the Indian context, with a specific focus on reducing possible threat to human health and the ecosystem. The AERB has set 60 μg L^{-1} as permissible limit of uranium contamination in water [62]. The permissible limits set by AERB for cadmium, zinc, chromium and iron are 0.01 mg L^{-1}, 5 mg L^{-1}, 0.05 mg L^{-1} and 0.3 mg L^{-1}, respectively [63].

1.5 Terms and Units

The basic terms used in radiation physics are given as under-

1.5.1 Activity

It is the number of nuclear disintegrations per unit time. SI unit of activity is Becquerel (Bq), where Bq is the one disintegration per second.

Half-life - The half-life of a radioactive element refers to the time span during which its number of atoms decreases to a half of its initial amount, as shown in figure 1.5 [4]. The equation for radioactive decay is given by

$$N(t) = N_0 e^{-\lambda t} \tag{1.3}$$

where N(t) denotes the no. of radionuclides at a given time t. N_0 represents the initial no. of radionuclides at the starting time t=0, and λ is the decay constant.

1.5.2 Radioactive equilibrium

Radioactive equilibrium occurs in a radioactive series once the progeny starts decaying at the same rate as they emanate from their parent nuclei. Therefore, when the quantity of atoms in a radioactive substance within a radioactive series reaches a stable state, radioactive equilibrium is reached.

Secular equilibrium - If the half-life of the parent isotopes (T_1) is significantly greater than the half-life of the daughter isotope (T_2), meaning that the decay constant of the daughter isotope (λ_2) is much larger than the decay constant of the parent isotopes (λ_1), the resulting condition is termed as secular equilibrium i.e $\lambda_2 >> \lambda_1$. The combined activity of the parent and daughter nuclei reaches its peak and remains relatively stable for several half-lives of the daughter product.

Transient equilibrium - During radioactive decay chain, transient equilibrium is reached when the decay rate of the parent isotope matches that of the daughter isotope, causing the activity of daughter isotope to closely match that of parent isotope for a specific period.

No equilibrium - If the decay constant of the parent radionuclide exceeds that of the daughter nuclide i.e. $\lambda_1 > \lambda_2$, an equilibrium state is not achieved.

Disequilibrium - It arises whenever one or more decay products within a decay series are entirely or partially eliminated or introduced into the system.

1.5.3 Exposure

Environmental exposure refers to the interaction of living beings with physical, biological or chemical agents present in air, food, soil or water that could adversely affect health.
Radiation exposure - It refers to the amount of ionization produced in air by gamma and X-rays. Its unit is Roentgen (R) where

$$1\text{R} = 2.58 \text{ x } 10^{-4} \text{ C kg}^{-1}$$

Exposure can be internal and external.

Internal exposure - It happens when pollutants are breathed in, swallowed or otherwise enters the bloodstream. The cessation occurs when a pollutant is eradicated from the body, either naturally or due to medical intervention.

External exposure - Its occurrence is attributed to the existence of pollutants in the soil and other substances in close proximity to our bodies, including the air. It can be eliminated from the body solely through washing.

1.5.4 Radiation dose

It is the risk faced by the individual which is based on various factors of exposure, which include site, amount of contaminants in the environment, time, and the individual's living habits such as diet, breathing rate, etc.

Absorbed dose - In 1954, ICRP gave a new parameter, absorbed dose which is defined as the amount of energy that is deposited in tissue due to exposure to ionising radiation. It extends to all fields involving ionising radiation, regardless of whether the radiation is directly or indirectly ionising, in addition to any source of ionizing radiation that is dispersed throughout the absorbing medium. Its unit is Gray.

Equivalent dose - Radiation characterised by a low linear energy transfer (LET) exhibits a comparatively reduced capacity to induce detrimental effects on a biological system per unit dose, in contrast to radiation with high LET. The term "equivalent dose" is used to characterise radiation with high linear energy transfer thus, distinguishing it from low LET values. The impact of specific radiation on the tissue is defined by the equivalent dose. The equivalent dose is the same as the absorbed dosage at low linear energy transfer. For heavy ion particles and neutrons (high LET), absorbed dose is multiplied by a factor to calculate equivalent dose.

$$H = QD \tag{1.4}$$

where H is the equivalent dose, Q is absorbed dose and D is dimensionless quantity that depends on LET. Sievert is the SI unit of equivalent dose.

Effective dose - It is contingent upon three factors: the absorbed dosage to all organs of the body, the relative damage caused by the radiation, as well as the degree of sensitivity of each organ to radiation. The consideration of sensitivity is based on the fact that radiation has distinct effects, such as the lungs having a different impact compared to the brain.

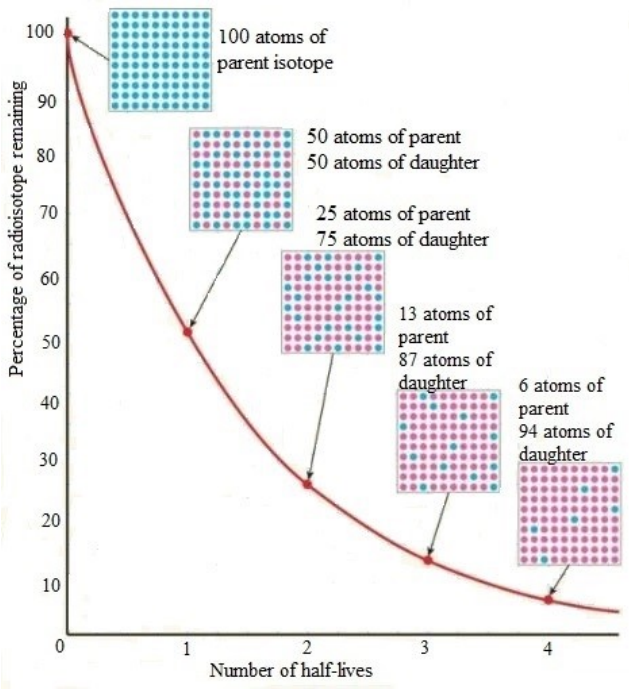

Figure 1.5: Radioactive decay curve [4].

1.6 Exposure pathways and health risks

Exposure routes include ingestion, inhalation and external exposure. The presence of pollutants in potable water and food offers a potential route to internal exposure. The presence of pollutants in the atmosphere serves as a significant contributor to both external and internal exposure to human beings. The environmental routes of pollutants are shown in figure 1.6 [64]. The cumulative radiation exposure encompasses both naturally occurring ionising radiation and anthropogenic sources, such as nuclear waste, mining activities, and weapon testing. The person who lives by the sea receives the average effective dose rate of about 3 mSv per year [65]. The radiation dose received from various sources is listed in table 1.2. The natural dose from radiation can be greater in high altitudes due to more cosmic ray intensities and in soil with higher radioactive content, which may vary from one place to another. Terrestrial radionuclides lead to health concerns, both carcinogenic and non-carcinogenic, due to their radioactive properties and chemical toxicity [66]. The absorption and distribution of these radionuclides inside the human body, and therefore the possible health consequences, are contingent upon the chemical characteristics of the compound to which an individual might be subjected to, as well as the pathway through which exposure occurs [67]. Water-soluble uranium compounds are known to have acute systemic effects. Excessive consumption of uranium has been found to have detrimental effects on the proximal tubules, potentially leading to renal failure. Pavlakis *et al.* [68] reported that the extended intake of uranium can lead to severe symptoms such as nausea, diarrhoea, vomiting as well as paralytic ileus. A study by Gueye *et al.* [69], observed a decline in radial cortical bone development and a decrease in mRNA expression of genes associated with trabecular bone metabolism. The majority of reproductive effects caused by

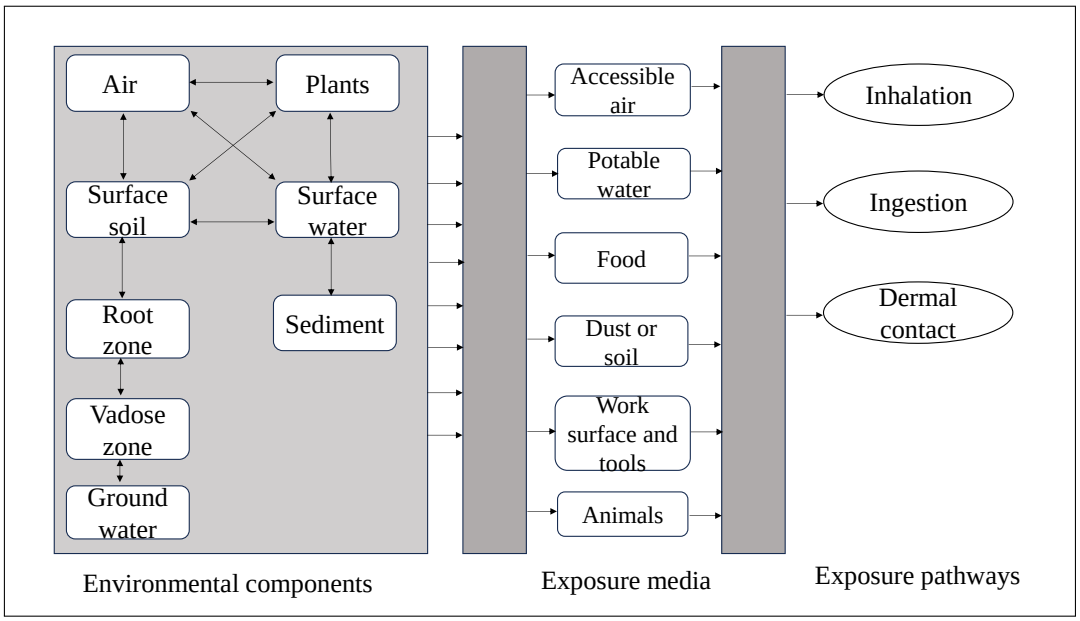

Figure 1.6: Environmental routes of pollutants through which they can enter human body [64].

uranium have been ascribed to its chemical characteristics [70]. For thorium, the retention of insoluble thorium compounds is observed within the lungs, as well as in other tissues where ingested thorium continues to accumulate. The degree of lung sclerosis exhibits a clear correlation with both the radiation dosage and the quantity of inhaled thorium dioxide [71]. The health risk posed by ^{40}K is linked to cellular damage resulting from exposure to ionising radiation which has the potential to initiate the development of cancer [72]. However, despite fluctuations in intake, the concentration of ^{40}K in the human body remains under control due to the hemostatic balance even if its levels exceed the reference value [65]. Although small amounts of some heavy metals are essential for human health, excessive ingestion has been shown to affect several cellular organelles and components within biological systems, such as the membrane of a cell, nuclei in addition to mitochondria [73]. The detrimental effects of exposure to these pollutants on human health are well documented, with evidence indicating that such exposure can result in disorders across multiple systems like digestive, pulmonary, cardiovascular, cognitive, as well as hematologic systems [73].

1.6.1 Health implications caused by radiation exposure

The various effects of radiation exposure on human health include:

Stochastic effect - It refers to chronic and continuous long-term radiation exposure, which can cause mutations at the cellular or molecular level resulting in the unregulated proliferation of cells leading to cancer, as shown in figure 1.7. The likelihood of stochastic effects happening is directly related to the dosage, whereas the intensity of the impact remains unaffected by the dosage received. This effect is further divided into three categories, namely genetic, somatic and in-utero effects. Genetic effect is

Table 1.2: Average radiation dose due to naturally occurring sources [65].

Source	**Worldwide average annual effective dose (mSv)**	**Typical annual effective dose range (mSv)**
External exposure		
Cosmic rays	0.39	0.3 - 1[a]
Terrestrial radiation (Outdoors and indoors)	0.48	0.3 - 1[b]
Internal exposure		
Inhalation (mainly radon)	1.26	0.2 - 10[c]
Ingestion (food and drinking water)	0.29	0.2 - 1[d]
Total	2.4	1 - 13

[a] Range due to altitude and latitude.
[b] Range due to soil composition and building materials.
[c] Range due to radon levels in different regions.
[d] Range due to dietary habits and water sources.

caused to the descendants of the exposed individual whereas somatic effects impact the exposed individual itself. The in-utero impact is particularly relevant concerning embryonic exposure to radiation. In relation to stochastic radiation injuries, it has been observed that ^{232}Th exhibits a higher radiotoxicity compared to uranium with equivalent levels of activity [64].

Deterministic effect - There is a threshold for deterministic effects below which they don't happen. The threshold level can vary considerably between individuals. After the threshold has been surpassed, the magnitude of an impact escalates in proportion to the dosage. It is based on the direct proportionality of dose and effect [65]. The observed effects include organ malfunction, alterations in blood composition and oligospermia.

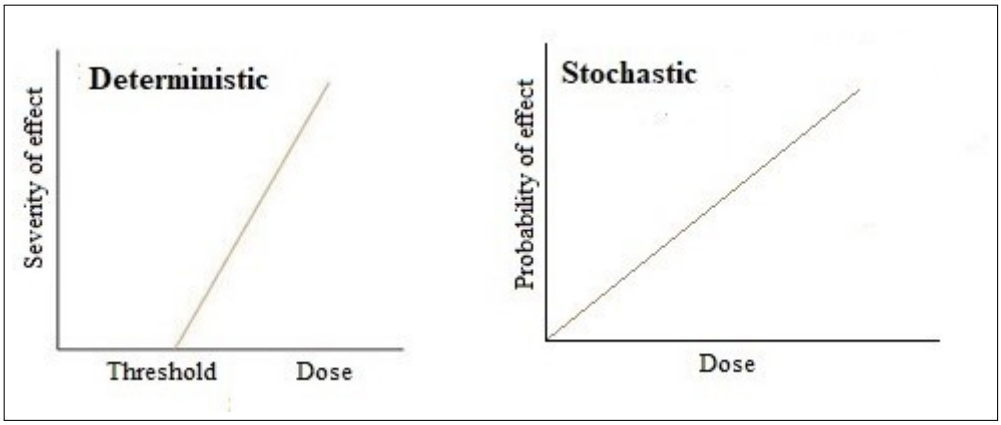

Figure 1.7: Graphical representation of deterministic and stochastic effects [74].

1.7 Literature survey

1.7.1 Groundwater

Uranium contamination measurements - The measurement of uranium poisoning in groundwater has been conducted over an extended period, resulting in the publication of a substantial volume of data on the same [77-81]. The inaugural publication of the WHO that addressed the subject of public drinking water quality was released in 1958 under the title 'International Standards for Drinking-water' [82]. Almeida *et al.* [83] found the elevated levels of uranium in Rio de Janerio state ranging from 0.2 to 667 μg L^{-1}. Similarly, Birke *et al.* [84] found the high uranium levels in Shanxi, China ranging between 0.02 to 288 μg L^{-1}. Wu *et al.* found uranium concentration to vary between 0.02-288 μg L^{-1} in Datong basin, China [85]. B Zhang *et al.* found uranium concentrations ranging from 0.18 to 453 μg L^{-1} in the Erlian Basin, located in north-east China [86]. In the Australian groundwater, the recorded uranium concentrations exhibited a range of 0.05 to 160 μg L^{-1} [87]. In a study conducted by Yamamoto *et al.* [88] in Kazakhstan, it was observed that the uranium levels were found to be below 30 μg L^{-1}. According to Ullah *et al.* [89], the uranium levels in Pakistan varied between 1.07 and 84.43 μg L^{-1}. In Indus basin, Punjab (Pakistan) uranium contamination varied between 0.1-556 μg L^{-1} [90]. The central valley aquifer in the United States has exceedingly elevated levels of uranium, with recorded values of $\leq$5400 μg L^{-1} [91]. Similarly, the values ranging from less than 0.5 to 5400 μg L^{-1} have been observed by Nolan and Weber in the same region [92]. In a different study, Fujii and Swain [93] also recorded values as high as 5400 μg L^{-1} for the same location. It was suggested that complexation with CO_3 and PO_4 may be pathways for the mobility of uranium in these groundwaters. The vast Plio-Pleistocene high plains aquifer in the central United States, having alluvial deposits, were reported to have uranium values ranging from 0.5 to 2670 μg L^{-1} [92]. In a study conducted by Steffanowski and Banning [94], it was found that the uranium contamination levels varied between 0.258 to 152 μg L^{-1} in Germany. The levels of ^{238}U and ^{222}Rn in drinkable water samples obtained from boreholes in the Migdonia valley, Greece were documented to be 48.9 μg L^{-1} for ^{238}U, whereas for ^{222}Rn it was 161 Bq L^{-1} [95]. In Sweden, the concentration of uranium in wells ranged from 0.20 to 470 μg L^{-1} [96]. In Dornogobi Aimag Province, Mongolia, the uranium levels varied between 0.24-429 μg L^{-1}. Moreover, shallower groundwater sources (<10 m) contained higher amounts of uranium compared to deeper sources (>50 m) in the region [97].

Several studies have been published on the activity concentration of ^{238}U in water samples collected from various parts of India. The uranium toxicity has been reported by Singh *et al.* [98], Singh *et al.* [99], Rana *et al.* [100] and Giri *et al.* [101]. Coyte *et al.* [102] found that 25% of the 324 wells tested in Rajasthan had uranium levels that were above the established limit set by WHO. Elevated uranium levels in Bihar predominantly occur along northwestern to southeastern region, situated along and eastward of the Gandak River [103]. In a study conducted by Sar *et al.* [104], it was observed that the majority of the samples collected from the groundwater of Balod district in Chattisgarh were below the limits set by the WHO. Similarly, in the region of Jammu and Kashmir, the concentration of uranium in groundwater varied in a range of 0.2 to 20.8 μg L^{-1} [105]. Kumar *et al.* [106] observed a range of uranium concentrations spanning from 0.005 to 2.0 μg L^{-1} in the Tummalapalle

uranium mining region located in Andhra Pradesh. Rani *et al.* [107] recorded uranium concentration ranging from 2.54 to 133 μg L^{-1} in northern Rajasthan, with the majority of values surpassing the allowable threshold of 30 μg L^{-1}. In Uttar Pradesh, Kumar *et al.* [108] found a range of uranium concentration between 11-63 μg L^{-1}, while in Tamil Nadu, Adithya *et al.* [109] reported a range of 0.8-72 μg L^{-1}. The groundwater samples from granitic rock formations of Telangana had uranium concentrations between 0.2 to 68 μg L^{-1} [110] and 7 to 370 μg L^{-1} [111].

The Malwa belt of Punjab is currently grappling with a significant issue of elevated levels of uranium pollution [112-114]. The uranium contamination in the Patiala district in groundwater was reported to be in a range from 38 to 267 μg L^{-1} [115]. The uranium levels in drinking water in the regions of Bathinda, Mansa, Faridkot and Ferozpur were found to vary between 0.5-579 μg L^{-1}. The data reveals that almost 68% of the water samples are above the permitted level set by WHO, while 43% of the samples beyond the limit recommended by AERB [116]. Kumar *et al.* [117] reported maximum values of 650 μg L^{-1}, whereas Sharma and Singh [118] observed concentrations as high as 1340 μg L^{-1}. Kochhar *et al.* [119] proposed Tusham area's high heat producing granites as the possible source of uranium contamination in the state. Siwalik sediments as the chief source for the high amount of uranium in groundwater was suggested by Patnaik and Phadke [120-121] while excess fertiliser usage was proposed as a possible reason by Kumar and Singh [117, 122] for high uranium concentration in groundwater.

Heavy metal contamination measurements - The dissolution of heavy metals in groundwater is affected by natural mechanisms like fluctuations in soil pH levels. The origins of heavy metal contaminants can be both natural and caused by human activity. Common natural sources of metal contamination in the environment include the chemical reactions between metal-containing rocks and the occurrence of volcanic eruptions [123]. In addition, groundwater can get polluted with heavy metals originating from sewage, mine tailings leachate, seepage from industrial waste, industrial spills and leaks, deep-well disposal of liquid wastes and landfill leachate [124]. The parameters of groundwater flow serve as an essential parameter in determining the movement of metal pollutants. Numerous heavy metals and metalloids are toxic to living beings, contingent upon the level of concentration and the duration of exposure [123].

The average concentration order in groundwater samples of Shiraz, Iran, has high levels of iron followed by copper, nickel, molybdenum, lead, zinc, arsenic and cobalt [125]. The amount of lead, nickel and iron in the groundwater samples of Warri, Nigeria, varied from 0.06 to 0.44 mg L^{-1}, 0.008 to 0.19 mg L^{-1} and 0.315 to 2.753 mg L^{-1}, respectively. Vanadium, chromium, zinc and cadmium were detected in very low concentrations, ranging from 0 to 0.85 $\times 10^{-3}$ mg L^{-1}. The concentrations of Ni, Fe and Pb surpassed the threshold limits of 0.02, 0.3 and 0.01 mg L^{-1}, respectively established by WHO [126]. The concentration of metals found in wells in Thailand and the overall mean was below the permitted limits for copper, arsenic, chromium, mercury, cadmium, nickel in addition to zinc in groundwater [127]. The level of heavy metal pollutants, such as nickel, copper, cadmium, lead, manganese, zinc, chromium and iron were measured in 129 groundwater samples in Vehari, Pakistan and their concentration was-lead (93% samples), cadmium (68% samples) and iron (100% samples), which were found to be exceeding WHO's recommended limits

[128]. In Kumasi (Ghana), the average content of lead, iron, cadmium and chromium transcended the acceptable thresholds set by the WHO for drinking water [129]. The groundwater samples collected from Tapiza, Albania, exhibit the following ranges of heavy metal concentrations: arsenic from 2.6 to 9.2 μg L^{-1}, cadmium from 0 to 0.61 μg L^{-1}, cobalt from 4.3 to 17.8 μg L^{-1}, copper from 7.5 to 28.4 μg L^{-1} and lead from 0.96 to 5.84 μg L^{-1} [130]. The mean concentrations of heavy metals in the borehole water of the Kilimambogo region were found to be 6.4 ppm for cadmium (Cd), 6.9 ppm for nickel (Ni), and 42.0 ppm for lead (Pb) [131].

Wagh *et al.* [132] took a total of forty groundwater samples from Nashik (India) of both dug and bore wells in rural areas for heavy metal analysis of zinc, cadmium, cobalt, lead, iron, chromium, nickel, manganese and copper. The analytical findings revealed that all samples have concentrations of lead and nickel exceeding the maximum permissible levels. Additionally, 95% of the samples had levels of Cr higher than the safe limits and 92.5% of the samples had levels of Fe exceeding the safe limits. The descending order of heavy metal concentrations measured in Jharkhand were as follows: iron (Fe) followed by zinc (Zn), manganese (Mn), aluminium (Al), barium (Ba), nickel (Ni), copper (Cu), lead (Pb), chromium (Cr), selenium (Se), arsenic (As) and cadmium (Cd). The concentration of Fe exceeded the desired limit in every sample [133]. The sixteen heavy metals were examined in Cauvery river basin in Tamil Nadu of groundwater with chromium exhibiting the highest concentration succeeded by zinc. Although the levels of chromium along with zinc in the groundwater samples were within Indian permissible limits [134].

Sharma *et al.* [135] observed the highest concentration of cadmium in Ferozpur at 2.9 mg L^{-1}, followed by Faridkot at 0.022 mg L^{-1}. Muktsar, Moga, and Mansa had a concentration of 0.009 mg L^{-1}, while Barnala and Sangrur had a concentration of 0.008 mg L^{-1}. The lowest concentration was reported in Bathinda at 0.006 mg L^{-1}, exceeding the BIS limit of 0.003 mg L^{-1} for cadmium. The highest recorded concentration of chromium (3.6 mg L^{-1}) was at Muktsar followed by Ferozpur (2.9 mg L^{-1}), Faridkot (2.89 mg L^{-1}) and Mansa (2.3 mg L^{-1}). However, the maximum permissible amount of chromium pollution in groundwater, according to BIS, is 0.05 mg L^{-1}. In comparison, low concentrations were reported in Bathinda, and Barnala has an even lower concentration [135]. Krishan *et al.* [136] reported the highest level of chromium content, up to 85.19 ppb, with an average concentration of approximately 1.47 ppb in Punjab. The concentration of iron in the samples from Punjab was measured up to 6830 (ppb), with an average concentration of 251 ppb.

1.7.2 Soil

The patterns of radionuclide distribution within the soil are influenced by geology, physical along with natural atmospheric interactions [137]. The extent of radioactivity found in soil is contingent upon the thickness of the soil cover, its type, its evolution and transport process along with moisture and temperature [138-141]. The environment contains radioactive pollutants that are both man-made and natural. Radionuclides pose significant risks to both environmental integrity and human health because of their high mobility, capacity for bioaccumulation and variety of biogeochemical processes [142]. In addition to serving as indicators of environmental and radiological pollution, soil can act as a source and a conduit

for radioactive migration [143]. Moreover, the extensive application of phosphate fertilisers in agricultural land has been recognised as a possible contributor of natural radionuclides in soils [144]. Warm humid tropical areas are typically characterised by significant soil weathering resulting from severe seasonal rainfall along with an elevated mean temperature. Moreover, a humid environment promotes the leaching of alkaline metals, contributing to the acidification of soil, which in turn can affect the mobility of uranium and thorium. In regions unimpacted by human intervention, the presence of uranium is predominantly associated with its dissolved or colloidal forms. Conversely, in proximity to mining operations, the transportation of uranium can occur in the form of particulate uranium minerals [145]. It is found that uranium sorption rises because organic matter and clay minerals act as exchange sites in soils. There is evidence that iron oxides and/or hydroxides, when present in the absence of carbonates, contribute significantly in the adsorption of uranium [146].

The Gajnjaca soils have the highest recorded concentration of uranium, with a total content of 2.91 mg kg^{-1} followed by alluviam soils [147]. In a comprehensive radiological assessment of Rio de Janeiro, ^{40}K activity was reported to vary between 12 and 1042 Bq kg^{-1}, for ^{226}Ra, activity ranged from 3 to 100 Bq kg^{-1}, and those for ^{228}Ra activity ranged from 5 to 511 Bq kg^{-1} [147]. According to the findings of Bister *et al.* [148], it was observed that alluvial soils in the flood basins of the Mulde river in Germany had elevated levels of uranium concentration in areas utilised for grazing, in comparison to croplands. Arnedo *et al.* [149] found the geometric mean of activity for ^{40}K, ^{226}Ra and ^{228}Ra to be 384.4, 25.2 and 28.9 Bq kg^{-1} for Canary Islands, Spain. Similarly, Laubenstein *et al.* [150] found activity of ^{40}K to be 486 Bq kg^{-1}, ^{226}Ra to be 31 Bq kg^{-1} and ^{228}Ra to be 41 Bq kg^{-1} in Molise, Italy. The activity concentrations in soil samples collected from North Cyprus exhibited a range from 49.7 to 147.6 Bq kg^{-1} for ^{226}Ra, 18.1 to 93.9 Bq kg^{-1} for ^{232}Th, 103.5 to 1468.6 Bq kg^{-1} for ^{40}K, and 4.3 to 15.9 Bq kg^{-1} for ^{137}Cs [151]. Similarly, the measured specific activity of soil samples in Nineveh province, Iraq, were found to be with average values of 32.52±6.48 Bq kg^{-1} for ^{226}Ra, 20.30±5.36 Bq kg^{-1} for ^{232}Th, 378.93±123.29 Bq kg^{-1} for ^{40}K and 8.17±5.55 Bq kg^{-1} for ^{137}Cs [152]. Singh *et al.* [153] found the activity of ^{226}Ra varying between 25.9 to 75.7 Bq kg^{-1}, ^{40}K varying between 143 to 242 Bq kg^{-1} and ^{232}Th between 80.7 to 122.8 Bq kg^{-1} in Himachal Pradesh. Srinivasa *et al.* found the average activity of ^{232}Th, ^{226}Ra and ^{40}K to vary from 14 to 86.2 Bq kg^{-1}, 15.2 to 58 Bq kg^{-1} and 224 to 1650 Bq kg^{-1} [154]. It has been estimated by Sivakumar that the average activity of radionuclides ^{238}U, ^{232}Th, and ^{40}K in the soil is 41.5 Bq kg^{-1}, 78.0 Bq kg^{-1}, and 295.6 Bq kg^{-1}, respectively [155]. In Haryana, the average activity in soil for ^{238}U is found to be 27.9 Bq kg^{-1}, ^{232}Th to be 34 Bq kg^{-1} and ^{40}K to be 464.2 Bq kg^{-1} by Panghal *et al.* [156]. The measured activities of radium, thorium and potassium in the soils of the populated regions of Haryana were determined to be 50.76±1.88 Bq kg^{-1}, 154.69±5.76 Bq kg^{-1} and 1092.51± 112.58 Bq kg^{-1}, respectively [157]. The average radioactivity levels in the soils of Rajasthan were determined to be 24±10 Bq kg^{-1} for ^{226}Ra, 55±11 Bq kg^{-1} for ^{232}Th, and 549±145 Bq kg^{-1} for ^{40}K [158]. Narayana *et al.* reported the activity levels of ^{40}K, ^{226}Ra and ^{232}Th with median of 117.5 Bq kg^{-1}, 35.0 Bq kg^{-1}, 29.8 Bq kg^{-1}, in the coastal region of Karnataka [159]. The mean activity levels of ^{226}Ra, ^{232}Th and ^{40}K in the soils of Chikkamagaluru district, Karnataka, were determined to be 36.9±31.0, 51.6±1.3, and 566.97±11.0 Bq kg^{-1}, respectively [160].

Uranium content in soil samples in areas of Punjab is reported to range from 1.14 to 2.44 mg kg^{-1} [161]. In soil samples, the maximal value of uranium activity is 41.9±10.3 Bq kg^{-1} that is considerably greater than the average global uranium activity of 35 Bq kg^{-1}. It was observed that potassium and uranium contamination is highest in the Bathinda district. Bandhan *et al.* found the average activity in soils to be 28.58 Bq kg^{-1} for ^{238}U, 50.95 Bq kg^{-1} for ^{232}Th and 569.59 Bq kg^{-1} for ^{40}K in Ludhiana, Punjab [162]. According to Kaintura *et al.*'s findings [163] in the neutral terrain of Ropar (Punjab), the activity concentration of ^{232}Th, ^{238}U and ^{40}K varied from 55.58 to 106.82 Bq kg^{-1}, 37.00 to 76.13 Bq kg^{-1} and 381.37 to 526.26 Bq kg^{-1}, respectively.

1.7.3 Food

Natural radionuclides measurements in wheat grains - The contamination of food due to radionuclides into the environment is impacted by several factors, including the type of soil, its chemical attributes, and both the chemical and physical forms of the radionuclides found in the soil, the absorption of radionuclides by certain plants, and the subsequent accumulation levels in specific food items [164]. The radionuclides are absorbed by plants either by coming into contact with the external surfaces of the plant, such as through the leaves, or by being transferred from the soil to the plant through the roots. Soil functions as a natural buffering mechanism, controlling the distribution of chemical elements and compounds throughout various regions of the biosphere. However, plants can absorb harmful substances like radionuclides in conjunction with nutrients, which can subsequently be transmitted through the food chain [165].

The transfer factor is a measure of the ratio between the concentration of a particular radionuclide in plant tissue and the concentration of a particular radionuclide in the soil. A study was conducted to investigate the absorption of naturally occurring radionuclides by wheat plants in two distinct soils in India. The transfer factors (TF) for the soil-to-wheat grain transfer were estimated and found to vary from 6.0×10^{-3} to 2.4×10^{-2} for ^{232}Th, 4.0×10^{-4} to 2.1×10^{-3} for ^{238}U and 0.14-3.1 for ^{40}K [166]. The magnitude of accumulation of natural radioactive elements is influenced by the ability of plants to selectively absorb these elements. This helps maintain a balance in their environment, known as homeostasis [166]. Tufail *et al.* reported the transfer factors for ^{40}K, ^{226}Ra and ^{232}Th from soil to wheat grain to be 0.118±0.021, 0.022±0.004, and 0.036±0.007, respectively in Faislabad, Pakistan [167]. The transfer factors of natural radionuclides from soils to wheat grains grown in fertilised fields in Pakistan have been measured as 2-3$\times10^{-2}$ for ^{232}Th, 3-4$\times10^{-2}$ for ^{226}Ra and 17-20$\times10^{-2}$ for ^{40}K [168]. The transfer factors of the radionuclides ^{226}Ra, ^{232}Th and ^{40}K from soil to wheat flour of Kars, Turkiye were found to range from 0.30 to 1.29, 0.15 to 0.86, and 0.45 to 0.83, respectively [169]. The transfer factor from soil to wheat grains in Qassim, Saudi Arabia, is reported to be from 0.15 to 0.18 for ^{40}K and from 0.09 to 0.16 for ^{226} Ra [170]. Yadav *et al.* [165] found the transfer factors of ^{226}Ra, ^{232}Th and ^{40}K from soil to wheat grains ranged from below detection limit (BDL) to 0.01, BDL to 0.004 and 0.19 to 0.48, respectively. Similarly, the transfer factors (TF) of ^{226}Ra, ^{232}Th, and ^{40}K from different kinds of soil to wheat grains were estimated, and the TF values ranged from 0.11 to 2 for ^{226}Ra, from 0.14 to 1 for ^{232}Th and from 1.18 to 3.72 for ^{40}K near areas irrigated by Bahr Yussuf canal, Egypt [171].

These numbers for ^{226}Ra, ^{232}Th and ^{40}K are surpassing the default values of 0.04, 0.05 and 1, respectively, as proposed by the IAEA [171]. Pourimani *et al.* [172] reported that the transfer coefficients for the maximum values of ^{232}Th, ^{40}K, ^{226}Ra and ^{137Cs} were found to be 0.08, 0.90, 0.09 and 0.09, respectively for barley and least transfer occurred for wheat. Taher *et al.* [173] found that the transfer factor for ^{226}Ra from soil to Alfalfa was greater than that observed for wheat grains and palm dates in Qasim (Saudi Arabia). The findings reported by Najam *et al.* [174] indicate that the transfer factors from soil to dried vegetable samples varied between 0.56 and 0.65, 0.31 and 0.46, and 0.42 and 0.8, respectively for ^{40}K, ^{226}Ra and ^{232}Th. Van *et al.* found that the concentrations of thorium as well as potassium in leafy vegetables from Vietnam surpassed the established global estimates [175].

Lindahl *et al.* [176] found no significant disparity in the levels of activity concentrations of the four radionuclides (^{40}K, ^{226}Ra, ^{228}Ra and ^{228}Th) in wheat grains grown using organic farming in comparison to conventional farming methods in Belgium. Paiva *et al.* [177] found no significant differences in the levels of Ra and U in vegetables cultivated under organic farming versus conventional farming practices in Petrópolis, Brazil. However, the findings presented by Mehmet et al. [178] demonstrated that the activity concentrations of ^{210}Po, ^{228}Ra, ^{40}K, ^{226}Ra and ^{210}Pb in plant and soil samples from conventional farming regions exceeded those found in organic farming areas. In plants collected from organic fields, the relative concentration ranges of ^{210}Po, ^{210}Pb, ^{40}K were between 0.21 and 1.40 Bq kg^{-1}, 0.67 and 4.81 Bq kg^{-1}, ND (not detected) and 7.34 Bq kg^{-1}, respectively.

Heavy metals contamination in wheat grains measurements - Agroecological niches are threatened by rapidly expanding industry, unchecked xenobiotic pollution discharge, in addition to irrigation with poor-quality water. The plant's interaction with metals depends on soil parameters such as pH, organic matter amount and clay adsorption [179]. The heavy metals accumulate in the soil, penetrate through the food chain and eventually reach the public, causing health issues. The high concentration of heavy metals can harm plants by affecting membrane permeability, blocking enzymes and inactivating photosystems [180]. Heavy metal toxicity in plant tissues, especially wheat, can disrupt physiological processes and ultimately harm human health. The root development is particularly vulnerable to heavy metal pollution. High metal concentrations restrict root growth, resulting in shorter, ramified, and unstructured roots [181]. Furthermore, the functioning of antioxidant enzymes is reduced by the elevated amounts of heavy metals [182]. The quantification of seven heavy metals in wheat grains indicated that zinc was the most prevalent, in contrast to cadmium, which was recorded as the least prevalent metal [183]. The study also found that wheat tends to acquire more heavy metals than maize. In Kunschan (China), the order in which heavy metals were accumulated in wheat grains was: zinc followed by copper, lead, chromium, nickel, cadmium, arsenic and mercury [184]. The average amounts of copper, manganese, iron, chromium and zinc in wheat grains exceeded the tolerance limits specified by international law for wheat grains in Argentina [185]. The findings by Thabit *et al.* showed that while Cd was found in very small amounts in one sample of Ukrainian wheat whereas, arsenic, cadmium, mercury as well as lead were not found in the majority of wheat and barley samples. Three samples of polish wheat contained very minute amounts of lead [186].

1.8 Study area

Punjab state, with 23 districts in the Indian subcontinent, shares its borders with the states of Himachal Pradesh, Haryana and Rajasthan, along with the union territories of Chandigarh and Jammu and Kashmir. The state spans across 50,362 sq. km [187]. The majority of Punjab is situated in a fertile, sedimentary plain with year-round rivers and a comprehensive network of irrigation canals [187]. The state's northeastern region is characterised by a range of rolling hills that stretch along the base of the Himalayas. The average altitude of the area is 300 metres above sea level, varying from 180 metres in the southwest to over 500 metres at the northeastern boundary. The southwestern region of the state exhibits a semi-arid climate, gradually transitioning into the Thar Desert. The state is traversed by the Sutlej, Beas and Ravi rivers. The soil qualities are partially impacted by the geography, vegetation and parent rock. The regional climate changes further amplify the diversity in soil profile characteristics. The state is geographically categorised into three main regions based on soil types: central, eastern and southwestern.

Figure 1.8: The map of Punjab state, India [187].

Geographical setting - The Mansa district is approximately triangular in shape and is situated in the southern region of Punjab state. It spans an area of 2,171 km^2 and is positioned between the latitudinal coordinates of 29°32' to 30°12'N and longitudinal coordinates of 75°10' to 75°46'E. The region is geographically demarcated by Bathinda district to the northwest, Sangrur to the northeast, and the southern border is shared with Haryana state, as shown in the figure 1.8 [187]. The geomorphology of the district mostly consists of flat alluvial plains, which are occasionally broken by dune formations in the southern region. The district does not possess a perennial river. The region is predominantly irrigated by an extensive

network of canals. The region is situated within the Indo-Gangetic alluvial plains. The geological structures seen in the district consist of Quaternary-age Alluvium, as depicted in figure 1.9 [187]. The composition of this geological formation is characterised by the presence of successive strata of sand, silt and clay. The granular zones consist of thin layers of fine sand that alternate with rigid clay bands, located below a depth of 20 metres. The compactness of these zones increases as the depth increases. A continuous band of an impervious layer, with a thickness ranging from 2 to 4 metres, is present near the ground surface in the majority of the region. This layer serves as a barrier, preventing the infiltration of surface run-off [188]. The alluvial deposits of the region were created by the transportation of sediments from neighbouring regions, including Siwaliks, granites and other metamorphic rocks [189].

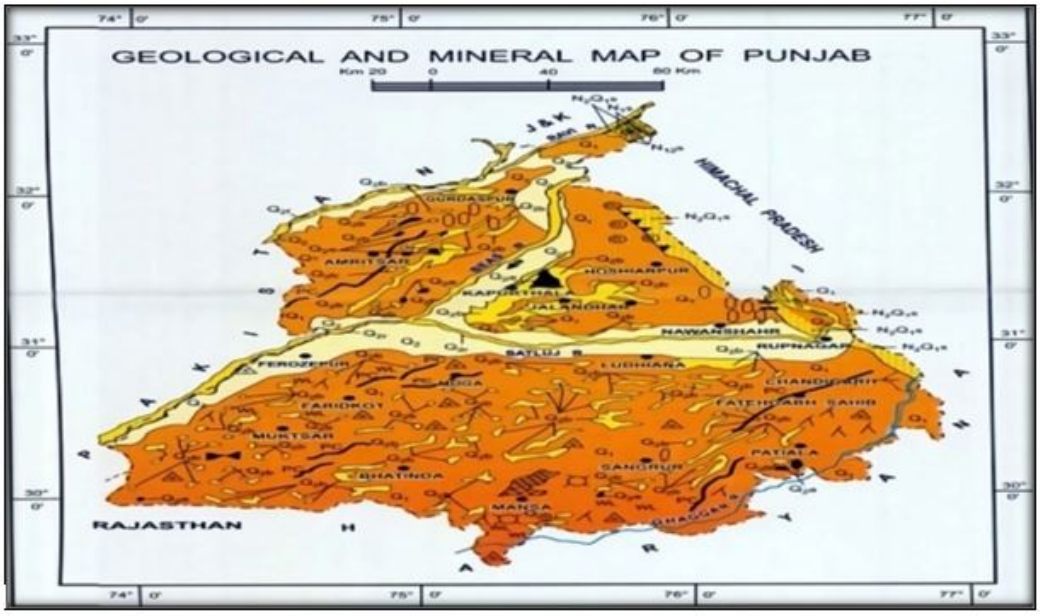

Figure 1.9: Geology and mineral map of Punjab [188].

1.8.1 Motivation

In India, the groundwater serves as the primary supply of potable water, as well as for agriculture and industry. In accordance with a recent report released by the Central Ground Water Board [188], Punjab has the highest level of groundwater exploitation in India. Hence, in accordance with the Sustainable Development Goals (SDG) 6 outlined in the United Nations Agenda 2030 [190], it is imperative to enhance water quality through the reduction of pollutants, mitigation of hazardous waste discharge, prevention of illegal waste disposal, and the promotion of widespread recycling and safe reuse practices. Numerous authors have confirmed the presence of uranium toxicity in the Malwa area of Punjab, India. According to the Federation of Indian Chambers of Commerce & Industry (FICCI) [191], the crude cancer incidence rate for the population of Punjab is 144.0 per lakh, making it one of the highest rates of crude cancer incidence in India. According to Blaurock-Busch *et al.* [192], the cancer rates in the Malwa area are notably elevated in the four districts of Mansa, Bathinda,

Faridkot and Muktsar. The increase in cancer incidence can be attributed to the soaring levels of uranium found in groundwater, as suggested by studies [193-194]. The state is currently experiencing a crisis as a result of these elevated levels of uranium and heavy metals in the groundwater table, which has been in the news for more than a decade for being the epicentre of debilitating diseases [195-196]. As the state has one of the highest rates of groundwater extraction in India, primarily for irrigation [197], therefore, it is pivotal to evaluate and periodically monitor the groundwater, soil and agricultural contamination due to natural radionuclides and heavy metals.

1.8.2 Objectives

The measurement of pollutants is indispensable to estimate the hazards to humans due to the interaction and interdependence of man and the environment. These measurements also provide baseline data to provide information for radiation activities, infer geological information, etc., as part of routine measurements, and to check possible changes with time. The pollutants that are present in soils and fertilisers find their way to the human body through a variety of geochemical mechanisms such as atmospheric dispersion, gravity settling in addition to plant uptake. The objectives of the research include -

1. To analyse the water contamination in the study region.
2. To analyse radioactivity in soil and food samples collected from the study region for radiological risk assessment.
3. To calculate soil to plant transfer ratio in Mansa district.
4. To compare the radioactivity in organic foods and regular staple food items available in the market.

1.9 References

1. Curie, P., & Sklodowska-Curie, M. (1898). Sur une substance nouvelle radioactive, contenue dans la pechblende. *CR Acad. Sci. Paris*, *127*, 175-178.
2. Rutherford, E. (1899). VIII. Uranium radiation and the electrical conduction produced by it. *The London, Edinburgh, and Dublin philosophical magazine and journal of science*, *47*(284), 109-163.
3. Rutherford, E. (1900). I. A radio-active substance emitted from thorium compounds. *The London, Edinburgh, and Dublin philosophical magazine and journal of science*, *49*(296), 1-14.
4. Krane, K. S. (1991). *Introductory nuclear physics*. John Wiley & Sons.
5. Kathren, R. L. (1998). NORM sources and their origins. *Applied radiation and isotopes*, *49*.
6. Twining, J. R., & Baxter, M. (Eds.). (2012). *Tropical radioecology* (Vol. 18). Elsevier.
7. Gavrilescu, M., Pavel, L. V., & Cretescu, I. (2009). Characterization and remediation of soils contaminated with uranium. *Journal of hazardous materials*, *163*(2-3), 475-510.
8. Waseem, A., Ullah, H., Rauf, M. K., & Ahmad, I. (2015). Distribution of natural uranium in surface and groundwater resources: a review. *Critical reviews in environmental science and technology*, *45*(22), 2391-2423.
9. Osburn, W. S. (1965). Primordial radionuclides: their distribution, movement, and possible effect within terrestrial ecosystems. *Health physics*, *11*(12), 1275-1295.
10. Smedley, P. L., Smith, B., Abesser, C., & Lapworth, D. (2006). Uranium occurrence and behaviour in British groundwater.
11. Cui, Q., Zhang, Z., Beiyuan, J., Cui, Y., Chen, L., Chen, H., & Fang, L. (2023). A critical review of uranium in the soil-plant system: Distribution, bioavailability, toxicity, and bioremediation strategies. *Critical reviews in environmental science and technology*, *53*(3), 340-365.
12. Edayilam, N., Ferguson, B., Montgomery, D., Al Mamun, A., Martinez, N., Powell, B. A., & Tharayil, N. (2020). Dissolution and vertical transport of uranium from stable mineral forms by plants as influenced by the co-occurrence of uranium with phosphorus. *Environmental science & technology*, *54*(11), 6602-6609.
13. National Council on Radiation Protection and Measurements (1988). *Exposure of the population in the United States and Canada from natural background radiation, NCRP Report No. 94*. Bethesda, MD.
14. Board on Radiation Effects Research National Research Council. (1999). *Evaluation of guidelines for exposures to technologically enhanced naturally occurring radioactive materials*. National Academy Press.

15. Kónya, J., & Nagy, N. M. (2018). *Nuclear and radiochemistry*. Elsevier.

16. Mernagh, T. P., & Miezitis, Y. (2008). *A review of the geochemical processes controlling the distribution of thorium in the Earth's crust and Australia's thorium resources* (p. 48). Canberra, Australia: Geoscience Australia.

17. USPEA (1999). Cancer risk coefficients for environmental exposure to radionuclides.

18. Fesenko, S. V., & Emlutina, E. S. (2021). Thorium concentrations in the environment: A review of the global data. *Biology bulletin*, *48*, 2086-2097.

19. Rachkova, N. G., Shuktomova, I. I., & Taskaev, A. I. (2010). The state of natural radionuclides of uranium, radium, and thorium in soils. *Eurasian soil science*, *43*, 651-658.

20. Boyle, R. W. (2013). *Geochemical prospecting for thorium and uranium deposits*. Elsevier.

21. Rao, A. Y., Panda, N. K., Kumar, K. R., & Sinha, D. K. (2022). Implications of Magnetic Properties in the Concentration and Distribution of REEs in Beach Placer Monazites: A Case Study from Chhatrapur Coast, Odisha. *Journal of the geological society of India*, *98*(8), 1121-1125.

22. Nguyen, V. D., & Trinh, D. H. (2022). Natural radioactivity and radiological hazard evaluation in surface soils at the residential area within Ban Gie monazite placer, Nghe An. *Journal of radioanalytical and nuclear chemistry*, *331*(2), 769-781

23. Ganapathi Rao, P., Bangaku Naidu, K., Reddy, K. S. N., Ravi Sekhar, C., Murali Krishna, K. N., & Anji Reddy, M. (2020). Geochemical studies of monazites from coastal sands of Kandivalasa–Dibbalapalem coast, Andhra Pradesh. *Journal of earth system science*, *129*, 1-17.

24. Anitha, J. K., Joseph, S., Rejith, R. G., & Sundararajan, M. (2020). Monazite chemistry and its distribution along the coast of Neendakara–Kayamkulam belt, Kerala, India. *SN applied sciences*, *2*, 1-18.

25. Veerasamy, N. *et al.* (2021). Geochemical characterization of monazite sands based on rare earth elements, thorium and uranium from a natural high background radiation area in Tamil Nadu, India. *Journal of environmental radioactivity*, *232*, 106565.

26. Ghiassi-Nejad, M., Mortazavi, S. M. J., Cameron, J. R., Niroomand-Rad, A., & Karam, P. A. (2002). Very high background radiation areas of Ramsar, Iran: preliminary biological studies. *Health physics*, *82*(1), 87-93.

27. Tao, Z. *et al.* (2012). Cancer and non-cancer mortality among inhabitants in the high background radiation area of Yangjiang, China (1979–1998). *Health physics*, *102*(2), 173-181.

28. Lahham, A., Fulop, M., Vladar, M., & Ragan, P. (1998). Body potassium content and radiation dose from 40K to the Slovak population. *Health physics*, *74*(3), 346-349.

29. Kathren, R. L. (1984). Radioactivity in the environment: Sources, distribution and surveillance.

30. Klement, A. W. (2019). Natural sources of environmental radiation. In *Handbook of environmental radiation* (pp. 5-21). CRC Press.

31. Airey, P., Hinton, T., & Twining, J. (2012). The scientific basis. In *Radioactivity in the environment* (Vol. 18, pp. 1-57). Elsevier.

32. Povinec, P. P., Hirose, K., Aoyama, M., & Tateda, Y. (2021). *Fukushima accident: 10 years after*. Elsevier.

33. Robertson, D. S. (1974). Basal Proterozoic units as fossil time markers and their use in uranium prospection. In *Formation of uranium ore deposits*.

34. Schauer, D. A., & Linton, O. W. (2009). NCRP report No. 160, ionizing radiation exposure of the population of the United States, medical exposure—are we doing less with more, and is there a role for health physicists? *Health physics*, *97*(1), 1-5.

35. Howell Jr, B. F. (1959). Introduction to geophysics. McGraw Hill Book Co., New York.

36. Schwarcz, H. P., Gascoyne, M., & Ford, D. C. (1982). Uranium-series disequilibrium studies of granitic rocks. *Chemical geology*, *36*(1-2), 87-102.

37. Tzortzis, M., & Tsertos, H. (2004). Determination of thorium, uranium and potassium elemental concentrations in surface soils in Cyprus. *Journal of environmental radioactivity*, *77*(3), 325-338.

38. Faure, G. (2013). *Origin of igneous rocks: the isotopic evidence*. Springer Science & Business Media.

39. Larsen, E. S., & Gottfried, D. (1960). Uranium and thorium in selected suites of igneous rocks. *American journal of science (US)*, *258*.

40. Reed, B. L., & Miller, T. P. (1980). *Uranium and thorium content of some tertiary granitic rocks in the southern Alaska Range* (No. 80-1052). US Geological Survey.

41. Dawood, Y. H. (2009). Radiogenic isotope fractionation as an indication for uranium mobility in the granites of El Shallal area, west-central Sinai, Egypt. *Earth sciences*, *20*(1).

42. Saha, A. K., Sankaran, A. V., & Bhattacharyya, T. K. (1970). *Preliminary study of the distribution of uranium and thorium in the granitic rocks of Singhbum* (No. CONF-681088-11). Presidency Coll., Calcutta.

43. Zhang, L., Chen, Z., Li, X., Li, S., Santosh, M., & Huang, G. (2018). Zircon U-Pb geochronology and geochemistry of granites in the Zhuguangshan complex, South China: Implications for uranium mineralization. *Lithos*, *308*, 19-33.

44. Sarangi, A. K., & Singh, A. S. (2006, May). Vein type uranium mineralisation in Jaduguda, uranium deposits, Singhbhum, India. *In proceedings of the international symposium on understanding the genesis of ore deposits to meet*

the demands of 21st Century, association on the genesis of ore deposits, Moscow, Russia (Vol. 12, pp. 54-61).

45. Heier, K. S. (1979). The movement of uranium during higher grade metamorphic processes. *Philosophical transactions of the royal society of London. Series A, mathematical and physical sciences*, *291*(1381), 413-421.

46. Rogers, J. J., & Ragland, P. C. (1961). Variation of thorium and uranium in selected granitic rocks. *Geochimica et Cosmochimica Acta*, *25*(2), 99-109.

47. Adams, J. A., & Weaver, C. E. (1958). Thorium-to-uranium ratios as indicators of sedimentary processes: example of concept of geochemical facies. *AAPG Bulletin*, *42*(2), 387-430.

48. McLennan, S. M., Nance, W. B., & Taylor, S. R. (1980). Rare earth element-thorium correlations in sedimentary rocks, and the composition of the continental crust. *Geochimica et Cosmochimica Acta*, *44*(11), 1833-1839.

49. Balaram, V., Rani, A., & Rathore, D. P. S. (2022). Uranium in groundwater in parts of India and world: A comprehensive review of sources, impact to the environment and human health, analytical techniques, and mitigation technologies. *Geosystems and geoenvironment*, *1*(2), 100043.

50. Water, S., & World Health Organization. (2000). WHO guidelines for drinking water quality: training pack.

51. Mohod, C. V., & Dhote, J. (2013). Review of heavy metals in drinking water and their effect on human health. *International journal of innovative research in science, engineering and technology*, *2*(7), 2992-2996.

52. Tchounwou, P. B., Yedjou, C. G., Patlolla, A. K., & Sutton, D. J. (2012). Heavy metal toxicity and the environment. *Molecular, clinical and environmental toxicology: volume 3: environmental toxicology*, 133-164.

53. He, Z. L., Yang, X. E., & Stoffella, P. J. (2005). Trace elements in agroecosystems and impacts on the environment. *Journal of trace elements in medicine and biology*, *19*(2-3), 125-140.

54. Ra, G. O. Y. (1991). Toxic effects of metals. *Casarett and Doull's toxicology.*

55. Shallari, S., Schwartz, C., Hasko, A., & Morel, J. L. (1998). Heavy metals in soils and plants of serpentine and industrial sites of Albania. *Science of the total environment*, *209*(2-3), 133-142.

56. Nriagu, J. O. (1989). A global assessment of natural sources of atmospheric trace metals. *Nature*, *338*(6210), 47-49.

57. Charles, M. (2001). UNSCEAR Report 2000: Sources and effects of ionizing radiation.

58. Asante, K. A., Agusa, T., Subramanian, A., Ansa-Asare, O. D., Biney, C. A., & Tanabe, S. (2007). Contamination status of arsenic and other trace elements in drinking water and residents from Tarkwa, a historic mining township in Ghana. *Chemosphere*, *66*(8), 1513-1522.

59. WHO (2022). Guidelines for drinking-water quality incorporating the first and second addenda. 4th Edition. WHO chronicle.

60. WHO. (2020). Chromium in drinking-water.

61. Clarke, R. H., & Valentin, J. (2009). The History of ICRP and the Evolution of its Policies: Invited by the Commission in October 2008. *Annals of the ICRP*, *39*(1), 75-110.

62. AERB (2004). Drinking water specifications in India.

63. https://www.aerb.gov.in/english/publications/codes-guides

64. Eisenberg, N. and McKone, T. E. (1998). Decision-Tree Method for the Classification of Chemical Carcinogens. *Environmental Health Perspectives*, 106(Suppl 6), 1425-1434.

65. Charles, M. (2010). Effects of Ionizing Radiation: United Nations Scientific Committee on the Effects of Atomic Radiation: UNSCEAR 2006 Report, Volume 1-*Report to the General Assembly, with Scientific Annexes A and B.*

66. Cotruvo, J. A. (2017). 2017 WHO guidelines for drinking water quality: first addendum to the fourth edition. *Journal-American Water Works Association*, *109*(7), 44-51.

67. ATSDR. U. S. (1997). Agency for toxic substances and disease registry. *Case studies in environmental medicine.*

68. Pavlakis, N., Pollock, C. A., McLean, G., & Bartrop, R. (1996). Deliberate overdose of uranium: toxicity and treatment. *Nephron*, *72*(2), 313-317.

69. Wade-Gueye, N. M., Delissen, O., Gourmelon, P., Aigueperse, J., Dublineau, I., & Souidi, M. (2012). Chronic exposure to natural uranium via drinking water affects bone in growing rats. *Biochimica et Biophysica Acta (BBA)-General subjects*, *1820*(7), 1121-1127.

70. Wang, S., Ran, Y., Lu, B., Li, J., Kuang, H., Gong, L., & Hao, Y. (2020). A review of uranium-induced reproductive toxicity. *Biological trace element research*, *196*, 204-213.

71. Chen, X. A., Cheng, Y. E., & Rong, Z. (2005). Recent results from a study of thorium lung burdens and health effects among miners in China. *Journal of radiological protection*, *25*(4), 451.

72. Strang, C., Cushman, S. J., DeRubeis, D., Peterson, D., & Pfaffinger, P. J. (2001). A central role for the T1 domain in voltage-gated potassium channel formation and function. *Journal of biological chemistry*, *276*(30), 28493-28502.

73. Wang, S., & Shi, X. (2001). Molecular mechanisms of metal toxicity and carcinogenesis. *Molecular and cellular biochemistry*, *222*, 3-9.

74. USEPA (1999). Draft guidelines for carcinogen risk assessment Washington Review Draft.

75. Rump, A., Hermann, C., Lamkowski, A., Popp, T., & Port, M. (2023). A comparison of the chemo-and radiotoxicity of thorium and uranium at different

enrichment grades. *Archives of toxicology*, *97*(6), 1577-1598.

76. Streffer, C., Bolt, H., Follesdal, D., Hall, P., Hengstler, J. G., Jacob, P., & Swaton, E. (2004). Low dose exposures in the environment: dose-effect relations and risk evaluation (Vol. 23). Springer Science & Business Media.

77. Kaufmann, R. F., Eadie, G. G., & Russell, C. R. (1976). Effects of uranium mining and milling on ground water in the Grants Mineral Belt, New Mexico. *Groundwater*, *14*(5), 296-308.

78. Mangini, A., Sonntag, C. H., Bertsch, G., & Müller, E. (1979). Evidence for a higher natural uranium content in world rivers. *Nature*, *278*(5702), 337-339.

79. White, A. F., Delany, J. M., Narasimhan, T. N., & Smith, A. (1984). Groundwater contamination from an inactive uranium mill tailings pile: 1. Application of a chemical mixing model. *Water resources research*, *20*(11), 1743-1752.

80. Orloff, K. G. *et al.* (2004). Human exposure to uranium in groundwater. *Environmental research*, *94*(3), 319-326.

81. Gregory, K. B., & Lovley, D. R. (2005). Remediation and recovery of uranium from contaminated subsurface environments with electrodes. *Environmental science & technology*, *39*(22), 8943-8947.

82. WHO (2004). Guidelines for drinking water quality (3rd ed.).

83. Almeida, R. M., Lauria, D. C., Ferreira, A. C., & Sracek, O. (2004). Groundwater radon, radium and uranium concentrations in Regiao dos Lagos, Rio de Janeiro State, Brazil. *Journal of environmental radioactivity*, *73*(3), 323-334.

84. Birke, M., Rauch, U., Lorenz, H., & Kringel, R. (2010). Distribution of uranium in German bottled and tap water. *Journal of geochemical exploration*, *107*(3), 272-282.

85. Wu, Y., Wang, Y., & Xie, X. (2014). Occurrence, behaviour and distribution of high levels of uranium in shallow groundwater at Datong basin, northern China. *Science of the total environment*, *472*, 809-817.

86. Zhang, B., Wang, X., Zhou, J., Han, Z., Liu, W., Liu, Q., & Dou, B. (2020). Regional geochemical survey of concealed sandstone-type uranium deposits using fine-grained soil and groundwater in the Erlian basin, north-east China. *Journal of geochemical exploration, 216*, 106573.

87. Landstetter, C., & Katzlberger, C. (2009). Determination of ^{3}H, ^{226}Ra, ^{222}Rn and ^{238}U in Austrian ground-and drinking water. *Journal of radioanalytical and nuclear chemistry*, *282*, 467-471.

88. Yamamoto, M., Tomita, J., Sakaguchi, A., Ohtsuka, Y., Hoshi, M., & Apsalikov, K. (2010). Uranium isotopes in well water samples as drinking sources in some settlements around the Semipalatinsk Nuclear Test Site, Kazakhstan. *Journal of radioanalytical and nuclear chemistry*, *284*(2), 309-314.

89. Ullah, H., Rehman, A., Ahmad, I., Khattak, N. U., Fozia, A., Ali, N., & Wasim, A. (2013). Estimation of uranium concentration in drinking water sources of

Tehsil Takht-e-Nasrati, District Karak, Khyber Pakhtunkhwa, Pakistan using fission track technique. *Journal of the chemical society of Pakistan*, *35*.

90. Ali, W., Aslam *et al.* (2019). Unraveling prevalence and public health risks of arsenic, uranium and co-occurring trace metals in groundwater along riverine ecosystem in Sindh and Punjab, Pakistan. *Environmental geochemistry and health*, *41*, 2223-2238.

91. Coyte, R. M., Jain, R. C., Srivastava, S. K., Sharma, K. C., Khalil, A., Ma, L., & Vengosh, A. (2018). Large-scale uranium contamination of groundwater resources in India. *Environmental science & technology letters*, *5*(6), 341-347.

92. Nolan, J., & Weber, K. A. (2015). Natural uranium contamination in major US aquifers linked to nitrate. *Environmental science & technology letters*, *2*(8), 215-220.

93. Fujii, R., & Swain, W. C. (1995). *Areal distribution of selected trace elements, salinity, and major ions in shallow ground water, Tulare Basin, southern San Joaquin Valley, California* (Vol. 95, No. 4048). US Department of the Interior, US Geological Survey.

94. Steffanowski J. and Banning A. (2017). Uraniferous dolomite: a natural source of high groundwater uranium concentrations in northern Bavaria, Germany. *Environmental earth sciences*, 76:1-11.

95. Zouridakis, N., Ochsenkühn, K. M., & Savidou, A. (2002). Determination of uranium and radon in potable water samples. *Journal of environmental radioactivity*, *61*(2), 225-232.

96. Seldén, A. I., Lundholm, C., Edlund, B., Högdahl, C., Ek, B. M., Bergström, B. E., & Ohlson, C. G. (2009). Nephrotoxicity of uranium in drinking water from private drilled wells. *Environmental research*, *109*(4), 486-494.

97. Nriagu, J., Johnson, J., Samurkas, C., Erdenechimeg, E., Ochir, C., & Chandaga, O. (2013). Co-occurrence of high levels of uranium, arsenic, and molybdenum in groundwater of Dornogobi, Mongolia. *Global health perspect*ives, *1*(1), 45-54.

98. Singh, P., Rana, N. P. S., Azam, A., Naqvi, A. H., & Srivastava, D. S. (1996). Levels of uranium in waters from some Indian cities determined by fission track analysis. *Radiation measurements*, *26*(5), 683-687.

99. Singh, S., Malhotra, R., Kumar, J., Singh, B., & Singh, L. (2001). Uranium analysis of geological samples, water and plants from Kulu Area, Himachal Pradesh, India. *Radiation measurements*, *34*(1-6), 427-431.

100. Rana, B., Tripathi, R., Sahoo, S., Sethy, N., Sribastav, V., Shukla, A., & Puranik, V. (2010). Assessment of natural uranium and ^{226}Ra concentration in ground water around the uranium mine at Narwapahar, Jharkhand, India and its radiological significance. *Journal of radioanalytical and nuclear chemistry*, *285*(3), 711-717.

101. Giri, S., Singh, G., & Jha, V. N. (2011). Evaluation of radionuclides in groundwater around proposed uranium mining sites in Bagjata and Banduhurang,

Jharkhand (India). *Radioprotection*, *46*(1), 39-57.

102. Coyte, R. M., Singh, A., Furst, K. E., Mitch, W. A., & Vengosh, A. (2019). Co-occurrence of geogenic and anthropogenic contaminants in groundwater from Rajasthan, India. *Science of the Total Environment*, 688, 1216-1227.

103. Richards, L. A., Kumar, A., Shankar, P., Gaurav, A., Ghosh, A., & Polya, D. A. (2020). Distribution and geochemical controls of arsenic and uranium in groundwater-derived drinking water in Bihar, India. *International journal of environmental research and public health*, *17*(7), 2500.

104. Sar, S. K., Diwan, V., Biswas, S., Singh, S., Sahu, M., Jindal, M. K., & Arora, A. (2018). Study of uranium level in groundwater of Balod district of Chhattisgarh state, India and assessment of health risk. *Human and ecological risk assessment: an international journal*, *24*(3), 691-698.

105. Rohit, M., Anamika, K. M., & Praveen, M. (2018). A comparative study of uranium concentration using two different analytical techniques and assessment of physicochemical parameters in groundwater. *Journal of radiation and nuclear applications*, *3*(3), 149.

106. Kumar, M. P., Nagalakshmi, K., Jayaraju, N., Prasad, T. L., & Lakshmanna, B. (2020). Deciphering water quality using WQI and GIS in Tummalapalle uranium mining area, Cuddapah Basin, India. *Water science*, *34*(1), 65-74.

107. Rani, A., Mehra, R., Duggal, V., & Balaram, V. (2013). Analysis of uranium concentration in drinking water samples using ICPMS. *Health physics*, *104*(3), 251-255.

108. Kumar, M. P., Prerna, S., Akash, K., & Prasad, M. K. (2015). Uranium in ground water of eastern Uttar Pradesh, India: a preliminary study. *International journal of scientific and engineering research*, *4*(6), 70-74.

109. Adithya, V. S., Chidambaram, S., Keesari, T., Mohokar, H. V., & Prasanna, M. V. (2019). Occurrence of uranium in groundwater along the lithological contacts in central Tamilnadu, India: an isotope hydrogeochemical perspective. *Exposure and health*, *11*, 277-290.

110. Brindha, K., Elango, L., & Nair, R. N. (2011). Spatial and temporal variation of uranium in a shallow weathered rock aquifer in southern India. *Journal of earth system science*, *120*, 911-920.

111. Keesari, T., Mohokar, H. V., Sahoo, B. K., & Mallesh, G. (2014). Assessment of environmental radioactive elements in groundwater in parts of Nalgonda district, Andhra Pradesh, South India using scintillation detection methods. *Journal of radioanalytical and nuclear chemistry*, *302*, 1391-1398.

112. Singh, J., Singh, L., & Singh, S. (1995). High U-contents observed in some drinking waters of Punjab, India. *Journal of environmental radioactivity*, *26*(3), 217-222.

113. Mehra, R., Singh, S., & Singh, K. (2007). Uranium studies in water samples belonging to Malwa region of Punjab, using track etching technique. *Radiation measurements*, *42*(3), 441-445.

114. Saini, K., Singh, P., & Bajwa, B. S. (2016). Comparative statistical analysis of carcinogenic and non-carcinogenic effects of uranium in groundwater samples from different regions of Punjab, India. *Applied radiation and isotopes*, *118*, 196-202.

115. Virk, H. S. (2023). A Study of Groundwater Contamination of Patiala District as a 'HOT SPOT' in Punjab. *Journal of water pollution & purification research*, *10*(1), 1-13p.

116. Bajwa, B. S., Kumar, S., Singh, S., Sahoo, S. K., & Tripathi, R. M. (2017). Uranium and other heavy toxic elements distribution in the drinking water samples of SW-Punjab, India. *Journal of radiation research and applied sciences*, *10*(1), 13-19.

117. Kumar, M., Singh, S., & Mahajan, R. K. (2006). Trace level determination of U, Zn, Cd, Pb and Cu in drinking water samples. *Environmental monitoring and assessment*, *112*, 283-292.

118. Sharma, N., & Singh, J. (2016). Radiological and chemical risk assessment due to high uranium contents observed in the ground waters of Mansa District (Malwa region) of Punjab state, India: an area of high cancer incidence. *Exposure and health*, *8*, 513-525.

119. Kochhar, N., Dadwal, V., & Balaram, V. (2012). Uranium in Malwa region of Punjab, India.

120. Patnaik, R *et al.* (2016). Study of uranium mobilization from Himalayan Siwaliks to the Malwa region of Punjab state in India. *Journal of radioanalytical and nuclear chemistry*, *308*, 913-918.

121. Phadke, A. V., Mahadevan, T. M., Narayan, D., & Saraswat, A. C. (1985). *Uranium mineralisation in some Phanerozoic sandstones in India* (No. IAEA-TECDOC--328).

122. Singh, L., Kumar, R., Kumar, S., Bajwa, B. S., & Singh, S. (2013). Health risk assessments due to uranium contamination of drinking water in Bathinda region, Punjab state, India. *Radioprotection*, *48*(2), 191-202.

123. Ali, H., Khan, E., & Ilahi, I. (2019). Environmental chemistry and ecotoxicology of hazardous heavy metals: environmental persistence, toxicity, and bioaccumulation. *Journal of chemistry*, *2019*.

124. Evanko, C. R., & Dzombak, D. A. (1997). *Remediation of metals-contaminated soils and groundwater* (pp. 5-13). Pittsburgh, PA, USA: Ground-water remediation technologies analysis center.

125. Shakeri, A., Moore, F., Mohammadi, Z., & Raeisi, E. (2009). Heavy metal contamination in the Shiraz industrial complex zone groundwater, South Shiraz, Iran. *World applied sciences journal*, *7*(4), 522-530.

126. Shakeri, A., Moore, F., Mohammadi, Z., & Raeisi, E. (2009). Heavy metal contamination in the Shiraz industrial complex zone groundwater, South Shiraz, Iran. *World applied sciences journal*, *7*(4), 522-530.

127. Wongsasuluk, P., Chotpantarat, S., Siriwong, W., & Robson, M. (2014). Heavy metal contamination and human health risk assessment in drinking water from shallow groundwater wells in an agricultural area in Ubon Ratchathani province, Thailand. *Environmental geochemistry and health*, *36*, 169-182.

128. Khalid, S. *et al.* (2020). Heavy metal contamination and exposure risk assessment via drinking groundwater in Vehari, Pakistan. *Environmental science and pollution research*, *27*, 39852-39864.

129. Boateng, T. K., Opoku, F., & Akoto, O. (2019). Heavy metal contamination assessment of groundwater quality: a case study of Oti landfill site, Kumasi. *Applied water science*, *9*(2), 33.

130. Deda, A., Alushllari, M., & Mico, S. (2019). Measurement of heavy metal concentrations in groundwater. In *AIP conference proceedings* (Vol. 2109, No. 1). AIP Publishing.

131. Nyambura, C., Hashim, N. O., Chege, M. W., Tokonami, S., & Omonya, F. W. (2020). Cancer and non-cancer health risks from carcinogenic heavy metal exposures in underground water from Kilimambogo, Kenya. *Groundwater for sustainable development, 10*, 100315.

132. Wagh, V. M., Panaskar, D. B., Mukate, S. V., Gaikwad, S. K., Muley, A. A., & Varade, A. M. (2018). Health risk assessment of heavy metal contamination in groundwater of Kadava River Basin, Nashik, India. *Modeling earth systems and environment*, *4*, 969-980.

133. Kumar, S., Toppo, S., Kumar, A., Tewari, G., Beck, A., Bachan, V., & Singh, T. B. N. (2022). Assessment of heavy metal pollution in groundwater of an industrial area: a case study from Ramgarh, Jharkhand, India. *International journal of environmental analytical chemistry*, *102*(18), 7290-7312.

134. Vetrimurugan, E., Brindha, K., Elango, L., & Ndwandwe, O. M. (2017). Human exposure risk to heavy metals through groundwater used for drinking in an intensively irrigated river delta. *Applied water science*, *7*, 3267-3280.

135. Sharma, R., & Dutta, A. (2017). A study of heavy metal pollution in groundwater of Malwa Region of Punjab, India: Current status, pollution and its potential health risk. *International journal of engineering research and applications*, *7*(3), 81-91.

136. Krishan, G. *et al.* (2021). Concentration of heavy metals in groundwater and heavy metal pollution index in Punjab. *The main sponsor of this issue: NABARD*.

137. Rajendran Selvakumar, R. S., Govindarajan Ramadoss, G. R., Menon, M. P., Karuppuli Rajendran, K. R., Palanisami Thavamani, P. T., Ravi Naidu, R. N., & Mallavarapu Megharaj, M. M. (2018). Challenges and complexities in remediation of uranium contaminated soils: a review.

138. Dent, D. L., MacMillan, R. A., Mayr, T. L., Chapman, W. K., & Berch, S. M. (2013). Use of airborne gamma radiometrics to infer soil properties for a forested area in British Columbia, Canada. *Journal of ecosystems and management*, *14*(1).

139. Beamish, D. (2013). Gamma ray attenuation in the soils of Northern Ireland, with special reference to peat. *Journal of environmental radioactivity*, *115*, 13-27.

140. Snezana Dragovi, Bosko Gaji, Ranko Dragovi, Ljiljana Jankovi-Mandi, Latinka Slavkovi-Beskoski, Nevena Mihailovi, Milan Mom ilovi, and Mirjana Cuji (2012). Edaphic factors affecting the vertical distribution of radionuclides in the different soil types of Belgrade, Serbia. *Journal of environmental monitoring*,14(1):127–137.

141. Jananee, B., Rajalakshmi, A., Thangam, V., Bharath, K. M., & Sathish, V. (2021). Natural radioactivity in soils of Elephant hills, Tamilnadu, India. *Journal of radioanalytical and nuclear chemistry*, *329*, 1261-1268.

142. Külahcı, F., Aközcan, S., & Günay, O. (2020). Monte Carlo simulations and forecasting of Radium-226, Thorium-232, and Potassium-40 radioactivity concentrations. *Journal of radioanalytical and nuclear chemistry*, *324*, 55-70.

143. Duong, N. T., Van Hao, D., Duong, D. T., Phan, T. T., & Le Xuan, H. (2021). Natural radionuclides and assessment of radiological hazards in MuongHum, Lao Cai, Vietnam. *Chemosphere*, *270*, 128671.

144. Saueia, C. H. R., & Mazzilli, B. P. (2006). Distribution of natural radionuclides in the production and use of phosphate fertilizers in Brazil. *Journal of environmental radioactivity*, *89*(3), 229-239.

145. Martin, A. *et al.* (2020). An integrated approach combining soil profile, records and tree ring analysis to identify the origin of environmental contamination in a former uranium mine (Rophin, France). *Science of the total environment*, *747*, 141295.

146. Mitchell, N., Pérez-Sánchez, D., & Thorne, M. C. (2013). A review of the behaviour of U-238 series radionuclides in soils and plants. *Journal of radiological protection*, *33*(2), R17.

147. Castilhos, Z. C., Alamino, R. C. J., Cesar, R. G., Ribeiro-Duthie, A. C., Schneider, C. L., & Souza, E. F. (2018). Treatment of Coal Mining Tailings to Reduce the Leaching of Metals including Uranium and Thorium. In *Naturally Occurring Radioactive Material (NORM VIII). Proceedings of an international symposium.*

148. Bister, S. *et al.* (2015). Impact of former uranium mining activities on the floodplains of the Mulde River, Saxony, Germany. *Journal of environmental radioactivity*, *144*, 21-31.

149. Muñoz, D. R. *et al.* (2017). Analysing the effect of land use and vegetation cover on soil infiltration in three contrasting environments in northeast Spain. *Cuadernos de investigación geográfica: Geographical research letters*, *43*(1), 141-169.

150. Laubenstein, M. *et al.* (2013). Radionuclide mapping of the Molise region (Central Italy) via gamma-ray spectrometry of soil samples: relationship with geological and pedological parameters. *Journal of radioanalytical and nuclear chemistry*, *298*, 317-323.

151. Abbasi, A., Kurnaz, A., Turhan, Ş., & Mirekhtiary, F. (2020). Radiation hazards and natural radioactivity levels in surface soil samples from dwelling areas of North Cyprus. *Journal of radioanalytical and nuclear chemistry, 324*, 203-210.

152. Najam, L. A., Younis, S. A., & Kithah, F. H. (2015). Natural radioactivity in soil samples in Nineveh Province and the associated radiation hazards. *International journal of physics*, 3(3), 126-132.

153. Singh, S., Singh, B., & Kumar, A. (2003). Natural radioactivity measurements in soil samples from Hamirpur district, Himachal Pradesh, India. *Radiation measurements*, *36*(1-6), 547-549.

154. Srinivasa, E., Rangaswamy, D. R., Suresh, S., & Sannappa, J. (2022). Natural radioactivity levels and associated radiation hazards in soil samples of Chikkamagaluru district, Karnataka, India. *Journal of radioanalytical and nuclear chemistry*, 1-8.

155. Sivakumar, R. (2014). An assessment of natural radioactivity levels and radiation hazards in the soil of Coonoor, South India. *Environmental earth sciences*, *72*, 5063-5071.

156. Panghal, A., Kumar, A., Kumar, S., Singh, J., Singh, P., & Bajwa, B. S. (2018). Estimation of natural radionuclides and exhalation rate in surface soils of four districts of Haryana, India. *Journal of the geological society of India*, *92*, 695-703.

157. Devi, V., Kumar, A., & Chauhan, R. P. (2019, August). Radiation doses due to background radioactivity in soil from inhabited area of Northern Haryana. *In AIP Conference Proceedings* (Vol. 2142, No. 1). AIP Publishing.

158. Mittal, S., Rani, A., Mehra, R., & Ramola, R. C. (2018). Estimation of natural radionuclides in the soil samples and its radiological impact on human health. *Radiation effects and defects in solids*, 173(7-8), 673-682.

159. Narayana, Y., Somashekarappa, H. M., Karunakara, N., Avadhani, D. N., Mahesh, H. M., & Siddappa, K. (2001). Natural radioactivity in the soil samples of coastal Karnataka of South India. *Health physics*, 80(1), 24-33.

160. Srinivasa, E., Rangaswamy, D. R., Suresh, S., & Sannappa, J. (2022). Natural radioactivity levels and associated radiation hazards in soil samples of Chikkamagaluru district, Karnataka, India. *Journal of radioanalytical and nuclear chemistry*, 1-8.

161. Singh, S., Kumar, M., & Mahajan, R. K. (2005). The study of indoor radon in dwellings of Bathinda district, Punjab, India and its correlation with uranium and radon exhalation rate in soil. *Radiation measurements*, *39*(5), 535-542.

162. Badhan K, Mehra R (2012). Primordial radioactivity (^{238}U, ^{232}Th and ^{40}K) measurements for soils of Ludhiana district of Punjab, India. *Radiation protection dosimetry* 152(1–3):29–32.

163. Kaintura, S. S., Thakur, S., Kaur, S., Devi, S., Tiwari, K., Sharma, A., & Singh, P. P. (2024). Investigating radioactivity in soil samples from neutral

and vegetation land of Punjab/India.

164. Samavat, H., Seaward, M. R. D., Aghamiri, S. M. R., & Reza-Nejad, F. (2006). Radionuclide concentrations in the diet of residents in a high level natural radiation area in Iran. *Radiation and environmental biophysics*, *45*, 301-306.

165. Yadav, P., Garg, V. K., Singh, B., Pulhani, V., & Mor, S. (2018). Transfer factors and effective dose evaluation due to natural radioactivity in staple food grains from the vicinity of proposed nuclear power plant. *Exposure and health*, *10*, 27-39.

166. Pulhani, V. A., Dafauti, S., Hegde, A. G., Sharma, R. M., & Mishra, U. C. (2005). Uptake and distribution of natural radioactivity in wheat plants from soil. *Journal of environmental radioactivity*, *79*(3), 331-346.

167. Tufail, M., Akhtar, N., & Akhter, J. (2010). Assessment of annual effective dose from natural radioactivity intake through wheat grain produced in Faisalabad, Pakistan. *Journal of radioanalytical and nuclear chemistry*, *283*, 585-590.

168. Akhtar, N., & Tufail, M. (2007). Natural radioactivity intake into wheat grown on fertilized farms in two districts of Pakistan. *Radiation protection dosimetry*, *123*(1), 103-112.

169. Bilgici Cengiz (eker), G., Çağlar, İ., & Çağlar, A. (2020). Determination of transfer factors of natural radionuclides from soil-to-wheat flour consumed by Kars people. *Caucasian journal of science*, 7(2), 140-152.

170. Alharbi, A., & El-Taher, A. (2013). A study on transfer factors of radionuclides from soil to plant. *Life science journal*, *10*(2), 532-539.

171. Mostafa, A. M. A., Uosif, M. A. M., Elsaman, R., & Moustafa, E. (2016). Transfer factors of radionuclides from soil to wheat grains. *International journal of scientific and engineering research, 7*(2), 642-644.

172. Pourimani, R., & Shahroodi, S. M. M. (2018). Radiological assessment of the artificial and natural radionuclide concentrations of wheat and barley samples in Karbala, Iraq. *Iranian Journal of medical physics, 15(2)*, 126-31.

173. Alharbi, A., & El-Taher, A. (2013). A study on transfer factors of radionuclides from soil to plant. *Life science journal, 10(2)*, 532-539.

174. Mheemeed, A. K., Najam, L. A., & Hussein, A. K. (2014). Transfer factors of ^{40}K, ^{226}Ra, ^{232}Th from soil to different types of local vegetables, radiation hazard indices and their annual doses. *Journal of radioanalytical and nuclear chemistry, 302,* 87-96.

175. Van, H. D., Nguyen, T. D., Peka, A., Hegedus, M., Csordas, A., & Kovacs, T. (2020). Study of soil to plant transfer factors of ^{226}Ra, ^{232}Th, ^{40}K and ^{137}Cs in Vietnamese crops. Journal of environmental radioactivity, 223, 106416.

176. Lindahl, P., Maquet, A., Hult, M., Gasparro, J., Marissens, G., & De Orduna, R. G. (2011). Natural radioactivity in winter wheat from organic and conventional agricultural systems. *Journal of environmental radioactivity*, *102*(2), 163-169.

177. Paiva, A. K., Pereira, W. S., Lopes, J. M., Silva, L. B., Carmo, A. S., Tarre, R. M. & Silva, A. X. (2022). Intake of natural radionuclides present in organic and conventional foods: radiological aspects. *Journal of radioanalytical and nuclear chemistry,* 331(2), 903-911.

178. Bakım, M., & Görgün, A. U. (2015). Radioactivity in soils and some terrestrial foodstuffs from organic and conventional farming areas in Izmir, Turkey. *Journal of radioanalytical and nuclear chemistry*, *306*, 237-242.

179. Rizvi, A., Zaidi, A., Ameen, F., Ahmed, B., AlKahtani, M. D., & Khan, M. S. (2020). Heavy metal induced stress on wheat: phytotoxicity and microbiological management. *Royal society of chemistry advances*, *10*(63), 38379-38403.

180. Al-Othman, Z. A., Ali, R., Al-Othman, A. M., Ali, J., & Habila, M. A. (2016). Assessment of toxic metals in wheat crops grown on selected soils, irrigated by different water sources. *Arabian Journal of Chemistry*, *9*, S1555-S1562.

181. Rees, F., Sterckeman, T., & Morel, J. L. (2016). Root development of non-accumulating and hyperaccumulating plants in metal-contaminated soils amended with biochar. *Chemosphere*, *142*, 48-55.

182. Fryzova, R., Pohanka, M., Martinkova, P., Cihlarova, H., Brtnicky, M., Hladky, J., & Kynicky, J. (2018). Oxidative stress and heavy metals in plants. *Reviews of environmental contamination and toxicology volume 245*, 129-156.

183. Wang ShiYu, W. S., Wu WenYong, W. W., Liu Fei, L. F., Liao RenKuan, L. R., & Hu YaQi, H. Y. (2017). Accumulation of heavy metals in soil-crop systems: a review for wheat and corn.

184. Huang, M., Zhou, S., Sun, B., & Zhao, Q. (2008). Heavy metals in wheat grain: assessment of potential health risk for inhabitants in Kunshan, China. *Science of the total environment*, *405*(1-3), 54-61.

185. Bermudez, G. M., Jasan, R., Plá, R., & Pignata, M. L. (2011). Heavy metal and trace element concentrations in wheat grains: assessment of potential non-carcinogenic health hazard through their consumption. *Journal of hazardous materials*, *193*, 264-271.

186. Thabit, T. M., Shokr, S. A., Elgeddawy, D. I., & El-Naggar, M. A. (2020). Determination of heavy metals in wheat and barley grains using ICP-MS/MS. *Journal of AOAC international*, *103*(5), 1277-1281.

187. Groundwater management circle water resources department (2022). Groundwater resources of Punjab state, SAS Nagar, Mohali.

188. CGWB (2013). Ministry of Jal Shakti. Groundwater information booklet, Mansa district, Punjab.

189. Krishan, G., & Chopra, R. P. S. (2015). Assessment of water logging in south-western (SW) parts of Punjab, India–a case study from Muktsar district. *ND-CWWC Journal (A half yearly journal of New Delhi Centre of WWC)*, *4*(1), 7-10.

190. Handl, G. (2012). Declaration of the United Nations conference on the human environment (Stockholm Declaration), 1972 and the Rio Declaration on

Environment and Development, 1992. *United Nations audiovisual library of international law*, *11*(6), 1-11.

191. FICCI (2022). Call for action: Making cancer care more accessible and affordable in India. FICCI, Government of India.

192. Blaurock-Busch, E., Busch, Y. M., Friedle, A., Buerner, H., Parkash, C., & Kaur, A. (2015). Comparing the metal concentration in the nails of healthy and cancer patients living in the Malwa region of Punjab, India with a random European group-a follow up study. *British journal of medicine and medical research*, *5*(4), 480.

193. Shrivastava, B. K. (2015). Elevated uranium and toxic elements concentration in groundwater in Punjab state of India: extent of the problem and risk due to consumption of unsafe drinking water. *Water quality, exposure and health*, *7*(3), 407-421.

194. Bjørklund, G., Semenova, Y., Pivina, L., Dadar, M., Rahman, M. M., Aaseth, J., & Chirumbolo, S. (2020). Uranium in drinking water: a public health threat. *Archives of toxicology*, *94*, 1551-1560.

195. Hindustan Times, *Water in 29% wells in Punjab has uranium concentration*

196. The Hindu, *Groundwater contaminated, Punjab battles uranium curse*

197. CGWB (2023). National Ccmpilation on dynamic groundwater resources of India. Ministry of Jal Shakti, Government of India.

Chapter 2

Instrumentation and methodology

This chapter commences with a description of the sampling procedure in section 2.1 and the methods employed for sample preparation. It focuses on the apparatuses and experimental methodologies used in the current investigation to examine the levels of natural radioactivity in water, soil and food within the study area. Moreover, the heavy metal measurements are also performed for water and food samples and the respective methodology is also discussed.

Environmental monitoring is the utilisation of methods and strategies to identify, examine and characterise environmental elements in order to evaluate and understand the effects of different activities on the environment. Throughout the years, a multitude of sophisticated techniques have been developed to precisely assess the concentration of pollutants in various environments. Accurate identification and thorough examination of environmental pollutants are essential when employing measurement methods to evaluate the contamination in any region.

2.1 Sampling procedure

The Mansa district was chosen as the study area. The grids were made using the QGIS 3.10 Hannover.

2.1.1 Water samples

For collection of water samples, the bottles were acid-leached and then double cleaned with de-ionized water before sample collection. The water from the source was pumped out for a period of seven to ten minutes to ensure that a fresh sample was obtained. The hermetically sealed polypropylene containers with a capacity of 500 ml were used. The water samples were passed through filter paper of 0.45 μm to eliminate undesired contaminants prior to examination in Radiation Monitoring and Assessment laboratory at Dr. B.R. Ambedkar National Institute of Technology, Jalandhar. The uranium contamination was measured using LED fluorimeter (Quantalase) and the heavy metals were measured using atomic absorption spectrophotometer, AAS-7000 (Shidmazu). The sampling points were chosen from a grid of 5 km $\times$ 5 km as shown in figure 2.1 [1].

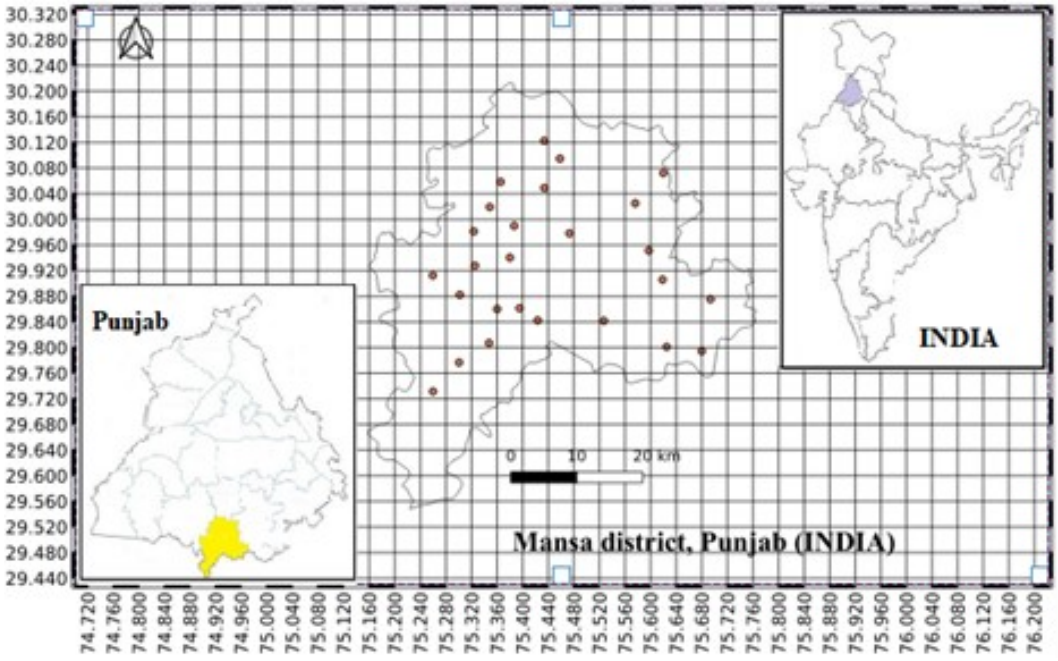

Figure 2.1: Map of Mansa district, Punjab showing locations from where water samples were collected [1].

2.1.2 Soil samples

The top layer of plants and roots was removed down to a depth of 5 cm before collecting each sample of soil. The soil samples were obtained from agricultural fields using a shovel. The entire sample was then mixed thoroughly, and an aliquot of approximately 2 kg was obtained and sealed in polythene bags from locations shown in figure 2.2. Ultimately, the samples were meticulously blended, and any superfluous substances such as vegetation, detritus, large stones, and pebbles were removed. The obtained samples were desiccated in direct sunlight for approximately two days till the soil's moisture was totally eradicated and were oven dried at 110 °C. The samples were sieved with a mesh size of 0.25 mm to ensure that every sample was well mixed. The samples were placed inside plastic containers and securely sealed. They were then labelled with codes according to their respective locations. Prior to taking measurements, the samples were stored at an ambient temperature for a period of about a month with the aim of achieving a state of equilibrium for the ^{238}U and ^{232}Th series along with their corresponding progenies [2].

2.1.3 Food samples

The wheat grains were collected from the fields, locations are shown in figure 2.2 and then labelled and transported into a plastic bag. In order to provide a representative sample from each location, six spots were chosen from each wheat plantation field. The size of each spot was 2m × 2m. Subsequently, the samples were carefully cleansed of roots, leaves, and any other form of residue [3]. For radiological analysis, the weight of the freshly obtained wheat grain samples was recorded. The grain samples were dried in an oven set to a temperature of 110°C for a duration of 24 hours. or until a constant weight was reached. The weights of the dried samples were then

recorded. Subsequently, the materials were pulverised using a powder grinder and filtered through a 1 mm sieve to get uniformly mixed samples [3]. Before conducting the measurements, the samples were maintained at an ambient temperature for approximately one month to allow the ^{238}U and ^{232}Th series to reach equilibrium.

For heavy metal analysis, the food samples were wet-digested for decomposition. A food sample weighing 0.5 g was measured and placed into a teflon beaker. Further, a mixture of 4 mL of 65% concentration HNO_3 and 2 mL of 30% concentration H_2O_2 was added to the sample. The mixture was left overnight under laboratory conditions to break down organic components and minimise carbonaceous residues. The wet digestion method was carried out by heating the sample solution on a hot plate in a fume closet at a temperature of 120-140 °C. This process involved vaporising excess acids until the solution's volume was decreased to 2 mL followed by cooling it to room temperature. Further, each solution was filtered using Whatman No. 42 filter paper and subsequently transferred into a 30 mL volumetric flask. The resulting sample was then diluted with approx. 28 mL deionized water [4].

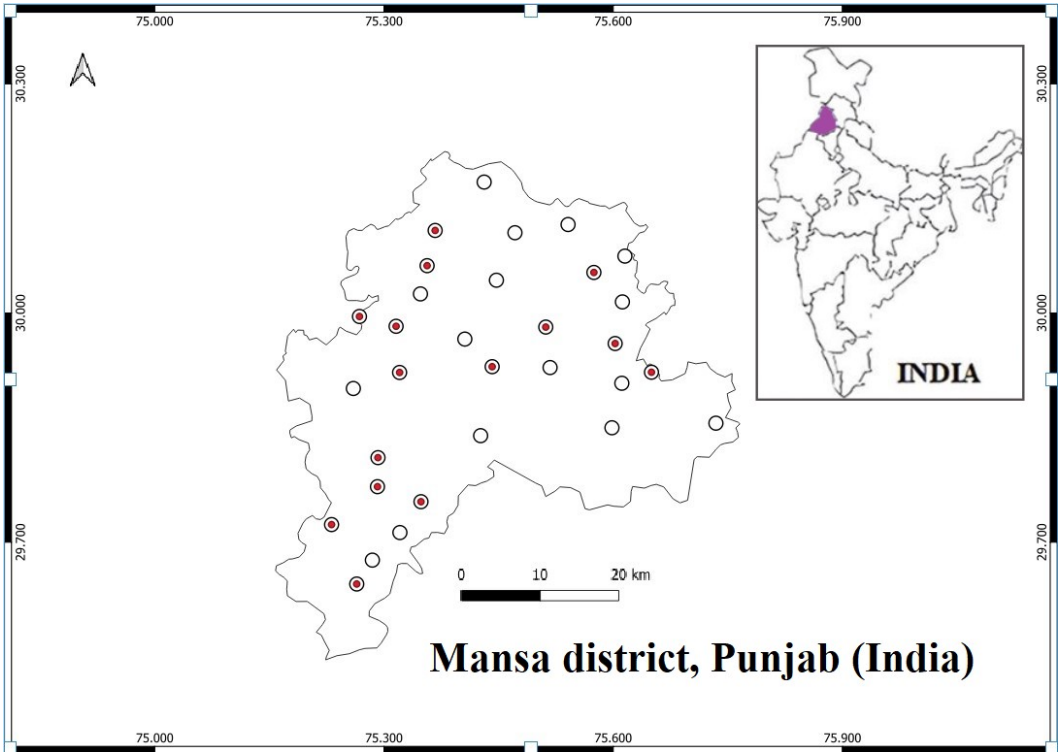

Figure 2.2: Map of Mansa district, Punjab showing locations from where soil (circled) and food (red dots) samples were collected.

2.2 Instrumentation

2.2.1 Measurement of uranium concentration in groundwater - LED flourimeter

Multiple analytical approaches can be employed to ascertain the concentration of uranium in water samples. The methodologies can be classified into two distinct

groups, namely, non-radiometric and radiometric methods. Radiometric methods refer to techniques that involve the measurement of radioactive decay specifically related to uranium. Some examples of techniques used in this field are alpha spectroscopy, gamma spectrometry, etc. Radiometric techniques have exceptional sensitivity and are capable of quantifying minute quantities of uranium. The non - radiometric approaches do not require the detection of radioactive decay. Some examples of analytical techniques are inductively coupled plasma mass spectrometry, (ICP-MS), atomic absorption spectrophotometer (AAS), kinetic phosphorescence analysis (KPA), and laser fluorimetry. Non-radiometric approaches are typically less hazardous and can be more efficient than radiometric procedures [5]. Nevertheless, it is crucial to acknowledge that the use of radiometric or non-radiometric procedures relies on the particular requirements and availability of the experimental setup.

The current research employed a pulsed LED fluorimeter, a highly sensitive technique, by Quantalase, Indore for measuring the concentration of uranium in water samples, as shown in figure 2.3 [6]. The quantification of green fluorescence emitted by uranium compounds is a widely recognised technique for determining the concentration of uranium in water samples [7]. The excitation spectra of uranium compounds often exhibit large peaks at wavelengths of 250 nm, 330 nm and 405 nm. The emission spectrum has prominent peaks at approximately 480 nm, 520 nm and 540 nm. The fluorimeter is capable of quantifying uranium concentrations ranging from 0.5 parts per billion (ppb) to 1000 ppb, achieving an accuracy level of 10%.

Figure 2.3: A photograph of LED fluorimeter by Quantalase, Indore [6].

The instrument relies on the Stokes fluorescence of a uranyl complex that results from fluran, a buffer in an aqueous sample. When the incident UV light lacks sufficient energy to dislodge electrons from atoms, the electrons transition to higher states. As a result of the relatively short life time of excited states, the electrons revert back to the ground state or lower states and release energy.

The instrument consists of

1. LED - The fluorimeter employs arrays of pulsed LEDs to stimulate fluorescence in the sample being examined. The LED output can be adjusted to align with the excitation specifications of the sample by modifying the wavelength, pulse duration and peak power.

2. Detection unit - It comprises of the photomultiplier tube (PMT) along with the cuvette chamber. The PMT is positioned in close proximity to the sample holder in order to gather fluorescence emitted by the sample. A cuvette chamber is a receptacle where a cuvette, which holds a sample, is placed. The PMT is deactivated when the chamber lid is in the open position.
3. Filters - Appropriate filters positioned between the LEDs and the photomultiplier tube serve to block the direct transmission of LED light to the PMT.
4. Microcontroller - The device is operated by a microcontroller that sends pulses to the LEDs and PMT. The microcontroller also governs the ADC, which transforms the fluorescence signal from the photomultiplier into a digital format for subsequent processing.
5. Other components - A single board computer is used for calculating and averaging the output of a photomultiplier across 2000 pulses.

There are three ways of measurement: the "Standard Addition Mode," commonly known as the spiking mode, "Uncalibrated Fluorescence Mode" which is frequently referred to as count mode in addition to "Calibrated Fluorescence Mode". The Standard Addition Mode is a self-calibrating feature that does not require any additional calibration. Additionally, it takes into consideration the phenomenon of fluorescence quenching that arises due to the existence of other compounds in the sample. Therefore, when there is suspicion of the presence of compounds that cause fluorescence quenching, it is recommended to use this method of testing. The equipment undergoes calibration in Calibrated Fluorescence Mode by quantifying the fluorescence emitted by established standard solutions. When conducting measurements on samples with unknown uranium concentrations, the device uses the previously determined calibration factor to determine and display the uranium level in the sample. The Uncalibrated Fluorescence Measurement Mode solely presents the fluorescence emitted by the sample, which is directly proportional to the amount of uranium present in the sample. It is frequently employed to do a high-throughput analysis of numerous samples in order to detect any instances of abnormally intense fluorescence. The uranium concentration in such samples can subsequently be ascertained using either of the remaining two methods.

Working – The prepared sample solution is contained in a cuvette, a small, transparent vessel made of quartz. Quartz cuvettes are used due to their transparency to ultraviolet light, which is commonly employed for fluorescence excitation. The cuvette, once filled with the sample, is positioned within the sample holder of the LED fluorimeter. The uranium complexes generate green fluorescence when stimulated by a pulsed UV light source (400 nm). This fluorescence is detected by a sensitive PMT to measure the concentration of uranium in water. The fluorescence is directly proportional to the intensity of the source excitation, which is in turn proportionate to the uranium concentration in the sample. A fluorescent uranyl species U(VI) is produced by combining 5 gm of sodium pyrophosphate, a buffered inorganic complexing agent, with 100 ml of distilled water and ortho-phosphoric acid known as fluran. This mixture helps to maintain a pH of 7. The dependence of fluorescence intensification on pH is crucial. By appropriately timing the activation of PMT and using optical filters that only allow longer wavelengths to get through,

it is possible to completely eliminate fluorescence emitted by organic substances.

The Beer-Lambert law, which is applied to the quantitative analysis of fluorescent compounds is as follow-

$$F_l = \phi I \varepsilon c l \tag{2.1}$$

where F_l is the intensity of fluorescence measured by the instrument, ϕ is the ratio of the number of photons emitted to the number of photons absorbed, I is the intensity of incident light, ε is the extinction coefficient in L $mol^{-1}cm^{-1}$, c and l are concentration of the sample in mol L^{-1} and length of the optical path in cm, respectively.

The reference material used is Accustandard's ICP-MS-66N-0.01X-1 (100 μg mL^{-1}). The calibration factor is determined by dividing the concentration of uranium in the standard solution by the difference in fluorescence between the standard and the water. To calibrate the device, 1 litre of water and 1 mL of HNO_3 with 1.78 gm of uranyl acetate dehydrate are mixed. For each analysis, a solution consisting of 10% fluran and 6 mL of water sample is prepared. The blank solution is utilised to calibrate the instrument by combining 1 part of buffer solution with 10 parts of double distilled water, resulting in a sample with no detectable uranium concentration. The quality assurance is conducted through the use of replication analysis and spike recovery.

2.2.2 Measurement of natural radionuclides in soil and food samples - gamma spectroscopy

The analysis of gamma ray spectra commences with an in-depth understanding of decay mechanisms of radionuclides. This approach has an advantage for radionuclide monitoring as it allows for the concurrent analysis of multiple radionuclides, often requiring minimal to no sample preparation [8].

2.2.2.1 Interaction of gamma rays with matter

Gamma rays can interact with matter through three main processes: photoelectric effect, Compton scattering and pair production. The significance of these three effects varies depending on the energy level of the incident photon ($h\nu_o$) and the atomic number (Z) of the impacted nucleus [9].

Photoelectric effect - The photoelectric effect is a prevalent occurrence at low energies, as shown in figure 2.4 [10]. A photon transfers its entire energy to an electron bound in a specific energy level. The energy of each individual photon must be greater than the binding energy of an electron for the photoelectric effect to occur. A part of incident photon energy is used to unbound the electron, and the remaining energy appears as the kinetic energy of the electron. The photoelectric effect primarily takes place in the inner electron shells of the atom, particularly in the K-electron shell. When an electron ejects from an inner atomic shell, electrons from outer shells migrate to inner electron shells in order to occupy the resultant vacancy. The shifts in electron energy levels necessitate the emission of energy by the atomic electrons, resulting in the generation of soft (low-energy) X-rays.

Compton effect - The photon relinquishes a portion of its energy to the electrons, leading to a reduction in its frequency. This typically involves the valence electrons. Nevertheless, the redirected photon persists in its trajectory through matter until it exhausts all of its kinetic energy through its interaction with other electrons in a comparable manner. The cross-sectional area for this phenomenon diminishes as the energy increases, however, the rate of decrease is slower compared to the photoelectric effect [11].

Pair production - At energies greater than 1.022 MeV, pair production takes place. When the photon approaches the atomic nucleus, it encounters the potent field of the nucleus. At this point, the photon is converted into electron-positron pairs. These electrons possess kinetic energies that are equivalent to $h\nu$ - $2m_oc^2$. The cross-section of this phenomenon exhibits a positive correlation with energy. The P/Z (where P is the cross-section and Z is the atomic number) ratio remains constant with energy up to 10 MeV. As the energy is increased further, the cross section decreases [12].

2.2.2.2 Gamma spectroscopy using NaI(Tl) detector

Gamma spectrometry, a direct and non-destructive technique, is used to identify and quantify gamma-emitting radioactive substances in food, soil etc, by analysing the energy distribution of the released gamma rays. The crystals of sodium iodide

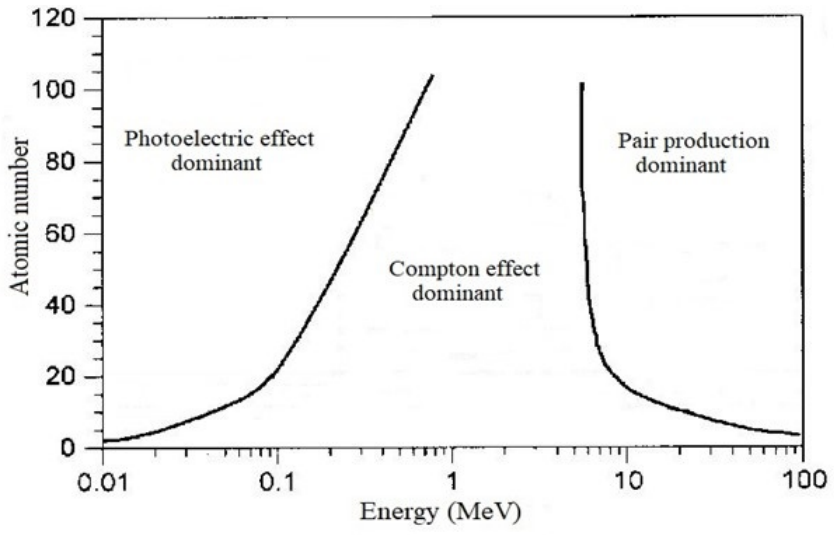

Figure 2.4: Interaction of gamma rays with matter [10]. The photoelectric effect prevails at lower energy levels, the Compton effect at intermediate gamma ray energies and pair production is predominant at higher gamma ray energies.

are commonly employed as scintillation material for gamma-ray spectroscopy. A thallium doped sodium iodide detector of 63 mm×63 mm AT1315 by Atomtex, Belarus detecting gamma radiation in the 50-3000 keV energy range is used for detecting natural radionuclides and a picture is shown in figure 2.5 [13]. It can operate at room temperature and has the highest output among scintillation detectors. One drawback of the few inorganic crystals, such as NaI (Tl), is their hygroscopic nature, which necessitates storing them in a hermetically sealed container to shield them from moisture.

The components of the instrument consist of -

1. Sodium iodide crystal - It is typically doped with a minute quantity of thallium. Thallium doping increases the light output and shifts the emission wavelength to approximately 415 nm, aligning well with the sensitivity of photomultiplier tubes (PMTs). When incoming gamma or X-ray photons interact with the crystal, it results in fluorescence, which generates a brief burst of light for each absorbed photon. The magnitude of the light pulse is directly proportional to the energy of the incident photon.

2. Photocathode - A photocathode is a slender film on a transparent substrate (quartz) that photons encounter after traversing the crystal. An electron is expelled as a result of the photons' interaction with the photocathode. The different types of materials used for making photocathode are bi-alkali like Cs-K-Sb, multi-alkali like Na-K-Cs-Sb and gallium arsenide.

3. Photomultiplier tube - The photomultiplier tube, which can be cylindrical or rectangular in shape, is situated immediately after the photocathode, as shown in figure 2.6 [14]. It is made up of a series of metal cups with voltage applied to each of them. This voltage accelerates the expelled electron, which in turn causes more electrons to be knocked loose and accelerate as well. The signal is amplified by repeating this process. They are shielded to protect the electron trajectories inside the tube from being influenced by external fields.

4. Signal Processing - The preamplifier is placed after the photomultiplier tube to optimise the signal and is also connected to the amplifier. The output pulses are converted into a digital number using an Analog to Digital Converter (ADC) that is integrated into a Multichannel Analyzer (MCA). The MCA is utilised for the purpose of capturing and preserving data, which is subsequently used for the analysis of pulse height distribution.

Figure 2.5: A photograph of the sodium iodide detector by Atomtex, Belarus [13].

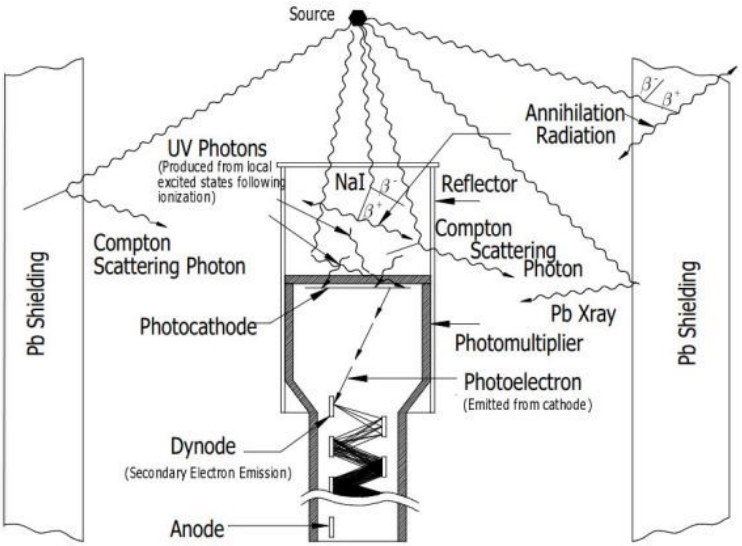

Figure 2.6: Schematic representation of a thallium doped sodium iodide detector [14]. The NaI(Tl) crystal which is surrounded by lead shielding designed to prevent interference from extraneous radiation. When gamma rays penetrate the detector, a fraction of them leads to the emission of photoelectrons within the crystal. The scintillation light generated from these interactions is then channelled to the photocathode of a PMT. The PMT is equipped with several dynodes, each serving to amplify the signal prior to its final conversion into an electrical pulse.

Working - The operational mechanism of a scintillation detector entails the conversion of the energy from incident radiation into optical energy using a scintillator. This process results in the production of flashes with different intensities [15]. The scintillation phenomenon in inorganic materials relies on the energy states dictated by the crystal lattice of the substance. Semiconductors or insulators are materials in which electrons possess only discrete energy bands. The valence band refers to the lower energy band in which electrons are tightly bound to lattice sites, whereas the conduction band have electrons that possess enough energy to freely move across the crystal [9]. The presence of thallium impurities generates electron orbitals between the conduction and valence bands, which are referred to as activation centers as shown in figure 2.7 [16]. In the ground state, both the valence band and the ground state of each activation center are occupied by electrons. Conversely, the conduction band and the excited energy levels of the activation centers remain unoccupied. As a result, without radiation, no electron movement occurs. When a gamma ray enters the crystal, one or more secondary electrons with elevated kinetic energy are produced. As these electrons traverse the material, they induce ionizations and excitations, resulting in the production of numerous low-energy electrons that also possess high kinetic energy which in turn generate additional low-energy electrons. While the majority of these low-energy electrons dissipate their energy as thermal energy, a subset possesses sufficient energy to transit to the conduction band. Each electron that is excited to the conduction band leaves behind a vacancy, or a hole in the valence band. The electrons that migrate into the conduction band are free to move within the crystal lattice; however, they are restricted from directly returning to the

valence band. Instead, they try to return to the lowest available energy levels, which correspond to the excitation states of activation centers. Meanwhile, the presence of holes allows electrons to move within the valence band, eventually leading to their filling by electrons from the activation centers, which creates vacancies in the ground state orbitals of these centers. When an electron fills a hole, it releases excess energy as a scintillation photon [16].

The gamma ray photon emitted during the radioactive decay of the nucleus interacts in the detector in various ways, leading to a complex detector response that is characterised by a continuous distribution of energy and distinct peaks at specific energy levels. The continuous energy distribution results from the incomplete absorption of energy of photon within the detector volume, causing the photon to exit the detector. The presence of complete energy peaks is a consequence of the complete absorption of gamma ray photons by the detector, either through the photoelectric effect or through multiple interactions. Due to the variability in the number of electrons, a photo-peak is created instead of a sharp line.

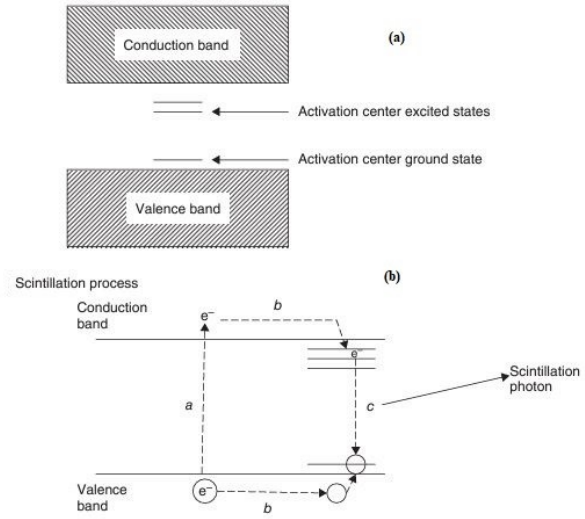

Figure 2.7: The figure (a) shows the activation centers between valence and conduction bands. Figure (b) shows scintillation mechanism: First, some of the free electrons generated by the interaction with gamma rays possess sufficient energy to overcome the energy gap and enter the conduction band. Second, these electrons, now within the conduction band, move towards the excited-state orbitals of the activation centers, while the holes in the valence band transition to the ground-state orbitals of the activation centers. Finally, the emission of a scintillation photon occurs when an electron transitions from an excited-state orbital of the activation center to its ground-state orbital [16].

Calibration of the detector - The energy scale stabilization of the gamma radiation line with the energy of 661.6 keV from the reference source of ^{137}Cs, 1170 keV and 1330 keV from ^{60}Co were carried out. The efficiency calibration was performed by using the standard set by IAEA of ^{238}U, ^{232}Th and ^{40}K i.e. RG-U, RG-Th and RG-K, respectively. The data was collected for a duration of 10800 seconds. This calibration determined the detector's detection efficiency based on the energy of the radiation. In order to reduce the inaccuracy caused by the weakening of gamma radiation, all

three standard sources were created with the same shape and composition. In order to prevent the accidental accumulation of gamma rays, a gamma ray standard with the same radionuclide as the one being monitored is employed. This calibration enables the formation of the correlation between the channel numbers of the analyser and the energy of the photons. The specific activity is calculated using-

$$C_{\mathrm{n}} = \frac{N_{\mathrm{n}}}{\gamma_{\mathrm{d}} \times \eta_{\mathrm{E}} \times T \times W} \tag{2.2}$$

where C_{n} is the specific activity in Bq/kg, N_{n} is the net counts, γ_{d} is γ ray emission probability, η_{E} is the detection efficiency, T is the counting time (sec), and W is the dry mass of the sample (kg). The uncertainity and limit of detection is calculated as

-

$$\sigma_{Cn} = C_n \cdot \sqrt{\left(\frac{\sigma_{Nn}}{N_n}\right)^2 + \left(\frac{\sigma_{\gamma d}}{\gamma_d}\right)^2 + \left(\frac{\sigma_{\eta E}}{\eta_E}\right)^2 + \left(\frac{\sigma_T}{T}\right)^2 + \left(\frac{\sigma_W}{W}\right)^2} \tag{2.3}$$

where $\sigma_{Cn}, \sigma_{Nn}, \sigma_{\gamma d}, \sigma_{\eta E}, \sigma_T, \sigma_W$ are the uncertainities of above mentioned factors.

$$LOD = \frac{3 \times \sqrt{b}}{\gamma_{\mathrm{d}} \times \eta_{\mathrm{E}} \times T \times W} \tag{2.4}$$

where b is the background count rate.

The minimum detectable activity is a crucial factor in low-level counting, particularly when the count rate of a sample is nearly indistinguishable from the count rate of the background [16-17]. In these circumstances, the background is assessed by using a blank, which consists of a sample holder, for example, a planchet and all other components that are included in the measurement of the real sample, provided that the blank does not contain any activity. The concentration of ^{40}K was determined by monitoring the 1460 keV rays that are emitted during the decay of ^{40}K. The activity concentration of ^{214}Bi, as estimated from its 1764 keV gamma ray peak, is selected to measure the presence of ^{238}U. For quantification of ^{232} Th, the activity concentration of ^{208}Tl is used at a gamma ray peak of 2615 keV.

2.2.3 Measurement of heavy metals in water - atomic absorption spectrometry

The selection of an analytical technique for quantifying heavy metals in water samples is contingent upon the type of sample, the concentration of heavy metal, its capacity to detect exceedingly low concentrations in addition to accuracy [18]. An assortment of analytical techniques are utilised, such as Inductively Coupled Plasma (ICP), Atomic Absorption Spectroscopy (AAS), UV spectroscopy, Fluorimetry, X-ray fluorescence along with electrochemical techniques. The atomic absorption spectrophotometer AAS-7000 manufactured by Shimadzu, is employed for the detection of heavy metals in water due to its sensitivity, precision and cost-effectiveness. The initial detection of atomic absorption dates back to 1802, when Wollaston noted the presence of indistinct bands in the solar emission spectrum. In the year 1859, both Kirchoff and Bunsen, who held professorships at the University of Heidelberg in Germany, accurately elucidated Wollaston's finding by demonstrating that the dark bands were a result of the absorption of emission radiation by atoms in the sun. The AAS was first developed in the 1950s by a group of Australian chemists. Sir

Alan Walsh led the team at the Division of Chemical Physics, located in Melbourne, Australia [19].

The sample is usually in a liquid state, and after undergoing vaporisation, the target elements are transformed into free atoms by being introduced into a flame via a nebulizer. The principle relies on the absorption of photons of light by unbound atoms in their ground state. A lamp emits light at precise wavelengths corresponding to the atoms present in a gaseous state within the flame. The absorption of light energy results in the elevation of electrons within atoms to an excited state, as shown in figure 2.8 [9]. Atomic absorption spectroscopy determines the wavelength of absorbed light based on the specific type of atom (element) present. Every wavelength is uniquely associated with a specific element and the absorption line's width is often only a few picometers (pm), giving the technique its ability to selectively identify elements. The absorbance is determined by Beer- Lambert's law, which is the logarithmic relationship between the intensity of the incident light and the intensity of the absorbing species [19].

$$A = \log\left(\frac{I_t}{I_0}\right) = \epsilon c l \tag{2.5}$$

where A represents the absorbance, $\log(I_o/It)$ represents the absorbance value, K represents the molar absorptivity (L m^{-1} mol^{-1}), l represents the length over which light travels (m), and c represents the concentration of atoms in the flame (mol L^{-1}).

The AAS-7000 is based on the generation of a calibration curve from standard solutions, which is then employed to ascertain the concentration of the element in an unknown sample with AAS measuring the absorbance.

The instrument includes

1. Light source - The light source is usually a hollow cathode lamp, as shown in figure 2.9, that emits specific spectral lines [20]. The lamp contains an inert gas, often argon, at a low pressure. When the high voltage is applied across the two electrodes, the filler gas will undergo acceleration towards the cathode. Moreover, the collision of atoms results in their excitation, followed by their return to the ground state, leading to the emission of radiation with a certain wavelength. The measured quantity is the absorbance of the light emitted by the lamp as it traverses the atomized material.

2. Sample introduction - The liquid sample is injected at a higher speed into the nebulizer through a thin capillary tube. Upon the high-velocity impact of a fluid sample with a glass bead, a fine mist of droplets, known as aerosol, are generated which are directed towards the spray chamber. Following nebulisation, the metal ions are finely dispersed into a high-temperature flame, where they reduce to their constituent atoms and then absorb light emitted by a hollow cathode lamp. The processes involved are desolvation, vaporisation, atomization and ionisation. Desolvation refers to the process of removing solvent or drying. The solvent is volatilized, leaving behind desiccated nanoparticles of the sample. Vaporisation refers to the particles that undergo a phase transition and are transformed into the gaseous state. Atomization refers to the process of

breaking down a substance into individual atoms or smaller particles. The focus of AAS analysis is on ground state atoms. Ionisation is defined as the process through which an atom or molecule is transformed into an ion by the addition or removal of one or more electrons. Under specific flame conditions, certain atoms will undergo ionisation, resulting in the formation of ions. The extent of ionisation will be influenced by factors such as the composition of the oxidant/acetylene gas mixture and the ionisation potential of the analytes in the solution.

3. 3D-double beam optics - The AAS-7000 series features 3D double-beam optics. The optical system has been engineered to achieve peak performance for every measurement minimising light losses in addition to optimising light beam.

4. Monochromator - To differentiate the radiation emitted by each element from other radiation produced by the source of radiation, the radiation is subsequently directed through a monochromator. The process is conducted by employing a prism monochromator.

5. Detector - The detector measures the magnitude of light that passes via wavelength selector. It quantifies the energy absorption from particular light wavelengths. The light that exits the output slit of the monochromator is directed towards the PMT, where it strikes a photodiode. This interaction results in the conversion of the light into an electrical signal. The generated electrical signal is then subjected to amplification via a series of dynodes prior to collection.

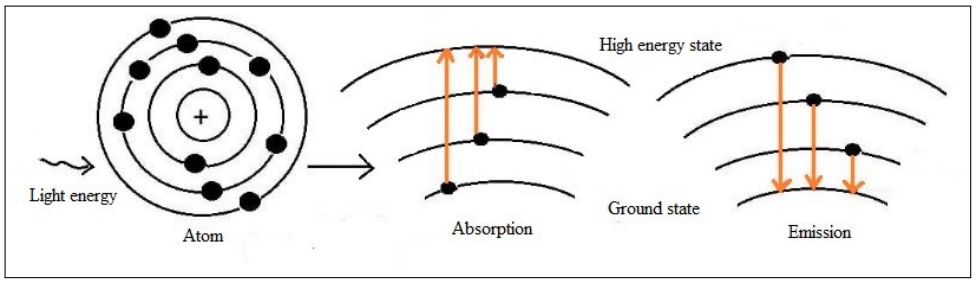

Figure 2.8: A schematic showing atomic absorption and emission process [9].

Accurate quantification of analytes is crucial in environmental monitoring. However, the presence of interfering species can lead to false readings or inaccuracies, making the study of interferences a necessary aspect of analytical method development [20]. Interferences can arise from a variety of sources, such as the formation of compounds that do not absorb at the desired wavelength or the inability of the instrument to distinguish between the analyte and the interfering species. Interferences in AAS are categorized into two distinct types: Spectral and non-spectral interferences. Spectral interference primarily occurs when another atomic line absorbs light, or when a molecule absorbance band is located near the spectral line of the element being studied. Non-spectral interferences are further divided into three categories, namely, matrix, ionisation and chemical interference. Matrix interference originates when a sample demonstrates increased viscosity or elevated surface tension in comparison to the standard, resulting in fluctuations in the rate at which the sample is taken up due to alterations in nebulization efficiency. During intense combustion, ionisation

interference is more prevalent. The process of dissociation goes beyond merely forming ground state atoms. A flame with high energy can ionize these atoms by removing electrons, resulting in a depletion of these atoms. Chemical interference takes place when a specimen mixed with an analyte, produces a molecule that is resistant to decomposition by the heat of the flame [21].

Analytical procedure - The AAS-7000 shown in figure 2.10 is calibrated using standard solutions. A calibration curve is constructed by plotting the concentration of the analyte against the absorbance after measuring the absorbance of each known solution. The groundwater sample is thereafter introduced into the instrument to measure its absorbance. The concentration of the element of interest, which is not known, is determined using a calibration curve. The observed concentration of the target element exhibits a direct proportionality to the number of ground state atoms present in the flame. The standard solutions are created by diluting a stock standard with a metal concentration of 1000 mg L^{-1}, (ISO-certified) and using de-ionised water. AAS-7000 has a limited analysis scope, focusing largely on metals and certain metalloids. It is not appropriate for analysing non-metal elements.

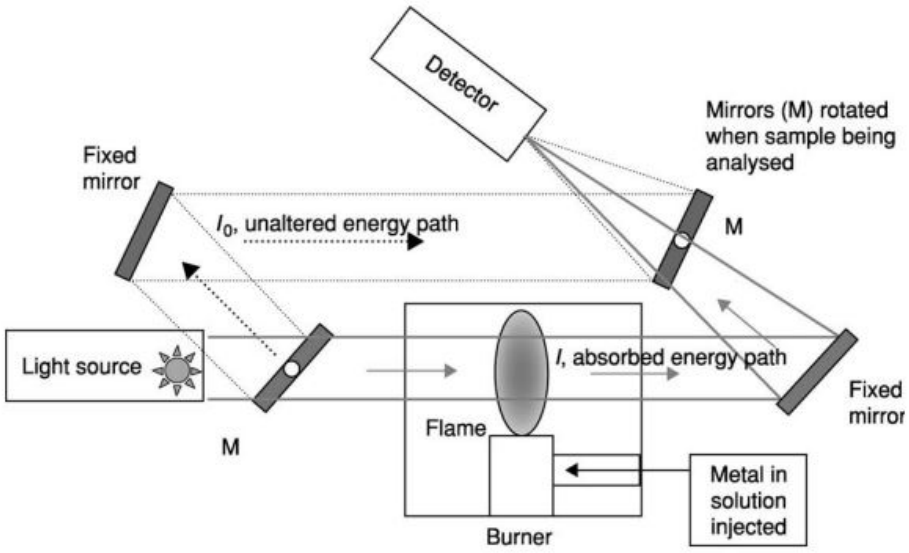

Figure 2.9: The components of atomic absorption spectroscopy. The liquid sample used for examination is introduced into the burner. The mirrors, designated as M, are rotated in order to assess the properties of both the incident and the absorbed light. The path deviated from the flame measures the unimpacted light intensity. The pathway traversed by the light through the flame, referred to as the absorbed energy route, quantifies the intensity of the light subsequent to its passage through a burner that contains the co-injected dissolved sample [21].

2.2.4 Measurement of heavy metals in food - inductively coupled plasma - optical emission spectroscopy

Inductively Coupled Plasma - Optical Emission Spectroscopy (ICP-OES) is a reliable analytical method employed to identify and measure the concentration of various elements. The commercial availability of ICP-OES began in 1974, and it has

subsequently gained widespread global usage, making it one of the most often employed analytical techniques. It is the preferred method for many applications that necessitate the analysis of a sample's elemental composition [22]. It is extensively utilised in diverse disciplines including environmental science, metallurgy, geology, petrochemistry, pharmaceuticals, materials science and food safety. The instrument has the capability to analyse many sorts of samples, such as aqueous and organic liquids and solids. It has several advantages compared to other elemental analysis techniques, such as an extensive linear dynamic range, significant tolerance to matrix effects and enhanced speed of analysis. ICP-OES has become the favoured technique for elemental analysis since it can measure several elements simultaneously. The Prodigy ICP-OES by Teledyne Leeman Labs [23] is used for analysing the concentration of heavy metals in wheat samples.

Figure 2.10: A picture of atomic absorption spectrophotometer-7000 by Shidmazu [24].

The approach is based on the principle that specific elements, when stimulated, emit light at a precise wavelength. An argon plasma is employed to stimulate the atoms. Upon returning to their ground state, these atoms release energy in the form of photons, which are then detected by the spectrometer. ICP-OES utilize a calibration curve constructed from standard solutions to determine the concentration of an element in an unknown sample with measuring emission intensity.

The instrument setup includes -

1. Sample introduction - The liquid sample is introduced into the nebulizer and is transformed into a fine aerosol by a stream of argon. The aerosol is further introduced into the spray chamber, where larger droplets are eliminated. The residual aerosol then advances into the plasma burner.

2. Excitation source - The ICP serves as the excitation source for the analysis. The plasma torch is composed of three concentric glass tubes. Argon gas circulates through the two outermost tubes, as shown in figure 2.11. An electric current

flows through the metallic coil encircling the glass torch, resulting in the generation of a magnetic field. When a spark is introduced into a flow of argon gas, it generates plasma. The metal coil surrounding the flame transfers energy to the argon gas, thereby maintaining the plasma. A separate flow of argon gas transports the aerosol of the sample through the centre of the plasma torch. The high temperature of the plasma causes the solvent in the sample to vaporise. The heat causes the sample molecules to dissociate into atoms and ions and supplies the necessary energy to stimulate the electrons in these atoms and ions, transitioning to higher energy states.

3. Radio-frequency generator - In ICP-OES, the ions are propelled using radiofrequency discharge (RF). The radio-frequency (RF) generator is an electronic apparatus that generates radio frequency energy, subsequently conveyed through the metallic coils encircling the plasma torch. The operator has the ability to manipulate the power of the radio frequency (RF), hence adjusting the energy level of the plasma.

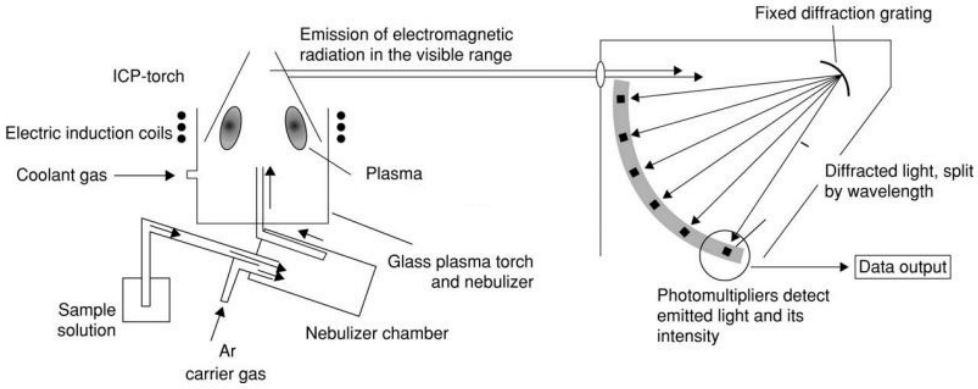

Figure 2.11: The fundamental constituents of ICP-OES. The induction coils generate a circular formation of plasma with temperatures about around 10,000 ^{o}C. The water sample is entrained and introduced into the plasma by the flowing carrier gas. Elements emit light as a result of being heated and excited. The use of a diffraction grating allows for the simultaneous analysis of a broad spectrum of light frequencies by dispersing the light [22].

4. Spectrometer - This component is utilised for the purpose of selecting specific wavelengths. Within the spectrometer, the light undergoes separation, similar to how a prism separates white light into a spectrum of colours. This allows for the exact measurement of light intensity at certain wavelengths. The spectrometer consists of two sections: the fore-optics and either a monochromator or a polychromator. After passing through the mono-or polychromator, the light is directed towards the detector.

5. Detector - The detector measures the intensity of light that traverses through the spectrometer. It quantifies the energy absorption from particular light wavelengths. Charge coupled devices (CCD) are often used where chip's surface is partitioned into pixels, with each pixel measuring photons of light at distinct wavelengths.

6. Signal processing - The electrons are collected at the anode of the PMT. The digital signal is then transmitted to the computer for further signal processing.

The Prodigy ICP-OES shown in figure 2.12 is calibrated using standard solutions from LGC standards (VHG labs, England). The intensity of the emitted light at particular wavelengths is measured and plotted in relation to the predefined concentrations. An ICP-OES system can be optimised for analysis by configuring it in one of three configurations: radial, axial, or dual-view, depending on the type of samples. Salsa software is utilised for the purpose of collecting data of concentrations of analytes in samples [24].

Figure 2.12: A picture of Prodigy ICP-OES [25].

2.2.5 Difference between AAS and ICP-OES

Atomic Absorption Spectroscopy involves the measurement of light absorption by vaporized atoms, with each element requiring a specific hollow cathode lamp for analysis. This technique operates sequentially, addressing one element at a time. In contrast, Inductively Coupled Plasma Optical Emission Spectroscopy (ICP-OES) measures the light emitted from atoms that are excited in a high-temperature plasma, facilitating the simultaneous analysis of multiple elements. AAS is characterized by higher detection limits and reduced sensitivity, making it suitable for samples with elevated concentrations. In contrast, ICP-OES offers lower detection limits and greater sensitivity, which is advantageous for trace element detection. AAS is inherently slower due to its sequential measurement approach, while ICP-OES is faster, allowing for the concurrent measurement of various elements. The choice between these techniques is influenced by their respective advantages, the specific analytical requirements, detection limits, sample matrix complexity, and financial considerations.

2.2.6 Physico-chemical properties of water

The salinity, total dissolved solids (TDS), pH and conductivity are crucial parameters for assessing water quality for drinking purposes. The measurement of TDS in water is an essential parameter used to evaluate the quality of a water sample. It is directly linked to higher levels of turbidity, hardness and conductivity in the water samples. It refers to the overall amounts of dissolved compounds in water like inorganic salts, minerals and organic matter. The acidity or alkalinity of a solution, as measured by

its pH, is influenced by the amount of hydrogen ions that are present within that solution. The salinity directly impacts the solubility of dissolved oxygen, which is pivotal to the survival of organisms inhabiting aquatic environments. Conductivity is a quantitative assessment of water's ability to transmit electrical current, which is directly correlated with the number of ions present in the water.

The physicochemical properties of water were measured using NPC-362D Microprocessor based digital water and soil analysis kit by Naina Semiconductor Limited, Noida, as shown in figure 2.13 [26]. The pH, conductivity, TDS and salinity of the water samples were measured for the analysis.

pH - The resolution for pH measurement is 0.01pH. There are two calibration options of auto and manual. The automatic calibration is done using the standard buffer solutions of 4.00, 7.00 and 9.20 pH.

TDS, conductivity and salinity - The instrument measures TDS in the range of 0-200 ppt with automatic range selection and resolution of 0.1ppm. The range of conductivity is from 0 to 1000 milli mho with automatic range selection, a resolution of 0.1 micro mho and an accuracy of ±0.5%. The salinity range for the instrument is from 0 to 50 ppt, resolution of 0.1 ppt, an accuracy of ± 0.5% and an automatic temperature component.

Figure 2.13: A photograph of NPC-362D Microprocessor kit [26].

2.3 References

1. Kaur Guron, B., Kalkal, S., & Mehra, R. (2024). The impact of uranium contamination in groundwater on human health: a toxicological risk assessment. *International journal of environmental analytical chemistry*, 1-15.

2. Akkurt, İ., Gunoglu, K., Gunay, O., & Sarıhan, M. (2022). Natural radioactivity and radiological damage parameters for soil samples from Cekmekoy-İstanbul. *Arabian journal of geosciences*, *15*(1), 53.

3. Yadav, P., Garg, V. K., Singh, B., Pulhani, V., & Mor, S. (2018). Transfer factors and effective dose evaluation due to natural radioactivity in staple food grains from the vicinity of proposed nuclear power plant. *Exposure and Health*, *10*, 27-39.

4. Acar, O., Tunçeli, A., & Türker, A. R. (2016). Comparison of wet and microwave digestion methods for the determination of copper, iron and zinc in some food samples by FAAS. *Food analytical methods*, *9*, 3201-3208.

5. Sonali, P. D. B., Ajay, K., Priyanka, J. R., Rupali, K., Rajesh, V. K., Rajvir, S., & Pradeepkumar, K. S. (2016). Comparison of radiometric and non-radiometric methods for uranium determination in groundwater of Punjab, India. *Journal of radioanalytical and nuclear chemistry*, *307*, 395-405.

6. Mehra, R., Gupta, D., & Jakhu, R. (2017). Risk assessment for natural uranium present in ground water of Mahendragarh district of Haryana. *Journal of radiation and nuclear applications*, *2*, 67-73.

7. Rathore, D. P. S., Tarafder, P. K., Balaram, V., Mishra, M., Pari, J., Bhujled, A. G., & Bhawalkard, D. D. (2023). Application of a differential technique in laser-induced fluorimetry/pulsed LED-fluorimetry: simple and reliable analysis of uranium raw materials in the nuclear fuel cycle-a mini-review. *Environment science: advances, 2*, 1340-1350.

8. Tolgyessy, J., & Harangozo, M. (2004). Radiochemical Methods-Food and Environmental Applications, No. 00526. *Encyclopedia of Analytical Sciences.* Elsevier.

9. Crouthamel, C. E., Adams, F., & Dams, R. (2013). *Applied gamma-ray spectrometry* (Vol. 41). Elsevier.

10. Knoll, G. F. (2010). *Radiation detection and measurement.* John Wiley & Sons.

11. Valkovic, V. (2000). *Radioactivity in the environment: physicochemical aspects and applications.* Elsevier.

12. James E. Penner-Hahn, J.E. (2019). X-ray Absorption Spectroscopy. *Encyclopedia of analytical science* (Ed. 3). Elsevier.

13. https://atomtex.com/sites/default/files/datasheets/at1315_0.pdf (accessed on June,2024)

14. Duggan, J. L. (1988). *Laboratory investigations in nuclear science.* Nucleus, Incorporated.

15. Sandupatla, A., Arulkumaran, S., Ing, N. G., Nitta, S., Kennedy, J., & Amano, H. (2020). Vertical GaN-on-GaN Schottky diodes as α-particle radiation sensors. *Micromachines*, *11*(5), 519.

16. Jenkins, D. (2020). *Radiation detection for nuclear physics: Methods and industrial applications*. IOP Publishing.

17. Done, L., & Ioan, M. R. (2016). Minimum Detectable Activity in gamma spectrometry and its use in low level activity measurements. *Applied radiation and isotopes*, *114*, 28-32.

18. Ahamed, M. I., Lichtfouse, E., & Altalhi, T. (Eds.). (2021). *Remediation of heavy metals*. Springer International Publishing.

19. Zulkifli, S. N., Rahim, H. A., & Lau, W. J. (2018). Detection of contaminants in water supply: A review on state-of-the-art monitoring technologies and their applications. *Sensors and Actuators B: Chemical*, *255*, 2657-2689.

20. Lagalante, A. F. (2004). Atomic absorption spectroscopy: A tutorial review. *Applied Spectroscopy Reviews*, *34*(3), 173-189.

21. Worden, R. H. (2005). Analytical Methods [Geochemical Analysis (Including X-ray)].

22. Khan, S. R., Sharma, B., Chawla, P. A., & Bhatia, R. (2022). Inductively coupled plasma optical emission spectrometry (ICP-OES): a powerful analytical technique for elemental analysis. *Food analytical methods*, 1-23.

23. https://info.teledyneleemanlabs.com/blog/-prodigy-plus-inductively-coupled-plasma-optical-emission-spectrometer (accessed on June 8, 2024).

24. https://www.shimadzu.com/an/products/elemental-analysis/atomic-absorption-spectroscopy/aa-7000/index.html (accessed on June 8, 2024).

25. https://www.scientech.com.tw/en/pages/teledyneleeman.aspx#ICP (accessed on June 8, 2024).

26. https://nainasemi.com/microprocessor-water-and-soil-analysis-kitNPC362D.html (accessed on June 8, 2024).

Chapter 3

Health risk assessment using deterministic and probabilistic approach

---

Monte-Carlo simulations serve as a valuable tool for assessing health risks by reducing the variabilities in the data. Therefore, simulations are carried out in MATLAB and Argo for risk assessment and sensitivity analysis of uranium and other heavy metals in Mansa region of Punjab. The hazard quotient, annual effective dose and excess cancer risk are calculated using both deterministic and probabilistic methodologies. The chapter commences with an introduction followed by materials and methods in section 3.2. Heavy metal indices and spatial distributions, along with health risk assessment using deterministic and probabilistic approaches are discussed in section 3.3 followed by the conclusion.

3.1 Introduction

Water, essential for human survival, is becoming contaminated with pollutants, resulting in a scarcity of safe drinking water. According to UNESCO [1], over 2 billion individuals worldwide, which accounts for 26%, an alarming fraction, is deprived of access to safe drinking water. In addition to sustaining life, water is essential for the maintenance of healthy ecosystems, the cultivation of food and the generation of energy [2]. The water sources are mainly polluted by heavy metals through human activities, which include mining, agricultural practices, hazardous waste sites, landfilling, urban wastewater and dredged sediments [3]. There exist two categories of aquatic heavy metal species, specifically stable and liable states. The formation of a liable state is observed with weak ligands, as they exhibit a high susceptibility. Consequently, these complexes can be easily discharged using conventional methods. On the other hand, strong ligands lead to the formation of heavy metal complexes that possess great stability, making them withstand conventional methods [4]. Although certain heavy metals are essential for humans in meagre quantities but due to biomagnification, heavy metals can cause significant adverse effects on human well-being. Chromium (+3) is a crucial nutrient, whereas

ingestion of Cr (+6) for a long period can cause breathing problems, skin irritation, and kidney and liver issues. Itai-itai disease, renal failure and nervous system damage are also consequences of higher chromium intake [5]. High iron intake can lead to hemochromatosis and can damage endocrine organs, resulting in necroptosis [6]. Zinc is classified as a trace element and plays a crucial role in supporting growth and development. However, excessive zinc intake can result in adverse effects such as cell proliferation, anaemia, and elevated insulin levels [7]. The half-life of cadmium varies from 10 to 33 years therefore, the persistent uptake impairs kidneys, nervous system and skeleton [8].

Uranium has garnered substantial interest in recent years in the realms of environmental and health-related studies attributable to its chemical toxicity. It is present in elevated concentrations in potable water and groundwater [9-10]. The groundwater in 16 states in India has been found to contain uranium. With the exception of north-west (NW) India, all states in India possess Pre-Cambrian rocks, which are inherently regarded as a potential uranium source [11]. Punjab, a north-western state, is currently experiencing a crisis as a result of elevated levels of uranium and other heavy metals in the groundwater table, which has been in the news for more than a decade for being the epicentre of debilitating diseases such as cancer [12-13]. Therefore, substantial research has been carried out over the past several years on the concentration of uranium in groundwater of south-western region of Punjab, India and high levels of uranium contamination is observed [14-20].

Health risk assessment, encompassing evaluations of both carcinogenic and non-carcinogenic risks, is widely acknowledged as a crucial method for identifying potential health hazards. The deterministic approach has been extensively applied to assess the health risks associated with pollutants in water. Nevertheless, because of variations in age, sex, and metabolic factors across individuals, different people are subjected to varying levels of risk [21]. Therefore, deterministic risk assessment may not accurately reflect the true extent of the danger. Since this approach relies on a single-point estimation, it has the potential to either underestimate or overestimate the consequences [22]. In order to address this issue, the Monte-Carlo simulations are carried out which are based on a probabilistic approach. There is a scarcity of research that employs a probabilistic technique for the assessment of health hazards due to contamination in groundwater in the Mansa region of Punjab. The following objectives are addressed -

(a) heavy metals, including uranium contamination analysis is conducted using both deterministic and probabilistic approaches to gain a more comprehensive understanding. The sensitivity analysis is also carried out to assess the impact of various input parameters.

(b) heavy metal indices are calculated.

(c) spatial distribution of heavy metals, including uranium contamination in Mansa district, Punjab, is estimated.

3.2 Materials and Methods

3.2.1 Study area

The Malwa region comprising of 11 districts, is situated to the south of Sutlej river. The Mansa district with 242 villages, is part of the Malwa region. The boreholes dug in the area up to a depth of 60 m indicate the existence of predominantly fine sand mixed with "kankar", and consist of two primary aquifer zones. Each aquifer zone has a thickness ranging from 4 to 25 metres and is divided by clay layers measuring 3 to 5 metres in thickness [23-24]. The southwest monsoon, commencing in the final week of June and concluding in late September, is responsible for precipitation. The yearly precipitation is 378 mm on an average in the region. The primary trajectory of groundwater movement in the region is oriented from the northeast towards the southwest. The seasonal agricultural practices are negatively affected by monsoonal waterlogging resulting from the regional hydraulic gradient, particularly in the southwestern parts, as well as the depletion of the water table due to excessive exploitation [25]. The Ghaggar river and Sirhind drain are the primary drainage systems in the region [26]. The canal irrigation system encompasses a significant area of 90 sq. km. while the remaining acreage is irrigated using groundwater. The groundwater in this region is characterised by poor quality, primarily due to elevated levels of salinity as well as alkalinity [26-27]. The water level in the district has been consistently decreasing at a rate ranging from -0.14 to -0.82 metres each year [26]. The predominant crops in the region are wheat, rice, cotton, and bajra, with corresponding areas of cultivation reaching 170,000 hectares, 74,000 hectares, 92,000 hectares, and 1,000 hectares [23].

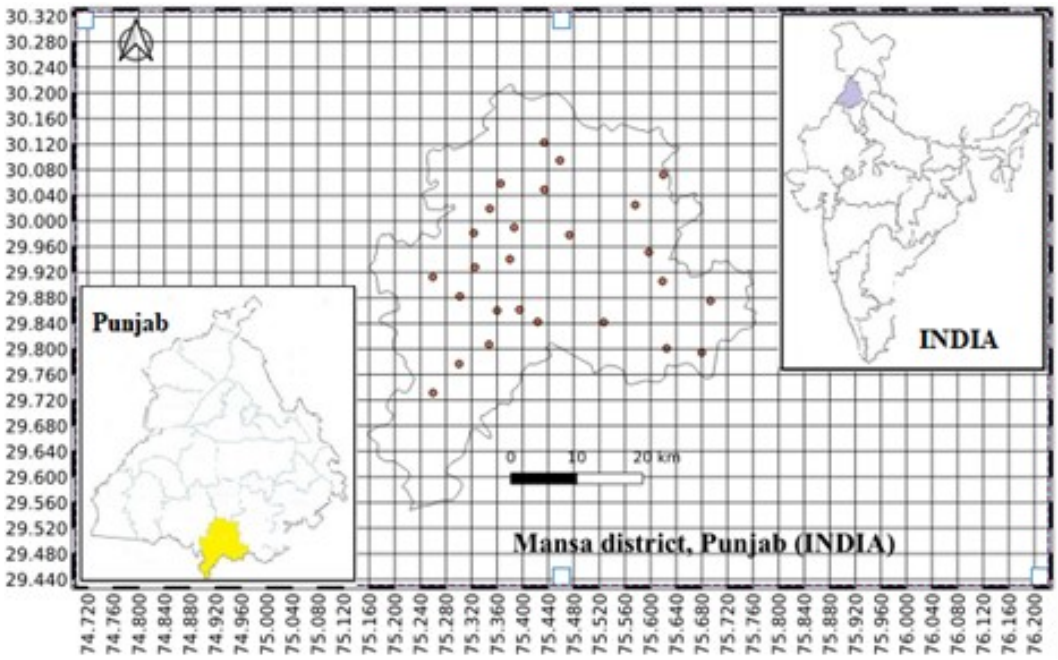

Figure 3.1: Map of Mansa district, Punjab showing locations from where water samples were collected.

Table 3.1: Heavy metal concentration (μg L^{-1}) in groundwater samples collected from different locations in Mansa, Punjab.

S.no.	Cadmium	Chromium	Zinc	Iron	Uranium
1	24.40 ± 1.20	1.50 ± 0.10	7.65 ± 0.70	48.15 ± 2.40	84.50 ± 0.67
2	64.60 ± 3.20	5.60 ± 0.50	8.90 ± 0.80	21.30 ± 1.90	43.43 ± 0.42
3	61.90 ± 3.10	15.70 ± 0.80	9.80 ± 0.90	35.60 ± 1.80	67.23 ± 1.70
4	4.60 ± 0.40	20.30 ± 1.00	16.70 ± 0.80	34.50 ± 1.70	131.72 ± 0.74
5	55.50 ± 2.80	32.50 ± 1.60	19.40 ± 1.00	41.60 ± 2.10	234.2 ± 1.78
6	17.50 ± 1.60	36.10 ± 1.80	19.73 ± 0.90	15.00 ± 1.40	48.34 ± 0.40
7	133.60 ± 4.00	44.20 ± 2.20	22.10 ± 1.10	22.00 ± 2.00	264.92 ± 1.63
8	23.40 ± 2.10	54.30 ± 2.70	23.23 ± 1.20	9.50 ± 0.90	279.09 ± 2.52
9	9.40 ± 0.80	70.60 ± 2.10	11.40 ± 1.00	3.80 ± 0.30	235.65 ± 1.97
10	166.30 ± 5.00	62.40 ± 1.90	16.90 ± 0.80	1.80 ± 0.20	111.71 ± 1.01
11	81.20 ± 4.10	72.60 ± 2.20	32.60 ± 0.70	4.50 ± 0.40	91.28 ± 1.15
12	211.90 ± 4.20	92.90 ± 1.90	73.40 ± 1.50	30.80 ± 1.50	449.79 ± 2.68
13	49.10 ± 2.50	85.80 ± 1.70	17.50 ± 1.60	11.60 ± 1.00	104.8 ± 0.92
14	47.00 ± 2.40	119.40 ± 2.40	19.00 ± 1.00	15.20 ± 1.40	182.85 ± 1.62
15	4.60 ± 0.40	111.70 ± 2.20	20.20 ± 1.10	3.50 ± 0.20	98.17 ± 1.04
16	54.20 ± 2.70	99.60 ± 2.00	118.10 ± 2.40	3.50 ± 0.40	65.72 ± 0.82
17	19.50 ± 1.80	106.20 ± 2.10	30.20 ± 1.50	1.70 ± 0.20	133.45 ± 0.96
18	4.90 ± 0.40	38.60 ± 1.90	17.50 ± 1.60	6.30 ± 0.30	239.99 ± 0.97
19	68.80 ± 3.40	135.20 ± 2.70	7.50 ± 0.70	1.90 ± 0.18	376.24 ± 2.34
20	4.60 ± 0.40	21.80 ± 1.10	12.10 ± 1.10	2.00 ± 0.20	135.68 ± 0.37
21	68.80 ± 3.40	23.90 ± 1.20	4.20 ± 0.40	14.00 ± 0.40	95.41 ± 1.94
22	4.60 ± 0.40	28.60 ± 1.40	48.50 ± 1.50	24.50 ± 0.70	116.63 ± 1.56
23	69.40 ± 3.50	33.30 ± 1.70	3.50 ± 0.30	15.40 ± 0.80	71.05 ± 0.66
24	114.70 ± 3.40	41.00 ± 2.10	8.40 ± 0.80	20.50 ± 1.00	147.11 ± 1.53
25	181.80 ± 5.50	46.80 ± 2.30	11.50 ± 1.10	9.40 ± 0.80	63.27 ± 0.60
26	9.20 ± 0.80	19.50 ± 1.80	14.50 ± 1.30	8.19 ± 0.70	134.27 ± 0.75

3.2.2 Measurement Technique

Atleast three samples of groundwater were collected from each location and were averaged for the respective location shown in figure 3.1. The heavy metal concentrations in the groundwater of the district are listed in table 3.1. Iron, cadmium, chromium and zinc were analysed using atomic absorption spectrophotometer AAS-7000 (Shimadzu). The elements were examined using the flame absorption method to atomize them in an Air-C_2H_2 atmosphere. The analytical line wavelengths for Cd, Cr, Zn and Fe were 228.80 nm, 357.87 nm, 213.85 nm, and 492.5 nm, respectively. In AAS, atoms of heavy metals absorb specific wavelengths of electromagnetic spectra after the excitation by acetylene flame. Before analysis, the samples were filtered using Whatman filter paper to get rid of impurities. All the standard guidelines were followed during the analysis. The linear calibration was done using wizAArd software prior to sample analysis with $R^2 = 0.99$. The concentration vs absorbance calibration curve exhibited strong linearity with absorbance less than 0.4. The blank samples were measured to reduce any effect of the instrument and environment on the absorbance value of a sample. The USEPA standards for the analysis of water

samples were followed. The samples were repeated for precision, and a spike test was conducted. The threshold for detecting cadmium and chromium is 0.2 ppb, in contrast to zinc and iron, which have a detection limit of 1.5 ppb. The LED LF-2a fluorimeter of Quantalase was used to quantify the uranium concentration in the samples. The uranium concentration from different locations is listed in table 3.1, ranging from 43.43 μg L^{-1} to 449.79 μg L^{-1}. The instrument has a detection range of 0.5-1000 μg L^{-1}. The quality assurance was conducted utilising Accustandard reference material. The LED fluorimeter underwent calibration using standard solutions of uranium with concentrations of 10 and 100 μg L^{-1} [18]. The detailed information regarding sample preparation and instrumentation is mentioned in chapter 2.

Table 3.2: Parameters used for calculating risk assessment using probabilistic and deterministic approach.

Parameters	**Probabilistic Approach**		**Deterministic Approach**		**References**
Concentration (mg L^{-1})	Child	Adult	Child	Adult	
Cr Cd Zn Fe	Weibull (Shape - 1.42, scale - 0.06) Exponential (Rate - 16.71) Weibull (Shape - 1.12, scale - 0.02) Weibull (Shape - 1.15, scale - 0.01)	Weibull (Shape - 1.42, scale - 0.06) Exponential (Rate - 16.71) Weibull (Shape - 1.12, scale - 0.02) Weibull (Shape - 1.15, scale - 0.01)	Mean	Mean	Current study
Ingestion rate (L day^{-1})	Lognormal (0.65±0.39)	Lognormal (1.38±0.71)	0.78	2.50	[28-29]
Body weight (kg)	Lognormal (10.22±1.43)	Lognormal (49.29±8.82)	10.22	49.29	[30]
Exposure duration (years)	Uniform (0,6)	Uniform (0,30)	6	30	[31]
Exposure frequency (days $year^{-1}$)	Triangular 345 (180-365)	Triangular 345 (180-365)	365	365	[31-32]
Average time (days)	2190	10950	2190	10950	
Permeability coefficient (cm hr^{-1})	Cr - 0.002, Cd - 0.001, Zn - 0.0006, Fe - 0.001	Cr - 0.002, Cd - 0.001, Zn - 0.0006, Fe - 0.001	Cr - 0.002, Cd - 0.001, Zn - 0.0006, Fe - 0.001	Cr - 0.002, Cd - 0.001, Zn - 0.0006, Fe - 0.001	[31]
Surface area (cm^2)	Lognormal (5838±920)	Lognormal (19771±3373)	6600	18000	[28]
Exposure time (hr day^{-1})	Triangular 0.2 (0.13-0.33)	Triangular 0.2 (0.13-0.33)	0.25	0.25	[33]
Conversion factor (L cm^{-2})	0.001	0.001	0.001	0.001	[34]

Average time for calculating carcinogenic risk is 70 years.

3.3 Health risk assessment for radiological and chemical risks

3.3.1 Chemical risk due to Cr, Zn, Cd and Fe contamination

The different ways of human exposure are via ingestion, inhalation and dermal based on the intake medium in which the pollutant is present. Ingestion and dermal contact are considered for water exposure to children and adults in this study for assessing health risks due to the presence of Cr, Cd, Zn and Fe in groundwater. To evaluate the non-carcinogenic risk linked to heavy metals, it is essential to calculate the average daily dose (ADD) for each route of exposure for children and adults. The parameters used for deterministic and probabilistic approaches are listed in table 3.2. The average daily dose is given as [35]-

$$ADD_{ing}\left(mg\ kg^{-1}day^{-1}\right) = \frac{(\ C \times IR \times EF \times ED)}{(AT \times BW)} \tag{3.1}$$

$$ADD_{der}\ \left(mg\ kg^{-1}day^{-1}\right) = \frac{(C \times K_p \times SA \times ET \times EF \times ED \times CF)}{(AT \times BW)} \tag{3.2}$$

where ADD_{ing} is the average daily dose for ingestion in mg kg^{-1} day^{-1}, C is the concentration in mg L^{-1}, IR is the ingestion rate in L day^{-1}, EF is the exposure frequency in days year^{-1}, ED is the exposure duration in years, AT is the averaging time in days, and BW is the body weight in kg. ADD_{der} is the average daily dose for dermal contact in mg kg^{-1} day^{-1}, K_p is the permeability coefficient in cm hr^{-1}, ET is exposure time, SA is the surface area in cm^2, and CF is the conversion factor in L cm^{-3}.

The risk assessment for a chemical pollutant, considering both ingestion and skin exposure is determined by calculating the hazard quotient in respect to the reference dosage. The hazard index (HI) quantifies the combined non-carcinogenic risks associated with a certain pollutant due to all probable pathways of exposure. When the hazard index (HI) is more than 1, it signifies the presence of hazardous non-carcinogenic toxicity in all age categories [35]. Hazard quotient is given as-

$$HQ_{ing} = \frac{ADD_{ing}}{R_d} \tag{3.3}$$

$$HQ_{der} = \frac{ADD_{der}}{R_{der}} \tag{3.4}$$

$$HI = \sum \left(HQ_{ing} + HQ_{der}\right) \tag{3.5}$$

where HQ_{ing} is the hazard quotient for ingestion, ADD_{ing} is the average daily dose for ingestion in mg kg^{-1} day^{-1}. For Cd and Cr, the reference dose, R_d is 5×10^{-4} mg kg^{-1} day^{-1} and 3×10^{-3} mg kg^{-1} day^{-1}, respectively. For Zn and Fe, R_d is 3×10^{-1} mg kg^{-1} day^{-1}. HQ_{der} is the hazard quotient for dermal contact, ADD_{der} is the average daily dose for dermal contact in mg kg^{-1} day^{-1} and R_{der} for Cd, Cr, Zn and Fe are 5×10^{-6}, 1.50×10^{-5}, 6×10^{-2} and 4.50×10^{-2} mg kg^{-1} day^{-1} [31].

The carcinogenic risk is assessed for chromium and cadmium, as they are identified as carcinogens. It is calculated as [32]-

$$Excess\ cancer\ risk = ADD_{ing} \times CSF_{ing} \tag{3.6}$$

where the cancer slope factor (CSF) for Cd is 3.80×10^{-1} and for Cr is 5×10^{-1} [28].

The heavy metal concentrations in the study region vary and are ordered as Cd > Cr > Zn > Fe. The cadmium concentration in all samples and the chromium concentration in approx. 42% samples is above the permissible limit of 0.003 mg L^{-1} and 0.05 mg L^{-1}, respectively [36-37]. The concentration of zinc and iron is below the recommended limit of 5 mg L^{-1} and 0.3 mg L^{-1} in the study region [36,38]. Bajwa *et al.* [39] also found that chromium was above the recommended limit in the same region, whereas, iron was well below the recommended limit. The excess cancer risk and hazard quotient are calculated using deterministic as well as probabilistic approaches. The excess cancer risk due to chromium and cadmium contamination for children using a deterministic approach is 2.13×10^{-3} and 1.71×10^{-3} , respectively. There is a prevalence of approx. 2 children at risk per 1000 for exposure to chromium and cadmium. In adults, the excess cancer risk is 1.42×10^{-3} and 1.15×10^{-3} due to chromium and cadmium contamination, respectively. There is more than 1 in 1000 adults at risk of developing cancer due to chromium and cadmium contamination in drinking water in the study region. The hazard quotient caused by ingestion of chromium contaminated water for children and adults using a deterministic approach is 1.38 and 0.92, respectively. The hazard quotient for children is greater than 1, which signifies that they are at higher risk. Chromium is commonly recognised as a significant carcinogen, and Zhang Z (2020b) [40] found that prolonged exposure to Cr (VI) leads to the development of cancerous tumours and enhances the occurrence of colorectal cancer in mice. Additional human investigations have shown that long-term exposure to Cr (VI) by drinking water can elevate the likelihood of developing stomach, bladder, kidney, and prostate cancer [41]. Similarly, the hazard quotient using a deterministic approach due to ingestion of cadmium contaminated water for children and adults is 9.00 and 6.06, respectively. Both adults and children are at risk due to the ingestion of high cadmium concentration in water. Cadmium tends to accumulate in the human body, particularly in the kidneys, leading to kidney disease known as renal tubular injury. Additional consequences of exposure to cadmium include disruptions in calcium metabolism, excessive excretion of calcium in the urine and the development of kidney stones [42]. The hazard quotient due to ingestion of zinc contaminated water for children is 5.6×10^{-3}, and for adults is 3.7×10^{-3} for adults. The hazard quotient due to iron ingestion is 4.0×10^{-3} for children and 2.68×10^{-3}. Due to dermal exposure to chromium contaminated water, the hazard quotient for children and adults is 1.17 and 0.66, respectively. The hazard quotient due to dermal exposure of cadmium in groundwater is 1.91 and 1.08 for children and adults, respectively. The hazard quotient of dermal exposure due to zinc in groundwater is 3.61×10^{-5} and 2.04×10^{-5} for children and adults, respectively. The hazard quotient of dermal exposure due to iron in groundwater is 5.60×10^{-5} for children and 3.16×10^{-5} for adults. The hazard quotient is lower than 1 for both zinc and iron. The deterministic hazard index for children and adults is 13.46 and 8.72, respectively, which is much larger than 1.

The reliability of health risk evaluation using a deterministic model is compromised by the use of fixed parameters. Therefore, probabilistic approach is employed, wherein each input variable adheres to a specific distribution. To establish the appropriate statistical distribution types for producing probability distribution functions (PDFs), the input variables/parameters were assessed by Anderson - Darling and Kolmogorov - Smirnov Test. The probabilistic approach for these metal contaminants is done using Argo - an Excel add on. The 5^{th} and 95^{th} percentiles are employed in a probabilistic method to prevent underestimation or overestimation of outcomes. For children, the 5^{th} percentile for excess cancer risk due to chromium contamination in groundwater is 2.40×10^{-5}, 50^{th} percentile is 4.11×10^{-4}, 95^{th} percentile is 2.51×10^{-3}. Similarly, for adults the 5^{th}, $50^{th,}$ 95^{th} percentile of excess cancer risk due to chromium contamination is 1.07×10^{-5}, 1.8×10^{-4}, 1.13×10^{-3}, respectively. The 50^{th} percentile of children and adults due to chromium contamination in groundwater has higher cancer risk than the permissible limit of 10^{-4} [43]. The 5^{th} percentile of excess cancer risk (children) due to cadmium contamination in groundwater is 8.93×10^{-6}, 50^{th} percentile is 2.6×10^{-4}, 95^{th} percentile is 2.8×10^{-3}. For adults, the 5^{th}, 50^{th}, 95^{th} percentile of excess cancer risk caused by the presence of cadmium in groundwater is 4.68×10^{-6}, 1.12×10^{-4}, 1.04×10^{-3}. The 50^{th} percentile children have higher chances of developing cancer than adults, which is approx. 2 in 10,000 as compared to approx. 1 in 10,000 for adults.

The non-carcinogenic risk assessment of ingestion and dermal pathways using a probabilistic approach for these metals is carried out. The 5^{th}, 50^{th}, 95^{th} percentile of hazard quotient for children due to chromium ingestion via groundwater is 1.52×10^{-2}, 0.27 and 1.70, respectively as shown in figure 3.2. The 5^{th}, 50^{th}, 95^{th} hazard quotient of adults due to chromium ingestion is 7.35×10^{-3}, 0.12 and 0.74, respectively as shown in figure 3.2. The 5^{th}, 50^{th}, 95^{th} percentile of hazard quotient for children due to cadmium ingestion via groundwater is 0.04, 1.4 and 12.03, respectively as shown in figure 3.2. The 5^{th}, 50^{th}, 95^{th} hazard quotient of adults due to cadmium ingestion is 0.02, 0.65 and 5.26, respectively as shown in figure 3.2. The 5^{th}, 50^{th}, 95^{th} percentile of hazard quotient for children due to zinc ingestion via groundwater is 3.91×10^{-5}, 9.07×10^{-4} and 7.24×10^{-3}, respectively. The 5^{th}, 50^{th}, 95^{th} hazard quotient of adults due to zinc ingestion via groundwater is 1.78×10^{-5}, 4.14×10^{-4}, 3.05×10^{-3}, respectively. The 5^{th}, 50^{th}, 95^{th} percentile of hazard quotient for children due to iron ingestion via groundwater is 2.66×10^{-5}, 6.37×10^{-4}, 4.94×10^{-3}. The 5^{th}, 50^{th}, 95^{th} hazard quotient of adults due to iron ingestion is 1.37×10^{-5}, 3.19×10^{-4} , 2.28×10^{-3}. The 5^{th}, 50^{th}, 95^{th} percentile of hazard quotient for children due to dermal exposure by chromium contamination via groundwater is 0.01, 0.25 and 1.22, respectively. The 5^{th}, 50^{th}, 95^{th} percentile of hazard quotient for adults due to dermal exposure to chromium contaminated groundwater is 0.01, 0.17 and 0.87, respectively. The 50^{th} and 95^{th} percentile of hazard quotient for children due to dermal exposure to cadmium contaminated groundwater is 6.9×10^{-4} and 2.58, respectively. The 5^{th}, 50^{th}, 95^{th} percentile of hazard quotient for adults due to dermal exposure to cadmium contamination via groundwater is 0.007, 0.23 and 1.68, respectively. The 5^{th}, 50^{th}, 95^{th} percentile of hazard quotient for children due to dermal exposure to zinc contaminated groundwater is 2.24×10^{-6}, 5.23×10^{-5} and 3.3×10^{-4}. The 5^{th}, 50^{th}, 95^{th} percentile of hazard quotient for adults due to dermal exposure to zinc contaminated groundwater is 3.12×10^{-7},7.24×10^{-6}, 4.82×10^{-5}. The 5^{th}, 50^{th}, 95^{th} percentile of hazard quotient for children due to dermal exposure

to iron is 5.87×10^{-7}, 1.17×10^{-5} and 7.13×10^{-5}, respectively. The 5^{th}, 50^{th}, 95^{th} percentile of hazard index for children is 0.79, 2.90 and 13.79, respectively. The 5^{th}, 50^{th}, 95^{th} percentile of hazard index for an adult is 0.43, 1.54 and 6.35, respectively. The 50^{th} percentile of children and adults are impacted by high concentration of these metals.

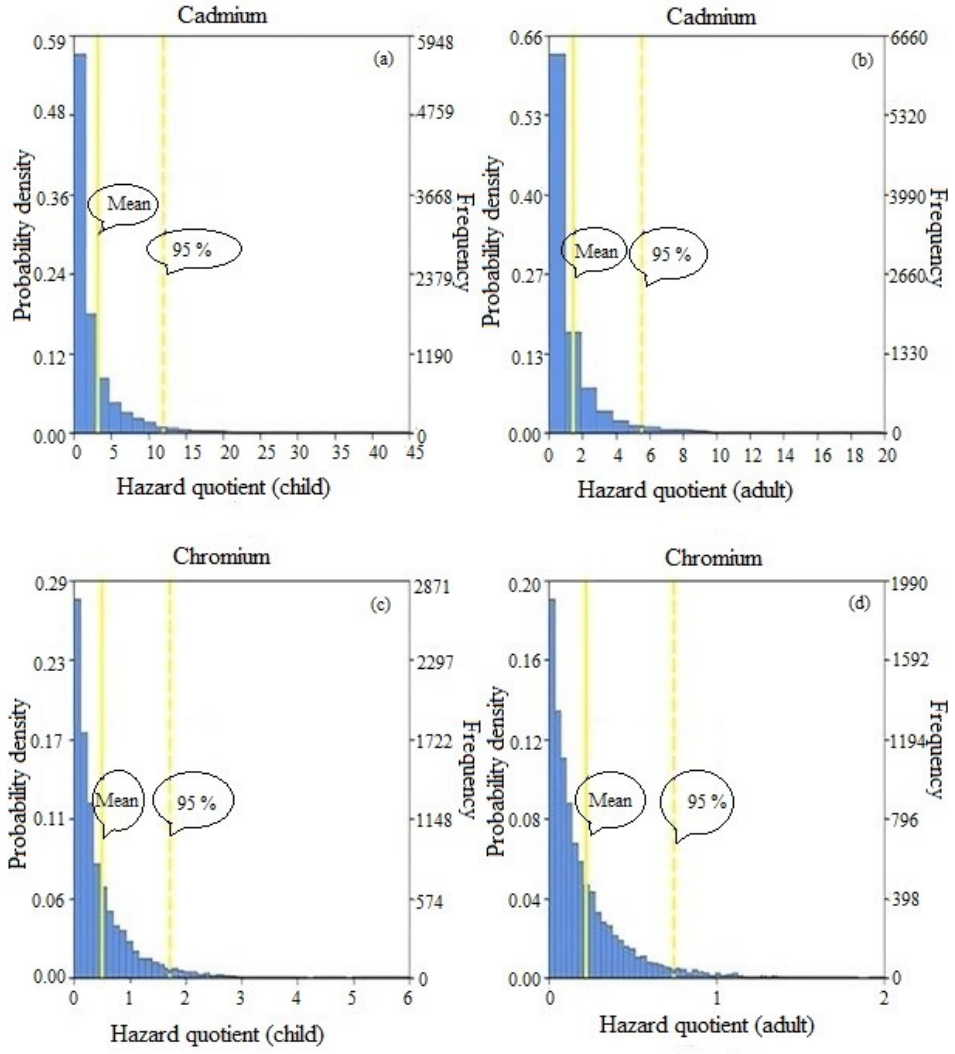

Figure 3.2: The probability density function of hazard quotient due to (a) water ingestion of cadmium (child), (b) water ingestion of cadmium (adult), (c) water ingestion of chromium (child) and (d) water ingestion of chromium (adult).

Sensitivity analysis: Uncertainty can be defined as a state of not having sufficient understanding about the true value of a parameter. The sensitivity analysis reveals the effect of the predictor factors on the accurate prediction that affects the assessment. The Spearman correlation is used for sensitivity analysis for ingestion and dermal contact of heavy metals using Argo - an Excel add-on. The concentration of heavy metal is the most dominant factor affecting the population, followed by exposure duration ingestion rate and exposure frequency, as shown in figure 3.3 and

3.4 for both ingestion and dermal contact.

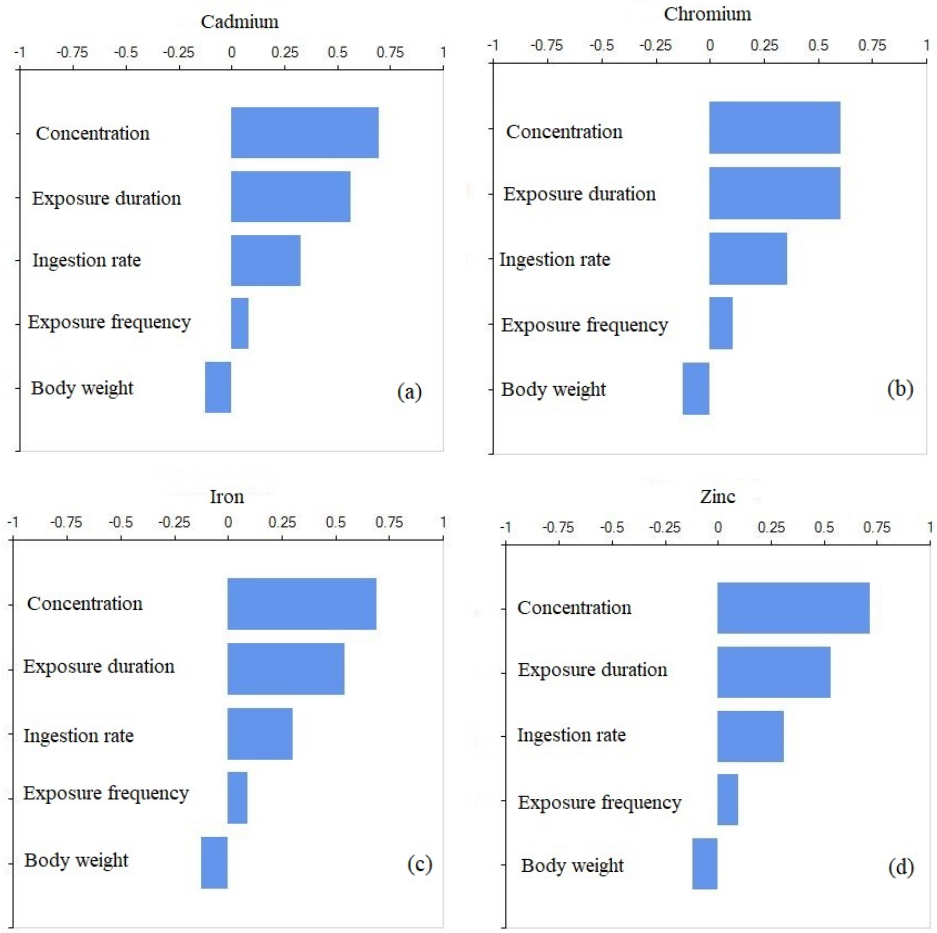

Figure 3.3: The sensitivity analysis for adults in (a), (b), (c) and (d) for ingestion pathway.

3.3.2 Heavy metal indices

Pollution indices are typically computed to assess the suitability of water for a certain intended purpose. The evaluation of these indices is based on the comparison between measured values of the parameters and the permissible concentrations of the relevant parameters.

Heavy metal evaluation index (HEI) - The level of heavy metals in water can be measured using HEI method and is calculated as [44]:

$$HEI = \sum_{j=1}^{n} \frac{C_j}{S_j} \tag{3.7}$$

where HEI is the heavy metal evaluation index where C_j is the concentration of j^{th} heavy metal and S_j is the standard permissible limit of j^{th} heavy metal. The S_j for chromium, iron, zinc and cadmium is 0.05 mg L^{-1} and 0.3 mg L^{-1}, 5 mg L^{-1} and 0.003 mg L^{-1}, respectively [36-38].

Heavy metal pollution index (HPI) - The HPI is an assessment method employed to evaluate the overall impact of particular elements on the quality of water. It is given as [45]-

$$HPI = \sum_{j=1}^{n} \frac{W_j Q_j}{W_j} \tag{3.8}$$

where W_j and Q_j is calculated as

$$W_j = \frac{1}{S_j}; Q_j = \left(\frac{C_j}{S_j}\right) \times 100 \tag{3.9}$$

where HPI is the heavy metal pollution index, W_j is the unit weight for j^{th} metal and Q_j is the sub-index of j^{th} heavy metal, S_j is the standard permissible limit, C_j is the concentration of j^{th} heavy metal.

Nemerow pollution index (NPI) - The Nemerow Pollution Index approach is a broader strategy for evaluating the quality of water, focusing on the primary sources of pollution while also taking into account for various supplementary factors in the evaluation process. This approach categorizes water quality through the calculation of an intricate pollution index, which is a multi-factor environmental quality index that considers the highest or most extreme values. It is given by [46]-

$$NPI = \sqrt{\frac{P_{\max}^2 + P_{avg}^2}{2}} \tag{3.10}$$

where NPI is the Nemerow pollution index, P_{max} is the maximum pollution index and P_{avg} is the average pollution index of the heavy metals involved.

The calculated HEI of heavy metals i.e. cadmium, chromium, zinc and iron, is 21.07, which indicates severe pollution. The calculated HPI determined all the heavy metals is around 1867.99. This large value shows a high amount of heavy metal contamination in the water samples of the study area. Cadmium is a dominant pollutant in the groundwater of the region. Similarly, the NPI is around 15.76, which is significantly greater than 1.

3.3.3 Radiological and chemical risk due to uranium contamination

A comprehensive assessment of radiological and chemical risks associated with uranium consumption through water is also done. It is crucial to evaluate these risks associated with the direct ingestion of contaminated groundwater in order to fully comprehend the adverse effects on human health. The excess cancer risk refers to the increased probability of developing fatal cancer associated with lifelong exposure to carcinogens [47]. It is given by the following equation [44]-

$$Excess\ cancer\ risk = C_u \times R_c \times IR \times ED \tag{3.11}$$

where C_u is the uranium concentration (Bq L^{-1}), R_c (risk coefficient mortality) is 1.13×10^{-9} Bq^{-1} for ^{238}U [43], IR is the ingestion rate (L day^{-1}) and ED is the total exposure duration of 25550 days (70 years × 365 days) [45]. The parameters used for deterministic and probabilistic calculations are given in table 3.3.

The assessment of chemical risk is required for uranium as it is a heavy metal. It is calculated as the lifetime average daily dose (LADD) as given in equation below [46]-

$$\mathrm{LADD}\,(\mu\mathrm{g\,kg^{-1}\,day^{-1}}) = \frac{C_u \times IR \times EF \times ED}{BW \times AT} \tag{3.12}$$

where C_u is the uranium concentration ($\mu g\ L^{-1}$), IR is the ingestion rate (L day^{-1}), EF is the exposure frequency (day year^{-1}) and ED is the exposure duration (year), BW is the body weight (kg), and AT is the average time (days). The values of these parameters are listed in table 3.3 for calculations using deterministic and probabilistic approach.

The hazard quotient is calculated as [46] -

$$HQ = \frac{LADD}{R_f d} \tag{3.13}$$

where LADD is the lifetime average daily dose (μg kg^{-1}day^{-1}) and R_fd is the reference dose of 0.6 μg kg^{-1}day^{-1}. If HQ is more than 1, it signifies that there is a surpassing of the non-cancer health criterion [48].

The annual effective dose (AED) is the total amount of radiation exposure to the complete body and is calculated by using the expression [49]-

$$AED\ \left(\mu Sv\ year^{-1}\right) =\ C_u \times ED\ \times AI \tag{3.14}$$

where C_u is the activity concentration of uranium in Bq L^{-1} of water, ED is the effective dose per unit intake as 0.045 μSv Bq^{-1} [50] and AI is the annual ingestion estimated to be 1350 L year^{-1} (3.7 L day^{-1} $\times$ 365 days) for male and 985 L year^{-1} (2.7 L day^{-1} $\times$ 365 days) for female. The recommended upper limit of the annual effective dose is 1 mSv year^{-1} for general population [51].

As the number of iterations increases in Monte Carlo simulations, the simulation's outcome becomes more stable, resulting in a larger range of possible input values being generated based on the probability distribution of each individual parameter [52-53]. To establish the appropriate statistical distribution types for producing probability distribution functions (PDFs), the input variables/parameters were assessed by the Anderson - Darling and Kolmogorov - Smirnov Test. The simulations took into account the range of possible values for each input as determined by the distribution functions. The distributions of parameters used in the calculations for risk assessment due to uranium contamination are given in table 3.3. The factors contributing to radiological risks include the concentration of uranium (log-normal distribution), the overall period of exposure (point value), the risk factor of uranium (point value) along with water ingestion (normal distribution). For chemical risks, the factors considered are the concentration of uranium (log-normal distribution), water ingestion (normal distribution), body weight (normal distribution), frequency (triangular distribution) as well as the duration of exposure (point value). The iterations are set to 50,000 in MATLAB. Different matrices such as concentration, ingestion rate, body weight, and frequency are pre-allocated to store numbers generated during the iterations. Within each iteration, random numbers are generated from respective distributions.

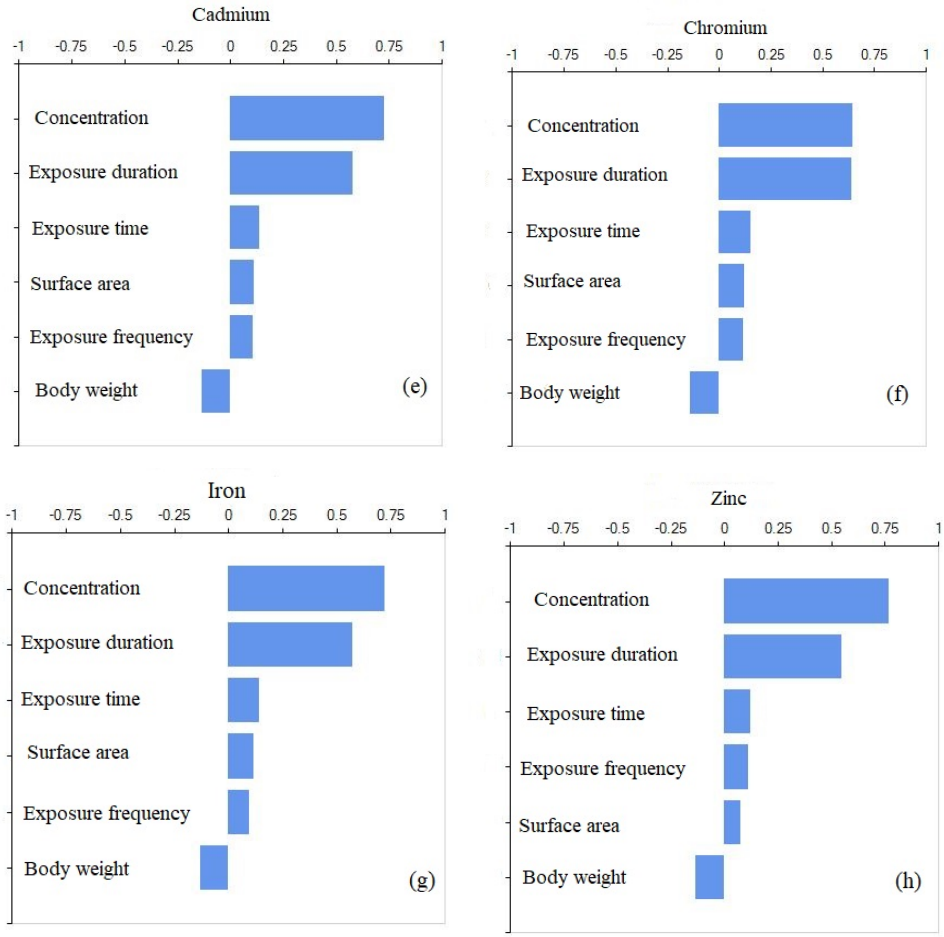

Figure 3.4: The sensitivity analysis for adults in (e), (f), (g) and (h) for dermal contact.

The uranium concentration in each sample exceeds the permissible limit set by WHO of 30 μg L^{-1} [58]. The statistical analysis which includes geometric mean, minimum and maximum using deterministic approach is given in table 3.4. N Sharma *et al.* [59] observed the uranium levels in the groundwater and municipal water supply samples varied from 0.13 to 1340 μg L^{-1} in the Mansa district. Similarly, D Sharma *et al.* [60] found the uranium concentration varying between 2.3 to 357 μg L^{-1} in the same region. However, the northern districts of the state have far less uranium concentration, with the mean uranium concentrations in groundwater samples of Pathankot, Amritsar, in addition to Gurdaspur districts being 3.0 $\mu g\,L^{-1}$, 8.6 $\mu g\,L^{-1}$, and 4.3 $\mu g\,L^{-1}$, respectively [61]. Saini *et al.* [62] reported that the average values recorded in North-East, South West and West Punjab were 4.74 μg L^{-1}, 84.69 μg L^{-1} and 23.86 μg L^{-1}, respectively. The uranium concentration in the study area is evaluated against the concentrations recorded in India and around the world in table 3.5. The current measurements show much higher uranium concentration as compared to other studies. Both male and female genders were taken into consideration for risk assessment. The excess cancer risk (mortality) for the male population is 4.12×10^{-4} and for female population is 3.00×10^{-4}. This indicates that the lifetime chance of cancer is more than 4 in 10,000 for men

Table 3.3: Parameters used for probabilistic and deterministic approach for calculations of risk assessment due to uranium contamination in groundwater.

Parameters	**Probabilistic approach (Distribution)**	**Deterministic approach**	**References**
Uranium concentration (μg L^{-1})	Log normal (154.09±102.48)	Mean	
Risk coefficient (Bq^{-1})	Point	1.13×10^{-9}	[43]
Ingestion rate (L day^{-1})			
Male	Normal (4±0.62)	3.7	
Female	Normal (3±0.37)	2.7	[51-52]
Exposure duration (years)	Point	70	[45]
Average time (days)	Point	25550	[45]
Exposure frequency (day $year^{-1}$)	Triangular 345(180-365)	365	[45,56]
Body weight (kg)			
Male	Normal (52.1±6.5)	51.5	
Female	Normal (45.4±7.0)	44.2	[54,57]

and 3 in 10,000 for women in the population. The male population has a higher excess cancer risk as their ingestion rate is higher in comparison to women. The higher ingestion rate observed in males may be attributed to factors such as their larger body size, which leads to increased food and water consumption rates. The calculated mean values of cancer mortality are higher than the general permissible limit of 10^{-4} [45]. The mean of lifetime average daily dose for males is 11.07 μg kg^{-1} day^{-1} and for females is 9.41 μg kg^{-1} day^{-1}. The mean hazard quotient for male and female population is 18.45 and 15.68, respectively. The hazard quotients due to uranium contamination in water are significantly higher than 1, indicating that the inhabitants in the study area are at substantial danger owing to uranium contamination in the groundwater. The calculated annual effective dose is 0.23 mSv $year^{-1}$, which is below the recommended value of 1 mSv $year^{-1}$ [29]. The health risks due to uranium contamination are calculated using Monte-Carlo simulations with 50,000 iterations in MATLAB. The lifetime average daily dose 5^{th}, 25^{th}, 50^{th}, 75^{th} and 95^{th} percentile of the male population is 2.58, 4.96, 7.77, 12.25 and 23.18 μg kg^{-1} day^{-1}, respectively. Similarly, for the female population lifetime average daily dose of 5^{th} percentile is 2.28 μg kg^{-1} day^{-1}, 25^{th} percentile is 4.34 μg kg^{-1} day^{-1}, 50^{th} percentile is 6.78 μg kg^{-1} day^{-1}, 75^{th} percentile is 10.69 μg kg^{-1} day^{-1} and 95^{th} percentile is 20.17 μg kg^{-1} day^{-1}. The predicted probability function of LADD for male and female population is shown in figure 3.5. The 5^{th} and 95^{th} percentiles are utilised as lower and upper bounds for estimation, rather than relying on the lowest and maximum values, in order to prevent underestimating and overestimation. The predicted probability function hazard quotient for male and female population is shown in figure 3.6. The 5^{th}, 25^{th}, 50^{th}, 75^{th} and 95^{th} percentile of hazard quotient for the male population is 4.36, 8.36, 13.08, 20.45 and 38.25, respectively. The 5^{th}, 25^{th}, 50^{th}, 75^{th} and 95^{th} percentile of hazard quotient for female population is 3.81, 7.27, 11.40, 17.80, 34.26. The predicted probability density function for excess cancer risk is shown in figure 3.7. The excess cancer risk for male population at 5^{th}, 25^{th},

50^{th}, 75^{th} and 95^{th} percentile are 1.31 × 10^{-4}, 2.40 × 10^{-4}, 3.64 × 10^{-4}, 5.59× 10^{-4}, 1.02×10^{-3}, respectively. For female population, 5^{th} percentile of excess cancer risk is 9.95×10^{-5}, 25^{th} percentile is 1. 81×10^{-4}, 50^{th} percentile is 2.74×10^{-4}, 75^{th} percentile is 4.16 ×10^{-4} and 95^{th}percentile is 7.62× 10^{-4}. The excess cancer risk for all male population is above the limit of 10^{-4} [45], whereas, only 5% of the women population is below the recommended limit. The 95^{th} percentile value of excess cancer risk male population shows that 10 in 10,000 men are at risk of cancer, and for female, it is around 8 in 10,000 population. The 5^{th}, 25^{th}, 50^{th}, 75^{th} and 95^{th} percentile of annual effective dose for male population is 0.74 mSv $year^{-1}$, 1.35 mSv $year^{-1}$, 2.08 mSv $year^{-1}$, 3.18 mSv $year^{-1}$ and 5.79 mSv $year^{-1}$, respectively. The 5^{th}, 25^{th}, 50^{th}, 75^{th} and 95^{th} percentile of annual effective dose for female population is 0.56 mSv $year^{-1}$, 1.03 mSv $year^{-1}$, 1.56 mSv $year^{-1}$, 2.37 mSv $year^{-1}$ and 4.33 mSv $year^{-1}$. The annual effective dose of 25^{th} percentile population is lower than the recommended dose of 1.0 mSv $year^{-1}$ [29]. The predicted probability function of annual effective dose for male and female population is shown in figure 3.8. Given the numerous characteristics involved in health risk assessment, identifying the most effective parameter can aid in gaining a better understanding of risk causing parameters [63]. The assessment of uncertainty is conducted by sensitivity analysis, which involves determining the impact of various input factors on the resulting conclusions [64]. As a result, a sensitivity analysis was conducted to rank the potential health effects caused by various input variables and their respective contributions. The sensitivity analysis using probabilistic parameters for calculating LADD for 50,000 iterations for Pearson correlation was done using MATLAB (R2023b). The results are presented as bar graphs in figure 3.9. The primary factor that has the greatest impact on both male and female populations is the concentration of uranium in groundwater, followed by ingestion and exposure frequency. The Pearson correlation between LADD and the concentration of uranium in groundwater is 0.92 for male and female. Similarly, the Pearson correlation between LADD and ingestion rate is 0.20 for male and 0.17 for female population. Exposure frequency and LADD have Pearson correlation of 0.19 for male and female, respectively. The body weight and LADD has negative correlation for both the male and female population.

Table 3.4: Descriptive statistics of the study region using a deterministic approach.

Parameter	**Geometric Mean**	**Minimum**	**Maximum**
Uranium concentration (μg L^{-1})	127.79	43.43	449.79
LADD (μg kg^{-1} day^{-1}) (Male)	9.18	3.12	32.31
LADD (μg kg^{-1} day^{-1}) (Female)	7.80	2.65	27.47
HQ (Male)	15.30	5.20	53.85
HQ (Female)	13.01	4.42	45.79
AED (μSv $year^{-1}$) (Male)	194.08	65.95	683.11
AED (μSv $year^{-1}$) (Female)	141.60	48.12	498.42

Table 3.5: Comparison of uranium concentration of the study area to India and world.

Location	**Concentration (μg L^{-1})**	**References**
Mansa	43.43 - 449.79	Present study
Jhajjar (Haryana)	5 - 91	[65]
Chattisgarh	0.5 - 26.4	[66]
Rajasthan	5 - 145	[67]
Austria	0.05 - 160	[68]
Germany	0.006 - 42.33	[69]
Turkey	0.05 - 900	[70]

3.4 Spatial Analysis of heavy metals

The spatial distribution is determined using QGIS 3.16 Hannover, utilising the inverse distance weighting interpolation approach. This method calculates the distribution based on the distance between the sites. This approach estimates the value at a particular location by considering the values at nearby known sites distributed around that point of interest. The spatial graphs are plotted for cadmium, chromium, zinc and iron in addition to uranium contamination. The spatial distribution for Cd, Cr, Zn and Fe contamination in groundwater of Mansa district is shown in figure 3.10. The natural factors and human activities add to the elevated concentrations of heavy metals in Mansa district (Punjab). The presence of trace metals in groundwater is controlled by natural factors such as aquifer type, severity of mineral weathering from the aquifer, frequency of precipitation, quality of infiltrating water along with physicochemical attributes, the leaching of subsurface contaminants as well as the mineral contents of underlying bedrock and sediments [70]. The arid and semiarid regions are facing increased water scarcity, not only because of low water availability but also due to poor water quality caused by both ongoing climate change and extensive human activity. Moreover, the application of fertilisers and pesticides in agriculture has resulted in the seepage of these heavy metals into groundwater. Mansa, characterised by a flat agricultural landscape, has experienced significant industrial growth during the past twenty years. Anthropogenic chromium mostly refers to the release of chromium in the form of Cr(VI). Industrial waste generated by refractory manufacturing, coal burning, dyes, wood preservation, leather tanning, and textile industries could be the reason for high chromium in groundwater [71]. Chromium-based compounds, which are a result of industrial activity get mixed with surface water and subsequently seep into the groundwater. Similarly, cadmium in groundwater has anthropogenic sources such as the deposition of combustion emissions and the utilisation of phosphate fertilisers [52]. The presence of iron in groundwater can represent significant risks, but in the study region, iron is well under the permissible limit of 0.3 mg L^{-1}. Fertilisers and pesticides can contribute to the poisoning of groundwater with zinc. Zinc is emitted into the environment from several sources such as metal production, coal combustion, waste incineration and the degradation of rubber tyres on vehicles [72].

The key determinants affecting the level of uranium in groundwater are the concentra-

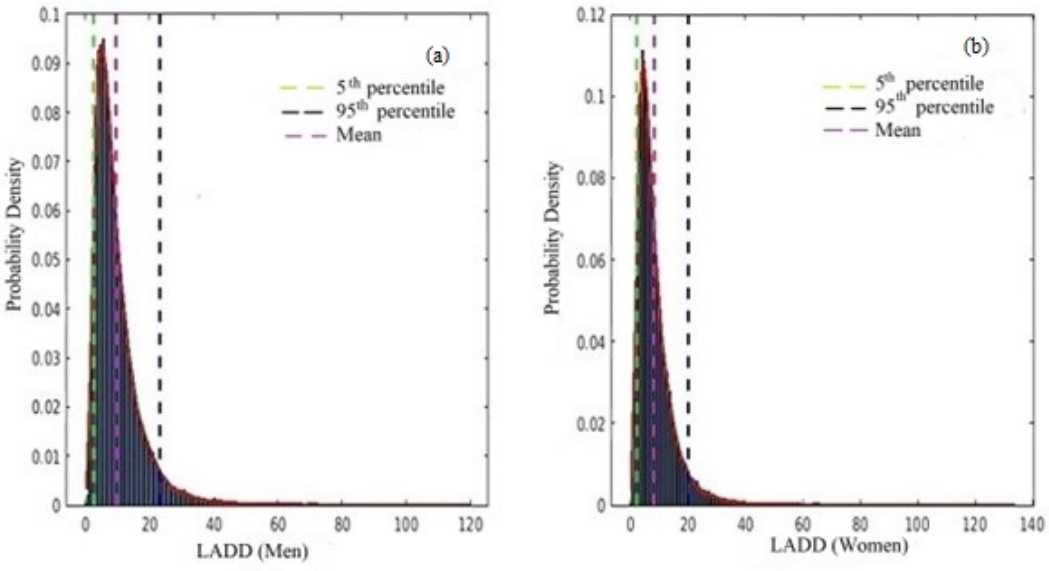

Figure 3.5: The probability density function for LADD (a) male and (b) female using Monte-Carlo simulations with 50,000 iterations due to uranium contamination in groundwater.

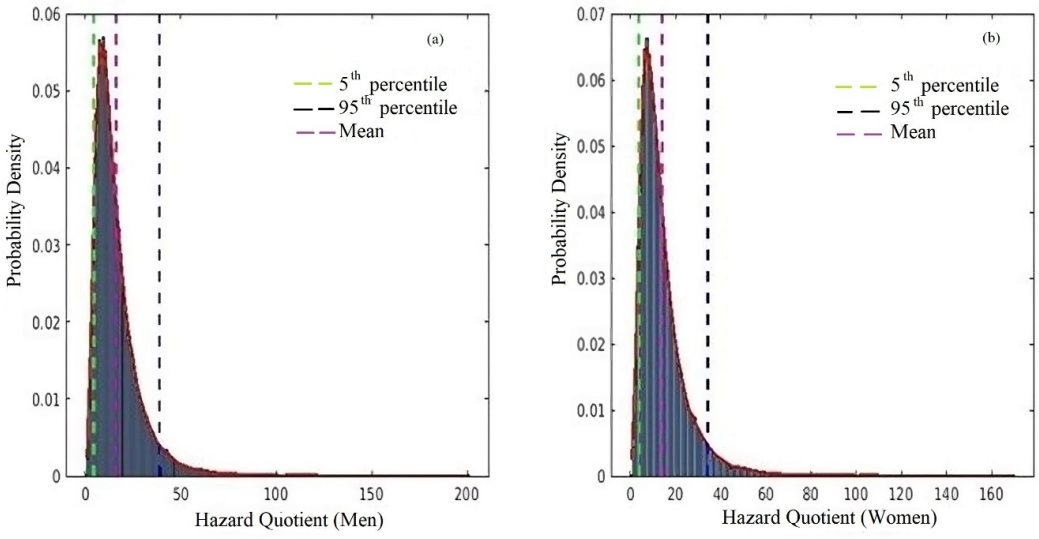

Figure 3.6: The probability density function for hazard quotient (a) male and (b) female using Monte-Carlo simulations with 50,000 iterations due to uranium contamination in groundwater.

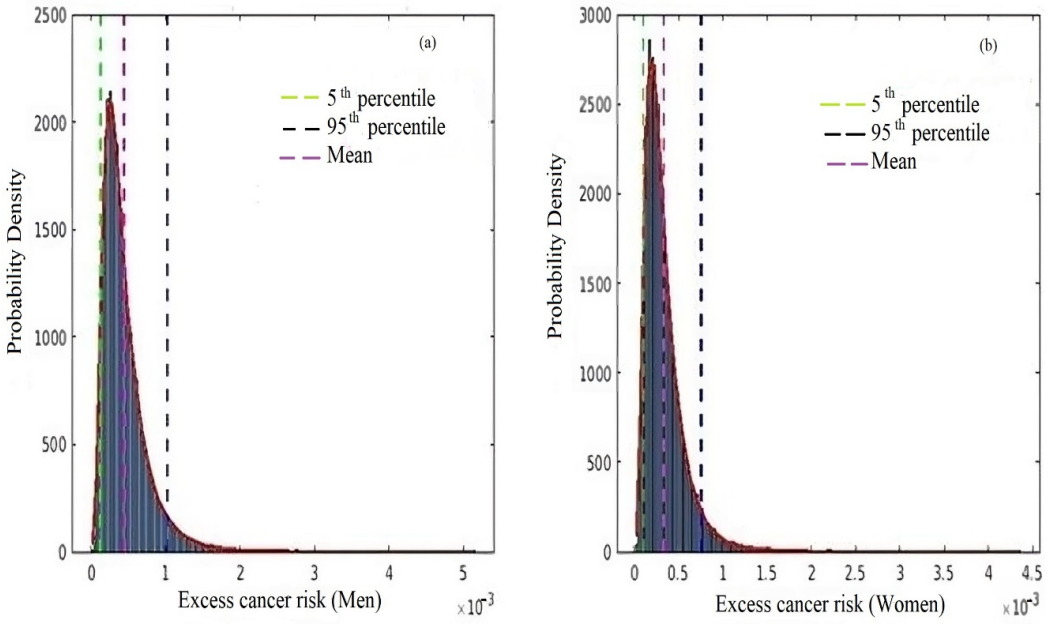

Figure 3.7: The probability density function for excess cancer risk (a) male and (b) female using Monte-Carlo simulations with 50,000 iterations due to uranium contamination in groundwater.

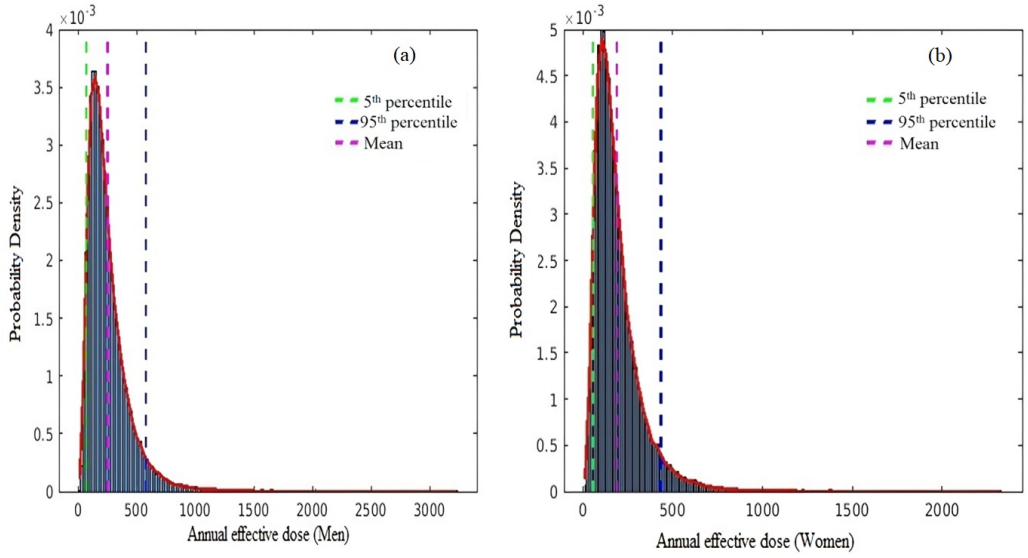

Figure 3.8: The probability density function for annual effective dose (a) male and (b) female using Monte-Carlo simulations with 50,000 iterations due to uranium contamination in groundwater.

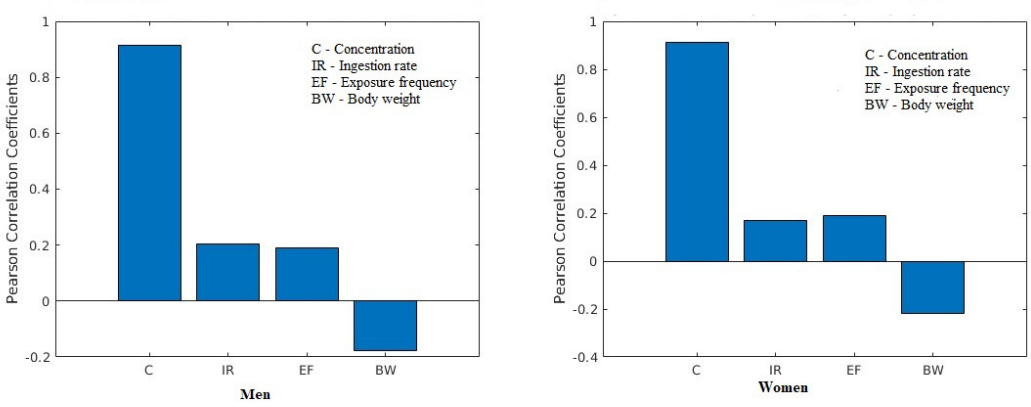

Figure 3.9: Sensitivity analysis of various parameters used in assessment of non-carcinogenic risk for men and women.

tion of uranium in the source rock, sediments/soils, and its leachability. Furthermore, the close proximity of water to rocks or minerals containing uranium, impacts the uranium concentration in groundwater. The pH and oxidation of water increase the solubility of uranium in water [73]. The spatial distribution of uranium contamination of groundwater in Mansa district is shown in figure 3.11. The groundwater of the district is significantly contaminated with uranium values greater than WHO limits [67]. The apex of the topography is situated in the middle vicinity, namely in Mansa and Budhlada, while the lowest elevation is found in the southeastern area. These variations in elevation are indicative of the topographic gradients. The hydraulic gradient is significant in the middle section due to the nature of formations in the northeastern half and the presence of finer sediments in the southeastern part [18]. The spatial distribution graph indicates a progressive rise in the concentration of uranium in the south-west direction. The current situation may be influenced by various factors, including regional groundwater flow and an increased groundwater table due to water logging [75].

The soaring levels of uranium could be due to the geology of the region. The elevated uranium levels in groundwater could be primarily caused by the release of uranium from the granitic rocks as well as pegmatites in the Himalayan region. This uranium is carried by rivers and accumulates in the alluvial aquifers of Punjab. The increased concentrations of uranium in these regions can also be linked to the presence of radioactive granitic rock formations in the Tosham hills of the neighbouring state of Haryana [74]. The uranium concentration in the sediments of Mansa district varies from 0.5 to 4.5 ppm, above the typical crustal abundance of 2.8 ppm [76]. Moreover, the groundwater in the region has alkaline pH, high bicarbonate levels and high electrical conductivity, which promote the solubility and movement of uranium in the aquifer [60]. The geo-spatial studies have confirmed the presence of calcium carbonate (kankers), which reacts with carbonic acid generated due to plant root respiration resulting in bicarbonate, that releases adsorbed uranium from the soil, further increasing uranium concentration in groundwater [62,65]. The possible source of high uranium concentration in Mansa could also be the utilization of phosphate fertilizers as this area is the cotton belt of Punjab. The long and continuous use of these fertilizers enhances the radionuclide concentration in the soil [77-78]. The

uranium contamination is more prevalent in shallow depths, while deeper aquifers exhibit lower levels of contamination, as shown in figure 3.12. Sahoo *et al.* [79] and Rishi *et al.* [80] reported comparable findings on southwest Punjab. While the quantities of dissolved uranium in deep zone groundwater are lower than those in shallow zone groundwater, they nevertheless exceed the recommended value set by the WHO for drinking purposes. The geology of the region reveals the presence of a distinct thick clay zone that serves as a boundary between the more recent and older alluvium [16, 80].

3.5 Conclusion

The risk assessment due to heavy metal contamination of groundwater is carried out using deterministic and probabilistic approaches for Mansa, Punjab. The hazard index using both approaches is greater than 1 for children and adults. However, the upper bounds of the probabilistic approach are greater than those using the deterministic approach. As a result, it is recommended that, if possible, probabilistic analysis should be used to estimate groundwater quality or associated contamination risk in order to better depict the actual scenario by accounting for variability. The evaluation of health risks indicated that children exhibit a greater susceptibility to health-related dangers compared to adults due to their lower body weight. The sensitivity analysis revealed that the concentration of heavy metals is the highest factor impacting the non-carcinogenic health risk assessment. Furthermore, the groundwater in the research area is deemed contaminated. The analysis also unveiled a significant level of uranium contamination in the groundwater, posing consequential health hazards to the people. The uranium concentration in all the samples is above the safe threshold established by the WHO. Both male and female population are at risk of developing cancer in the study area and are at chemical risk due to uranium with hazard quotient of 38.95 and 34.26, respectively, at 95^{th} percentile. The utilisation of probability-based assessment provided us with valuable insights such as the impact of concentration of uranium being highest on the risk assessment parameters. Although Monte-Carlo simulations have advantages but they can be intricate and necessitate a thorough comprehension of statistical methodologies. Moreover, exposure factors derived from short-term studies involving a large number of individuals may not precisely reflect long-term situations in small groups. Effective regulatory measures and their rigorous implementation, along with ongoing surveillance, are necessary to mitigate the health hazards faced by the population. If it is utilised for drinking and irrigation without proper pre-treatment for prolonged durations, it can present a substantial health risk. Furthermore, it is imperative to analyse the potential consequences of heavy metal pollution and devise a comprehensive plan for long-term restoration.

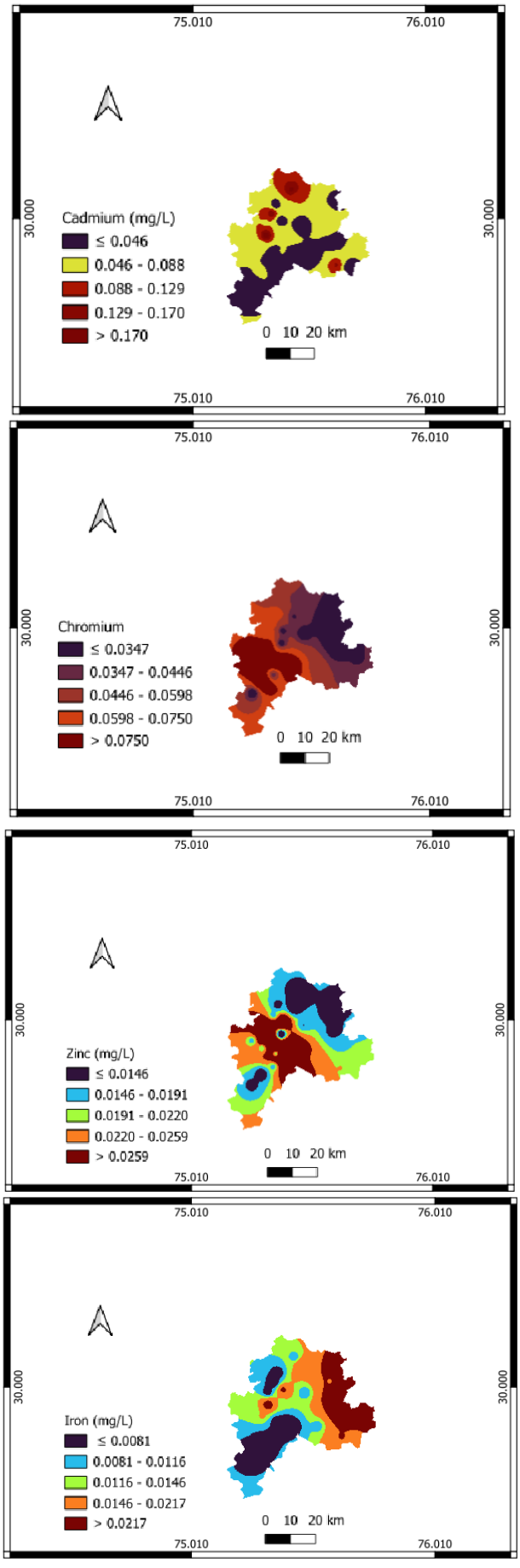

Figure 3.10: Spatial distribution of cadmium, chromium, zinc and iron in Mansa district, Punjab.

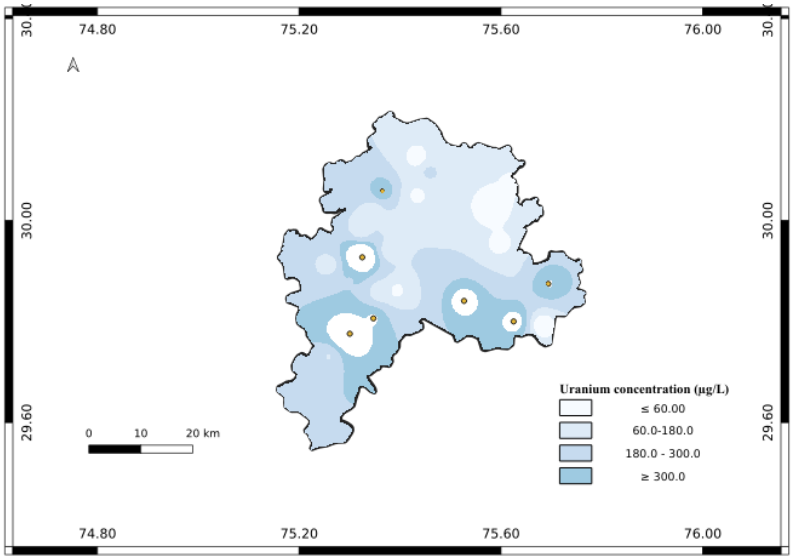

Figure 3.11: Spatial distribution of uranium contamination in groundwater of Mansa district.

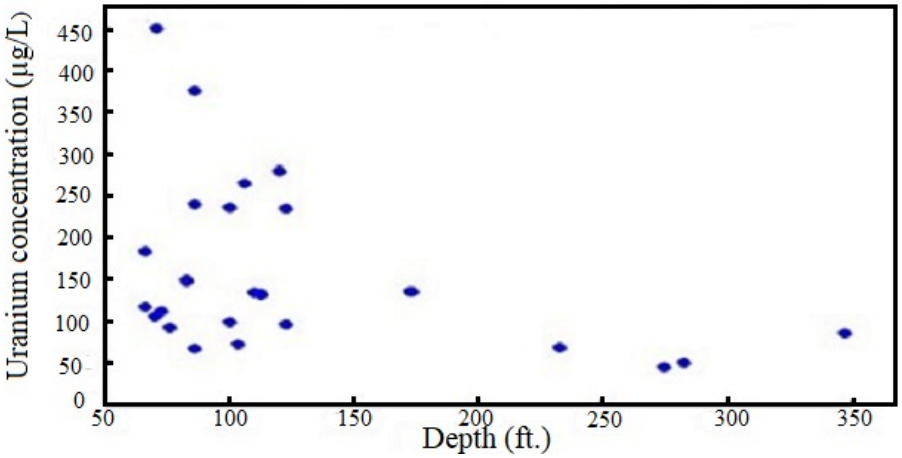

Figure 3.12: The variation of uranium contamination in groundwater with depth.

3.6 References

1. UNESCO (2023). The United Nations World Water Development Report.
2. UNESCO (2020). United Nations World Water Development Report 2020: Water and Climate Change. UNESCO, Paris, France.
3. Bradl, H. (Ed.). (2005). *Heavy metals in the environment: origin, interaction and remediation*. Elsevier.
4. Zhu, Y., Fan, W., Zhou, T., & Li, X. (2019). Removal of chelated heavy metals from aqueous solution: A review of current methods and mechanisms. *Science of the total environment*, *678*, 253-266.
5. Cuschieri, A., Azzopardi, J. I., & Blundell, R. (2023). Effect of Non-essential Heavy Metals on Human Health. In *Heavy Metals in the Environment: Management strategies for global pollution* (pp. 117-133).
6. van Swelm, R. P., Wetzels, J. F., & Swinkels, D. W. (2020). The multifaceted role of iron in renal health and disease. *Nature reviews nephrology*, *16*(2), 77-98.
7. Singh, K. B., & Taneja, S. K. (2009). Hazard effects of excess of zinc in diet. *Science vision*, *9*, 159-65.
8. Charkiewicz, A. E., Omeljaniuk, W. J., Nowak, K., Garley, M., & Nikliński, J. (2023). Cadmium Toxicity and Health Effects—A Brief Summary. *Molecules*, *28*(18), 6620.
9. Balaram, V., Rani, A., & Rathore, D. P. S. (2022). Uranium in groundwater in parts of India and world: A comprehensive review of sources, impact to the environment and human health, analytical techniques, and mitigation technologies. *Geosystems and geoenvironment*, *1*(2), 100043.
10. Waseem, A., Ullah, H., Rauf, M. K., & Ahmad, I. (2015). Distribution of natural uranium in surface and groundwater resources: a review. *Critical reviews in environmental science and technology*, *45*(22), 2391-2423.
11. Bala, R., & Das, D. (2022). Occurrence and behaviour of uranium in the groundwater and potential health risk associated in semi-arid region of Punjab, India. Groundwater sustainable development 17: 100731.
12. Hindustan Times, *Water in 29% wells in Punjab has uranium concentration* Water in 29% wells in Punjab has uranium concentration - Hindustan Times
13. The Hindu, *Groundwater contaminated, Punjab battles uranium curse* Groundwater contaminated, Punjab battles uranium curse - The Hindu
14. Singh, S., Rani, A., Mahajan, R. K., & Walia, T. P. S. (2003). Analysis of uranium and its correlation with some physico-chemical properties of drinking water samples from Amritsar, Punjab. *Journal of environmental monitoring*, *5*(6), 917-921.
15. Kumar, M., Prasher, S., & Singh, S. (2009). Uranium analysis in some food samples collected from Bathinda area of Punjab, India. *Indian journal of physics*, *83*, 1045-1050.

16. Singh, L., Kumar, R., Kumar, S., Bajwa, B. S., & Singh, S. (2013). Health risk assessments due to uranium contamination of drinking water in Bathinda region, Punjab state, India. *Radioprotection*, *48*(2), 191-202.

17. Shrivastava, B. K. (2015). Elevated uranium and toxic elements concentration in groundwater in Punjab state of India: extent of the problem and risk due to consumption of unsafe drinking water. *Water quality, exposure and health*, *7*(3), 407-421.

18. H.S. Virk (2017). Heavy Metals Contamination of Groundwater in Patiala District of Punjab State, India Research and reviews: A journal of toxicology 7:6-11.

19. Verma, M., & Loganathan, V. A. (2023). Hydrogeochemical constraints on uranium contamination of groundwater for drinking water supplies and associated health risks. *Groundwater for sustainable development*, *23*, 100973.

20. Kaur Guron, B., Kalkal, S., & Mehra, R. (2024). The impact of uranium contamination in groundwater on human health: a toxicological risk assessment. *International journal of environmental analytical chemistry*, 1-15.

21. Chen, H., Wang, L., Hu, B., Xu, J., & Liu, X. (2022). Potential driving forces and probabilistic health risks of heavy metal accumulation in the soils from an e-waste area, southeast China. *Chemosphere*, *289*, 133182.

22. Giri, S., Singh, A. K., & Mahato, M. K. (2020). Monte Carlo simulation-based probabilistic health risk assessment of metals in groundwater via ingestion pathway in the mining areas of Singhbhum copper belt, India. *International journal of environmental health research*, *30*(4), 447-460.

23. CGWB, *Ground water information booklet Mansa district, Punjab. Ministry of Water Resources, River Development & Ganga Rejuvenation, Government of India* (2013). cgwb.gov.in/old_website/District_Profile/Punjab/Mansa.pdf.

24. Chopra, R. P. S., & Krishan, G. (2014). Analysis of aquifer characteristics and groundwater quality in southwest Punjab, India. *Journal of earth science and engineering*, *4*(10), 597-604.

25. Chander, S., Bansal, S., Sharma, K., Dhiman, D., & Paikaray, S. (2021, November). Hydrogeochemical Perspective of Groundwater of Southwest Punjab, India. In *international conference on Mediterranean geosciences union* (pp. 61-65). Cham: Springer Nature Switzerland.

26. CGWB (2017). *Aquifer mapping and management plan Mansa district, Punjab.*

27. Sharma, T., Litoria, P. K., Bajwa, B. S., & Kaur, I. (2021). Appraisal of groundwater quality and associated risks in Mansa district (Punjab, India). *Environmental monitoring and assessment*, *193*, 1-21.

28. USEPA (2001) Reference Dose for Chronic Oral Exposure [EB/OL]. [2011-03-20]. http://www.epa.gov/ncea/iris/subst/0076.htm

29. Gupta, S., & Gupta, S. K. (2023). Application of Monte-Carlo simulation for carcinogenic and non-carcinogenic risks assessment through multi-exposure

pathways of heavy metals of river water and sediment, India. *Environmental geochemistry and health*, *45*(6), 3465-3486.

30. NNMB (2002) Diet and nutritional status of rural population Technical report no. 21.

31. USEPA (2011) Exposure factors handbook

32. Smith, R. L. (1994). Use of Monte-Carlo simulation for human exposure assessment at a superfund site. *Risk analysis*, *14*(4), 433-439.

33. Saha, N., Rahman, M. S., Ahmed, M. B., Zhou, J. L., Ngo, H. H., & Guo, W. (2017). Industrial metal pollution in water and probabilistic assessment of human health risk. *Journal of environmental management*, *185*, 70-78.

34. USEPA (2004). National Recommended Water Quality Criteria.

35. Mukherjee, I., Singh, U. K., Singh, R. P., Kumari, D., Jha, P. K., & Mehta, P. (2020). Characterization of heavy metal pollution in an anthropogenically and geologically influenced semi-arid region of east India and assessment of ecological and human health risks. *Science of the Total Environment*, *705*, 135801.

36. WHO (2022). Guidelines for drinking-water quality incorporating the first and second addenda. 4$^{\text{th}}$ Edition. *WHO chronicle*.

37. WHO. (2020). Chromium in drinking-water.

38. USEPA (2017). Secondary drinking water standards: Guidance for nuisance chemicals. *Drinking Water Contaminants-Standards and Regulations*.

39. Bajwa, B. S., Kumar, S., Singh, S., Sahoo, S. K., & Tripathi, R. M. (2017). Uranium and other heavy toxic elements distribution in the drinking water samples of SW-Punjab, India. *Journal of radiation research and applied sciences*, *10*(1), 13-19.

40. Zhang Z, Cao H, Song N, Zhang L, Cao Y, Tai J (2020b) Long-term hexavalent chromium exposure facilitates colorectal cancer in mice associated with changes in gut microbiota composition. *Food chemical toxicology*, *138*:111237

41. Astuti, R.D.P., Mallongi, A., Amiruddin, R. R., Hatta, M., & Rauf, A. U. (2023). Hexavalent chromium contamination in groundwater and its implication to human health: a Monte-Carlo model approach in Indonesia. *Sustainable water resource management.* 9, 2.

42. Idrees, N., Tabassum, B., Abd_Allah, E. F., Hashem, A., Sarah, R., & Hashim, M. (2018). Groundwater contamination with cadmium concentrations in some West UP Regions, India. *Saudi journal of biological sciences*, *25*(7), 1365-1368.

43. USEPA (1999). *Cancer risk coefficients for environmental exposure to radionuclides*. Federal Guidance *Report No* 13.

44. Rani, A., Parashar, K., Meena, R., Sharma, S. K., Tiwari, K. K., Ajaykumar, V., & Mondal, N. C. (2023). Hydrochemical characteristics and potential health risks of nitrate, fluoride, and uranium in Kota district, Rajasthan, India. *Environmental science and pollution research*, *30*(34), 82485-82505.

45. USEPA (2019). *Update for Chapter 3 of the Exposure Factors Handbook Ingestion of Water and Other Select Liquid.*

46. Ramesh, R., Subramanian, M., Lakshmanan, E., Subramaniyan, A., & Ganesan, G. (2021). Human health risk assessment using Monte Carlo simulations for groundwater with uranium in southern India. *Ecotoxicology and environmental safety*, *226*, 112781.

47. Freni, S. C. (1987). Application of estimated excess lifetime cancer risk in field situations. *Uncertainty in risk assessment, risk management, and decision making*, 339-347.

48. ATDSR, *Public health assessment guidance manual* (2005).

49. Archana, & Singh, J. (2021). Uranium estimation, radiation dose assessment and physico-chemical parametric study of ground water in Tarn Taran District, Punjab State, India. *Journal of radioanalytical and nuclear chemistry*, *330*, 1445-1452.

50. Eckerman, K., Harrison, J., Menzel, H. G., & Clement, C. H. (2012). ICRP publication 119: compendium of dose coefficients based on ICRP publication 60. *Annals of the ICRP*, *41*, 1-130.

51. ICRP, *The 2007 Recommendations of the International Commission on Radiological Protection.* ICRP Publication 103. Ann. ICRP 37 (2-4) (2007).

52. Kubier, A., Richard T. Wilkin, and T. Pichler (2019). Cadmium in soils and groundwater: A review. *Applied geochemistry.* Elsevier Science Ltd, New York, NY, 108:104388.

53. Mallongi, A., Rauf, A. U., Daud, A., Hatta, M., Al-Madhoun, W., Amiruddin, R.,& Astuti, R. D. P. (2022). Health risk assessment of potentially toxic elements in Maros karst groundwater: a Monte Carlo simulation approach. *Geomatics, natural hazards and risk*, *13*(1), 338-363.

54. Rahman, M. M., Sengupta, M. K., Ahamed, S., Chowdhury, U. K., Hossain, M. A., Das, B., & Chakraborti, D. (2005). The magnitude of arsenic contamination in groundwater and its health effects to the inhabitants of the Jalangi—one of the 85 arsenic affected blocks in West Bengal, India. *Science of the total environment*, *338*(3), 189-200.

55. H.S. Dang, D.D. Jaiswal, M. Parameswaran, S. Krishnamony, *Physical, Anatomical, Physiological and Metabolic data for reference Indian man-a proposal* (No. BARC--1994/E/043) Bhabha Atomic Research Centre (1994).

56. Smith, R. L. (1994). Use of Monte Carlo simulation for human exposure assessment at a superfund site. *Risk Analysis*, *14*(4), 433-439.

57. ICMR, *Nutrient requirements and dietary inta*ke, National Institute of Nutrition (2009).

58. WHO, *Guidelines for drinking-water quality: fourth edition incorporating the first addendum* (2017).

59. Sharma, N., & Singh, J. (2016). Radiological and chemical risk assessment due to high uranium contents observed in the ground waters of Mansa District (Malwa region) of Punjab state, India: an area of high cancer incidence. *Exposure and health*, *8*, 513-525.

60. Sharma, D. A., Rishi, M. S., Keesari, T., Pant, D., Singh, R., Thakur, N., & Sinha, U. K. (2017). Distribution of uranium in groundwaters of Bathinda and Mansa districts of Punjab, India: inferences from an isotope hydrochemical study. *Journal of radioanalytical and nuclear chemistry*, *313*, 625-633.

61. Sharma, T., Sharma, A., Kaur, I., Mahajan, R. K., Litoria, P. K., Sahoo, S. K., & Bajwa, B. S. (2019). Uranium distribution in groundwater and assessment of age dependent radiation dose in Amritsar, Gurdaspur and Pathankot districts of Punjab, India. *Chemosphere*, *219*, 607-616.

62. Saini, K., Singh, P., & Bajwa, B. S. (2016). Comparative statistical analysis of carcinogenic and non-carcinogenic effects of uranium in groundwater samples from different regions of Punjab, India. *Applied radiation and isotopes*, *118*, 196-202.

63. Soleimani, H., Azhdarpoor, A., Hashemi, H., Radfard, M., Nasri, O., Ghoochani, M., & Mahvi, A. H. (2022). Probabilistic and deterministic approaches to estimation of non-carcinogenic human health risk due to heavy metals in groundwater resources of torbat heydariyeh, southeastern of Iran. *International journal of environmental analytical chemistry*, *102*(11), 2536-2550.

64. Tarafdar, A., & Sinha, A. (2017). Cancer risk assessment of polycyclic aromatic hydrocarbons in the soils and sediments of India: a meta-analysis. *Environmental management*, *60*(4), 784-795.

65. Kumari, A., Panghal, A., Singh, B., Kataria, N., Dhiman, R., Rani, S., & Dalal, R. (2023). Analysis of Natural Uranium in Groundwater of Jhajjar District of Haryana, India using LED Fluorimeter. *Indian journal of Pure & Applied Physics*, *61*, 934-937.

66. Singh, M., Sahu, P., Tapadia, K., & Jhariya, D. (2022). Assessment of the groundwater quality by using multivariate approach and non-carcinogenic risk of uranium in the inhabitants of the Bastar district, Chhattisgarh, Central India. *Water supply*, *22*(4), 3863-3878.

67. Pant, D., Keesari, T., Roy, A., Sinha, U. K., Singh, M., Jain, S. K., & Tripathi, R. M. (2019). Study on groundwater quality in parts of Rajasthan with special reference to uranium contamination. *Journal of radioanalytical and nuclear chemistry*, *322*, 165-171.

68. Gruber, V., Maringer, F. J., & Landstetter, C. (2009). Radon and other natural radionuclides in drinking water in Austria: measurement and assessment. *Applied radiation and isotopes*, *67*(5), 913-917.

69. Post, V. E. A., Vassolo, S. I., Tiberghien, C., Baranyikwa, D., & Miburo, D. (2017). Weathering and evaporation controls on dissolved uranium concentrations in groundwater–A case study from northern Burundi. *Science of the total*

environment, *607*, 281-293.

70. Vu, C. T., Lin, C., Shern, C. C., Yeh, G., & Tran, H. T. (2017). Contamination, ecological risk and source apportionment of heavy metals in sediments and water of a contaminated river in Taiwan. *Ecological indicators*, *82*, 32-42.

71. Krishan, G., Taloor, A.K., Sudarsan, N., Bhattacharya, P., Kumar, S., Ghosh, N.C., Singh, S., Sharma, A., Rao, M.S., Mittal, S. and Sidhu, B.S., (2021). *Groundwater for sustainable development.*

72. Sharifi, S.A., Zaeimdar, M., Jozi, S.A. *et al.* Effects of Soil, Water and Air Pollution with Heavy Metal Ions Around Lead and Zinc Mining and Processing Factories. *Water air soil pollution 234*, 760 (2023).

73. Daniel, R., Tripathi, D., Singh, S., Sharma, N., Yuvraaj, A., Katyal, D., & Kumar, V. (2022). Uranium: occurrence, distribution across India and its potential health effects. *Journal of radioanalytical and nuclear chemistry*, *331*(7), 2805-2815.

74. WHO (2017). *Guidelines for drinking-water quality: fourth edition incorporating the first addendum.*

75. Karanveer, Bala, R., & Das, D. (2022). Geochemical and health risk assessment of potentially toxic trace elements and nitrate via groundwater in agro-ecosystem of alluvial plain Punjab, India. *Human and ecological risk assessment: An international journal*, *28*(9), 983-1011.

76. Chen, H., Wang, L., Hu, B., Xu, J., & Liu, X. (2022). Potential driving forces and probabilistic health risks of heavy metal accumulation in the soils from an e-waste area, southeast China. *Chemosphere*, *289*, 133182.

77. Boukhenfouf, W., & Boucenna, A. (2011). The radioactivity measurements in soils and fertilizers using gamma spectrometry technique. *Journal of environmental radioactivity*, *102*(4), 336-339.

78. Al-Jundi, J., Al-Ahmad, N., Shehadeh, H., Afaneh, F., Maghrabi, M., Gerstmann, U., & Oeh, U. (2008). Investigations on the activity concentrations of ^{238}U, ^{226}Ra, ^{228}Ra, ^{210}Pb and ^{40}K in Jordan phosphogypsum and fertilizers. *Radiation protection dosimetry*, *131*(4), 449-454.

79. Sahoo, P. K., Virk, H. S., Powell, M. A., Kumar, R., Pattanaik, J. K., Salomão, G. N., & Tiwari, R. P. (2022). Meta-analysis of uranium contamination in groundwater of the alluvial plains of Punjab, northwest India: Status, health risk, and hydrogeochemical processes. *Science of the total environment*, *807*, 151753.

80. Rishi, M. S., Keesari, T., Sharma, D. A., Pant, D., & Sinha, U. K. (2017). Spatial trends in uranium distribution in groundwaters of Southwest Punjab, India-A hydrochemical perspective. *Journal of radioanalytical and nuclear chemistry*, *311*, 1937-1945.

Chapter 4

Biokinetic modelling of uranium

All living beings are exposed to naturally occurring radionuclides. Uranium (^{238}U), identified as a primordial radionuclide, can form water-soluble compounds, facilitating its absorption into the human body via dietary intake and drinking water. This chapter commences with an introduction followed by the sampling procedure in section 4.2. The biokinetic model of uranium is described thereafter. The Pearson correlation and principal component analysis are also conducted to correlate uranium with other physico-chemical properties of water.

4.1 Introduction

Naturally occurring radionuclide materials (NORM) possess great health risk and uranium, being the primordial nucleus, because of its radioactive nature and chemical toxicity (heavy metal), engenders carcinogenic and non-carcinogenic health hazards [1]. The water-soluble uranium compounds like uranium hexafluoride and tetrachloride, uranyl nitrate, and fluoride lead to acute systematic effects whereas the insoluble uranium compounds, namely uranium peroxide, dioxide and trioxide are of the least concern. High uranium intake via ingestion can impair proximal tubes and cause renal failure [2-3]. Severe nausea, diarrhoea, vomiting and paralytic ileus can occur due to continuous uranium intake [4]. Van Gerwen *et al.* [5] established a notable correlation between elevated thyroglobin antibodies and uranium levels in urine. Uranium can accumulate in human bones [6]. Although the consequences of uranium on human reproductive organs are not well established but Wang et al. [7] observed it deteriorates fertility and lowers the level of sex hormones.

The sources of radiation of naturally occurring radioisotopes are terrestrial, which includes uranium mining, nuclear accidents, fertilizer production and cosmogenic, contributing to human exposure [8-11]. Uranium is found in rocks, water and soil [12]. Uranium reaches groundwater by desorption of adsorbed uranium from mineral surfaces and mineral dissolution [13]. It exists in different oxidation states in an aqueous solution. Uranium (VI) is easily found in the environment, whereas uranium (IV) governs in reducing environment with redox potential, $E_h < 200$ mV in waterlogged/wet soil. The higher solubility of uranium (VI) as a uranyl compound is

caused by its capacity of forming stable complexes with various organic as well as inorganic ligands [14-16]. Uranium (VI) is reduced to uranium (IV) in groundwater systems on reaction with compatible reductants [17]. Physico-chemical properties of water such as pH, total dissolved salts (TDS), salinity and conductivity give in-situ details of water quality [18]. These properties impact the uranium concentration in groundwater [19]. The most common route for uranium ingestion is by drinking water, which makes up a significant part of toxicological and radiological risks to human beings and being an alpha particle emitter, intense DNA damage can be caused when the concentration of uranium is extremely high [20]. Therefore, experimental and epidemiological research has been in focus from the past several decades, and various models are proposed [21-26] to delineate the consequences of uranium on the human body. The previous biokinetic model proposed by ICRP [26] was modified by Li *et al.* [27] to include the hair compartment as an excretion pathway. The groundwater usage is at the utmost in India, with 251 km^3 yr^{-1} [28]. Groundwater is the elementary source of drinking water, along with agricultural and industrial utilisation [29]. The safe limit of uranium intake through water set by the world health organisation (WHO) is 30 μg L^{-1} [30], whereas the Atomic Energy Regulatory Board of India has set the limit to 60 µg L^{-1} [31]. The overall crude cancer incidence rate for the population in Punjab is 144.0/lakh which is one of the highest crude cancer incidence rates in India [32]. The four districts, which include Mansa, Bathinda, Faridkot and Muktsar of Malwa region, have higher cancer rates [33]. The soaring cancer cases can be linked with enhanced uranium concentration in groundwater [20, 34-35]. Therefore,

(a) the biokinetics of uranium in human body using the hair compartment model is investigated in the Mansa district, Punjab, India.

(b) the annual effective radiation dose for various body organs is also estimated which could act as potential bio-indicators.

(c) the relationship of uranium contamination in groundwater with physico-chemical properties using Pearson correlation and principal component analysis is assessed.

4.2 Materials and methods

4.2.1 Geomorphology and soil characteristics

The Mansa district is roughly triangular, situated in the southern part of geosyncline Punjab, India. The area is close to the trans-Aravali Vindhyan basin and the basement rocks descend from Tusam to Bathinda [36]. The water elevation varies from 210 to 217 m above the mean sea level, with quality variations from fresh to highly saline. All five blocks of the district: Mansa, Bhikhi, Budhlada, Jhunir and Sardulgarh are over-exploited, leading to the depletion of groundwater resources [37]. The detailed geomorphology of the study region is given in chapter 1 and chapter 3.

4.2.2 Sampling procedure and measurement

A minimum of three samples were collected from each of the 26 locations. In total, 79 samples were collected at the beginning of the winter season. The water is used for drinking purposes for humans and cattle in addition to irrigation purposes. The

in-depth sampling procedure is discussed in chapter 2. The LED LF-2a Fluorimeter model by Quantalase (Indore) was used for the analysis of uranium which is based on the Stokes fluorescence [37]. The detailed measurement technique is also described in chapter 2. The pH, TDS, salinity and electrical conductivity were measured using NPC 362D by Naina Solaris. The concentration of uranium, pH, salinity, TDS and conductivity from 26 locations of Mansa district, Punjab is listed in table 4.1.

4.3 Biokinetic model of uranium

Uranium can be retained in the human body in different organs, specifically kidneys, bones and liver [38]. Li *et al.* [27] proposed the hair compartment model of uranium, which is the enhancement of the biokinetic model of ICRP [26] for ingestion of uranium, as it considers hair along with urine and faeces as removal pathways. It was concluded that the hair compartment model is applicable for elevated uranium ingestion via drinking water pathway. The model is suitable for acute intakes or chronic intakes at a constant rate over a fixed length of time. The model details the passage, absorption and retention of uranium using a mathematical simulation with the first-order differential equation for an adult when ingestion takes place by drinking water. The first order equation is

$$\frac{dq_f}{dt} = \sum_f \lambda_{gf} q_g - (\lambda_f + \ \lambda_r)\,.q_f, \quad f, g = 1, 2, 3 \ldots . n \tag{4.1}$$

where dq_f is the measure of change in the uranium quantity (in units of mass) in a specific compartment, dt represents the corresponding small time interval, λ_{gf} is the transfer rate amidst two distinct compartments (from compartment g to f), λ_f represents the transfer rate from the f^{th} compartment, λ_r is radioactive decay constant, and n represents the number of compartments.

There are different transfer rates between the compartments. Uranium can be transferred to hair from plasma and intermediate turnover soft tissue compartment (ST1). It is presumed that the ingested uranium is transferred from the small intestine to the blood, and then it is exchanged or transferred to different compartments. In the calculations, it is assumed that 0.6% of ingested uranium is absorbed from the small intestine on its amalgamation with blood plasma and thus reaches the whole body depending upon the transfer rate of that compartment and is further reabsorbed back in plasma. The different routes of uranium transportation are shown in figure 4.1. The biokinetic behaviour of ingested uranium in various body organs is estimated by calculating retention and excretion. The water intake is taken as 1.41 L day^{-1} [39], standard body weight as 68.83 kg [39], kidney mass as 310 g, food consumption rate as 0.253 kg day^{-1}, urine volume as 1.38 L day^{-1}, creatinine excretion in urine as 2 g day^{-1}, faeces mass as 135 g day^{-1} and hair growth rate at 0.1 g day^{-1}, GI absorption coefficient (f1) as 0.006 [27].

The retention and excretion of uranium in various organs of the population of the area studied are compiled in table 4.2 and 4.3. The standard error is calculated as

$$Standard\ error = \frac{\sigma}{\sqrt{n}} \tag{4.2}$$

where σ is the standard deviation of samples and n is the sample size (26 location points).

GI tract: The intake of water is through the GI tract and the ingested uranium reaches all the organs and tissues from the small intestine as the nutrients and compounds are absorbed by its walls. The mean value of retention of uranium in different components of the GI tract i.e. stomach, small intestine, upper large intestine and lower large intestine is 8.98 μg, 35.73 μg, 119.1 μg and 214.4 μg, respectively. Only 0.6% of uranium is transferred to blood plasma and red blood cells (RBC), while the remaining proceed towards the large intestine and get excreted through faeces [27]. The time dependence of retention of uranium for the mean value in the GI tract is shown in figure 4.2(a). The uranium concentration is lowest in the stomach and highest in the lower large intestine. After some time, uranium concentration in the upper and lower large intestine saturates. The lower large intestine exhibits a greater duration of transit compared to the upper large intestine, resulting in an extended period for uranium absorption and subsequent reabsorption in the lower large intestine [12].

Skeleton: Kurttio et al. [2] proposed that bones can be additional targets for uranium toxicity along with kidneys. Uranium enters trabecular bone (cancellous) and cortical bone (dense) through blood by Haversian and Volksmann's canals. It obeys a similar moving pattern as of Ca^{2+} distribution but does not participate in crystal formation [26]. The skeleton acts as the depository for uranium with values varying between 59.63 μg and 617.66 μg for cortical bone volume and 15.23 to 157.78 μg for trabecular bone volume. The lower porosity, along with the high volume fraction, is the reason for the excess uranium retention on the cortical bone. The mean values of uranium retention in the cortical bone surface and trabecular bone surface are 1.12 μg and 1.41 μg, respectively. The retention of uranium in the skeleton is shown in figure 4.2(b). It can be inferred from the figure that retention in the trabecular bone surface and the cortical bone surface gets saturated after a few days and in trabecular bone volume after approximately 22 years, whereas retention in cortical bone volume (non-exchangeable) increases with time.

Blood: The blood compartment within the biokinetic model serves a vital function in comprehending the transportation and dispersion of uranium in the human body after prolonged ingestion. It acts as the main pathway for the movement of uranium, impacting its distribution to various tissues, its retention and eventual excretion. The uranium retention is minimal in blood plasma, as shown in figure 4.2(c), which is obvious from the mean value of 0.09 μg with minimum and maximum values of 0.02 μg to 0.29 μg after 69.89 years of continuous water intake. The biological removal half-time is 0.0198 days and 2 days for plasma and RBC, respectively [27]. It serves as a transportation channel for uranyl ions (UO^{2+}) with bicarbonates, transferring (protein) and citrate for concerned organs and tissues [40].

Kidneys: The kidneys are essential organs that play a crucial role in filtration and excretion from the bloodstream. The kidneys not only filter uranium but also retain it depending on the binding affinities of uranium. The kidney can be categorized into two compartments: fast turnover compartment (urinary path) and slow turnover compartment (other kidney tissue), as shown in figure 4.2. The fast turnover compartment is characterized by the rapid filtration and excretion of

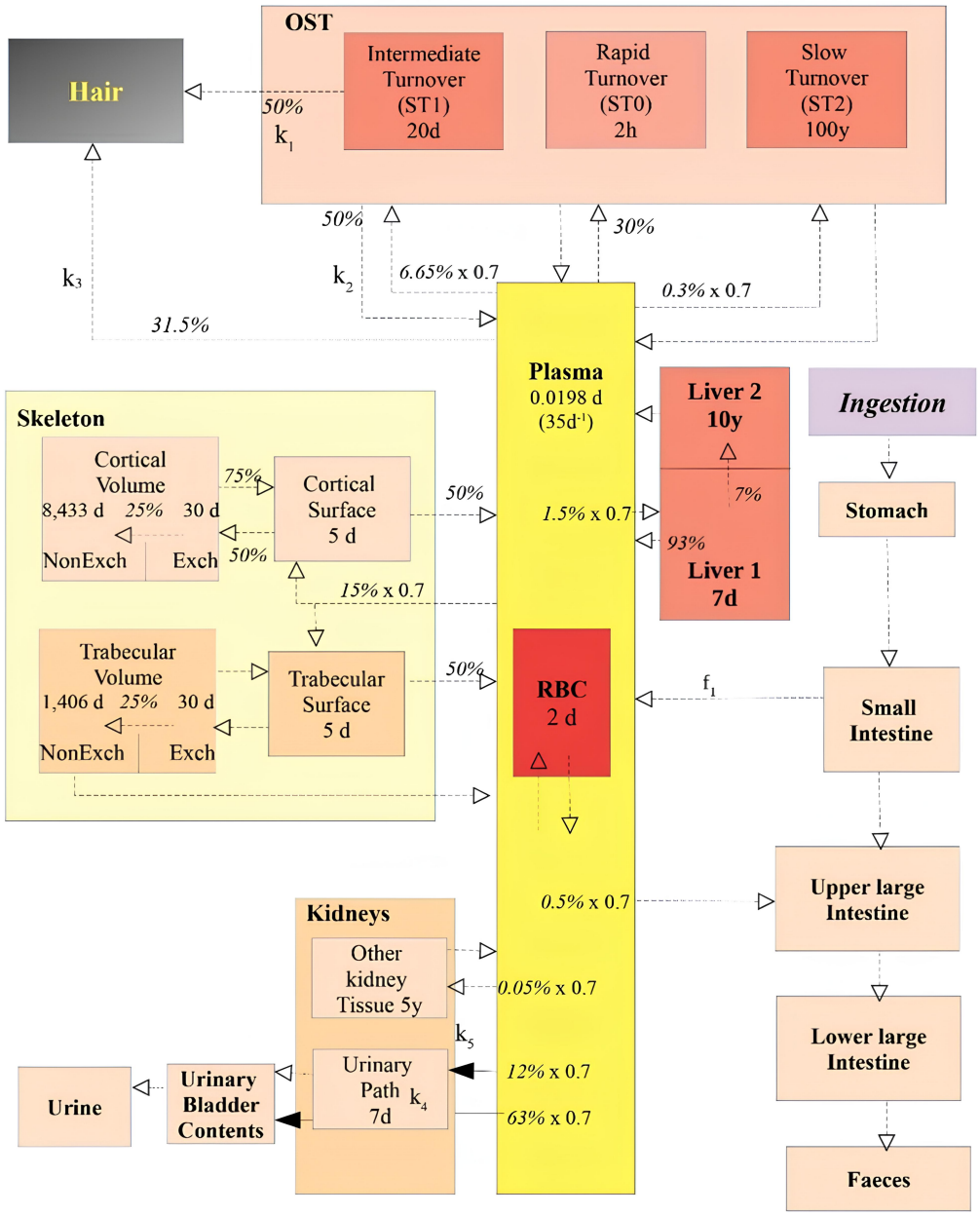

Figure 4.1: Hair compartment biokinetic model for uranium proposed by Li *et al.* [27] where transfer rates are given by k_i; i = 1, 2, 3, 4 and 5 while other transfer rates are similar to ICRP model [26]. The biological removal half-time is also mentioned in the compartments.

uranium. In this compartment, uranium has a brief retention duration, indicative of the swift clearance of soluble uranium species. The slow turnover compartment has uranium more firmly bound or sequestered, resulting in an extended retention duration. This may involve regions where uranium attaches to renal tissues or proteins, thereby reducing its rate of excretion. It gets stored as insoluble matter or organo minerals. The mean concentration and retention in kidneys is 8.56 ng g^{-1} and 2.65 μg, respectively. With higher exposure, tubule degeneration and cell necrosis can take place [41]. It can be noted from figure 4.2(c) that retention in kidneys with time is higher than blood and urinary bladder.

Liver: The liver plays a crucial role in the metabolism and detoxification of heavy metals, including uranium. Upon ingestion, uranium can be transported to the liver via plasma, where it may undergo various metabolic processes and exhibit different retention durations. The liver 1 and liver 2 are two sections of the liver. The first compartment, liver 1, is where uranium is quickly metabolized and either excreted into bile or returned to the bloodstream. Conversely, liver 2 represents regions of the liver where uranium binds more strongly to hepatic tissues or proteins, resulting in an extended retention time. This compartment is responsible for the accumulation of uranium within the liver, which can lead to prolonged exposure and potential toxic effects. The biological removal half-time of liver 1 is 7 days, and that of liver 2 is 10 years [27]. The former gets uranium from blood and further proceeds it to liver 2. The average uranium preserved in both livers is 8.08 μg, and its time dependence for mean value is shown in figure 4.2(c). The retention in the liver with time is higher than blood and urinary bladder.

Urinary bladder: The uranium reaches the bladder through kidney 1 after filtration with a transfer rate of $k_4 = 6.3$ day^{-1} and leaves the body through urine. The average retention of uranium in the bladder is 0.03 ng which is the least as shown in figure 4.2(c).

Other soft tissue (OST): Skin, fat, muscle and all other soft tissues are part of OST. The retention of uranium ranges between 25.79 μg and 267.12 μg. There are three compartments, namely ST0 (rapid) with removal half-time of 2h, ST1 (intermediate) of 20 days and ST2 (tenacious) of 100 years.

Excretory pathways for uranium: The uranium leaves the body through hair, urine and faeces. The faeces mass is taken as 135 g day^{-1}, urine volume as 1.38 L day^{-1} and hair growth as 0.1 g day^{-1}. The mean values of excretion of uranium via hair, faeces and urine are 0.82 μg day^{-1}, 214.43 μg day^{-1} and 0.44 μg day^{-1}, respectively. It can be noted from the data that uranium excretion through faeces is greater as compared to the other two. Uranium is mostly taken up in the gastrointestinal system and subsequently transferred to the liver, and reabsorbed back into the intestine from plasma. The reintroduced uranium is subsequently expelled through faeces, leading to a greater rate of excretion in faeces compared to urine. The excretion behaviour of uranium via these pathways as a function of time is shown in figure 4.2(d).

4.3.1 Dose to different organs of the human body

The radiological toxicity due to uranium retention and deposition can be harmful because it leads to radioactive decay in the organs/tissues. The doses in body organs

reckon on intake type, its pathway and time period along with chemical and physical properties. The effective dose coefficients given by [27] for adrenals, pancreas, bladder wall, lungs, brain, breasts, skin, thyroid, muscle, ovaries, uterus, spleen and thymus is 5.9 $\times$ 10^{-9} (Sv Bq^{-1}). The effective dose coefficients of the bone surface, stomach wall, small intestine wall, upper large intestine wall, and lower large intestine are 1.7$\times$ 10^{-9}, 6.9$\times$ 10^{-9}, 8.3$\times$ 10^{-9}, 2.1$\times$ 10^{-8} and 5.1$\times$ 10^{-8} (Sv Bq^{-1}), respectively. The kidneys have an effective dose coefficient of 6.1 $\times$ 10^{-8} (Sv Bq^{-1}) and liver have 2.3$\times$ 10^{-8} (Sv Bq^{-1}). The effective dose to different organs is calculated as [42] -

$$AED_{organ} = A \times DCF \times I \tag{4.3}$$

where AED_{organ} is the organ specific annual effective dose, A is the activity in Bq L^{-1}, DCF is the dose coefficient in Sv Bq^{-1} and I is the water intake in L day^{-1}. The bone surface has the highest annual effective dose of uranium with values ranging from 93.8 μSv to 976.4 μSv. As the effective dose coefficients are the same for few organs therefore, the values for adrenals, bladder wall, muscle, thyroid, brain, thymus, spleen, breasts, lungs, ovaries, pancreas, skin as well as uterus range from 3.26 μSv to 33.9 μSv with the mean value of 11.6 μSv. The stomach wall and lower large intestine have mean values 11.3 and 100 μSv, respectively. The kidney has a mean value of 120 μSv and lungs have 45.2 μSv as mean value. The red marrow has a mean value of 35.3 μSv whereas remainder mean is 12.7 μSv. The calculated doses for various body organs for samples collected are listed in table 4.4 and 4.5.

4.4 Statistical analysis

The dataset was interpreted using descriptive analysis with measures such as minimum, maximum, mean, median and Q1 and Q3 quartiles. Pearson correlation was used to evaluate the relationship between the variables. Kaiser-Mayer- Olkin (KMO) and Bartlett tests were conducted to assess the appropriateness of the data for factor analysis [43]. Principal component analysis (PCA) is a robust statistical technique which retains maximum variability while lowering the dimensionality of the dataset. The percentage of variance of significant components was calculated by obtaining eigen values and eigen vectors [44]. The SPSS software [45] was used for calculating Pearson correlation and PCA.

The descriptive statistics of uranium, pH, salinity, TDS and conductivity is given in table 4.6. The uranium concentration in the groundwater varies from 43.43 μg L^{-1} to 449.79 μg L^{-1} with a mean of 154.09 μg L^{-1}. The values of the first quartile and third quartile are 86.23 μg L^{-1} and 221.36 μg L^{-1}, respectively. The analysis of all collected samples indicates that their uranium concentrations exceed the limit established by WHO limit of 30 μg L^{-1}, and 96% of total samples have uranium concentration higher than the AERB limit of 60 μg L^{-1}. The pH of the region varies from 7.56 to 8.85. Therefore, the water of the study region is alkaline in nature. This phenomenon can be attributed to the prevalence of carbonate minerals within sediments [16, 19, 37]. The TDS in the region ranges from 350 to 3070 ppm with a mean of 1459.88 ppm and a median of 1350 ppm. The acceptable limit for TDS lies between 500 -1000 ppm, and 77% samples are above the acceptable limits in the study region. The mean salinity and conductivity of the study area is 1606.92 ppm and 2604.3 μS cm^{-1}, respectively. The comparative study of uranium concentration

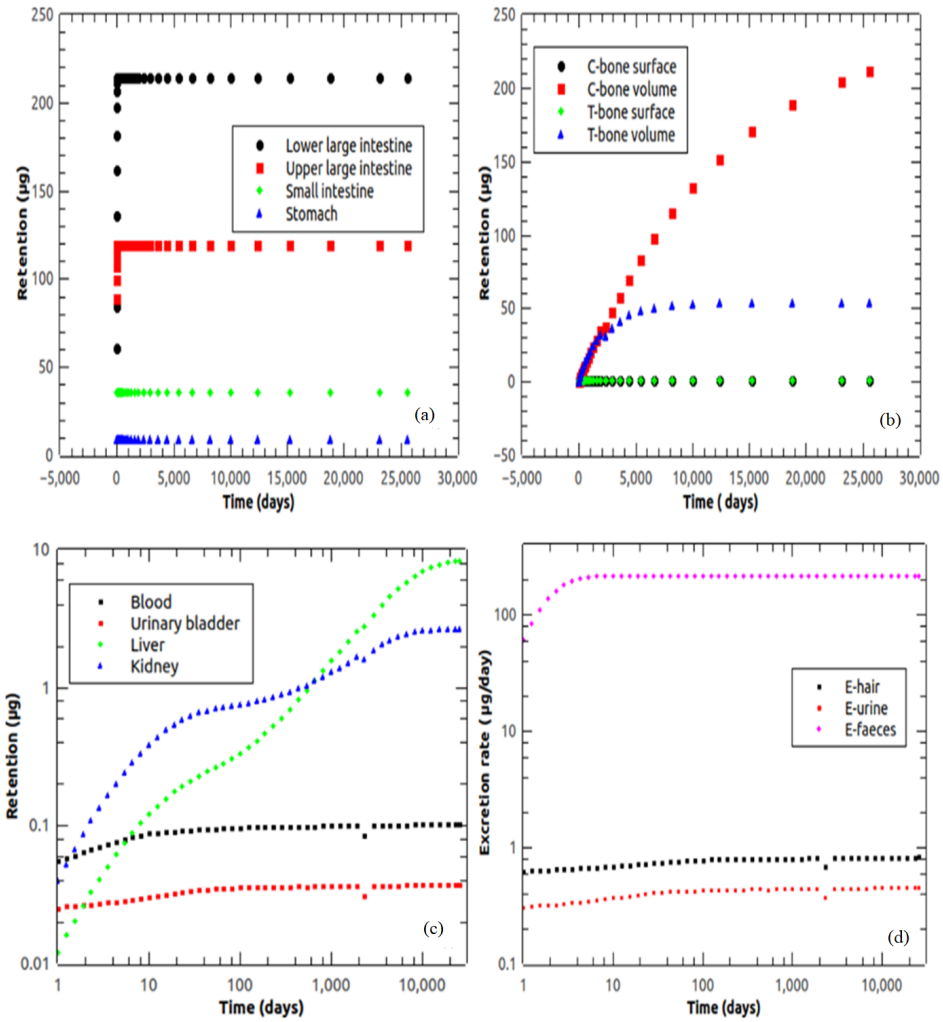

Figure 4.2: Uranium retention (or excretion) for the mean value of uranium concentration in groundwater in (a) stomach, small intestine, lower large intestine, upper large intestine, (b) cortical bone surface, cortical bone volume, trabecular bone surface, trabecular bone volume (c) blood, kidney, liver, urinary bladder and (d) hair, faeces and urine as a function of time.

in groundwater with other regions of the India and world is listed in table 4.7. The data presented in the table clearly indicates that groundwater in south-western Punjab has a relatively higher concentration of uranium.

4.4.1 Pearson Correlation Analysis

Pearson correlation is used to assess the association among two variables along with determining the degree of relationship they possess. If Pearson correlation coefficient, r>1, denotes a positive association between the variables whereas, if r<-1, signifies a negative association. If r = 0, then no relationship is between the variables. Pearson

correlation coefficient is given as [46]-

$$r = \frac{n\sum(PQ) - (\sum P)(\sum Q)}{\sqrt{[n\sum P^2 - (\sum P)^2]\,[n\sum Q^2 - (\sum Q)^2]}} \tag{4.4}$$

where n represents the total count of pairs, $\sum$(PQ) is the sum of the product of paired scores, $\sum$P and $\sum$Q represent the total of the individual scores while $\sum P^2$ and $\sum Q^2$ denote the totals of the squared scores.

The correlation between uranium, pH, TDS, salinity and conductivity is given in table 4.8. The correlations with values greater than 0.5 are significant at a significance level, $\alpha = 0.05$. The positive correlation coefficient, r = 0.68 is observed between uranium concentration and TDS. The salinity and uranium concentration have r = 0.51 correlation. The TDS have a high correlation of r = 0.81 and 0.61 with salinity and conductivity, respectively. The brackish groundwater of the region can be attributed to the occurrence of salt precipitation resulting from high rates of evaporation in addition to limited precipitation, particularly in arid and semi-arid environments [47]. The pH has a negative correlation with TDS and conductivity and a negligible correlation with uranium. Conductivity and salinity show a positive correlation (r = 0.66), which can be attributed to the existence of free ions.

4.4.2 Principal component analysis

The principal component analysis is given in table 4.9. The importance is given to eigenvalues that exceed a value of 1. Principal Component 1 (PCA1) is associated with the highest eigenvalue and accounts for the highest proportion of variance within the dataset and principal component analysis 2 (PCA2) accounts for the lower eigenvalue and explains the highest proportion of the remaining variance, and so on [45]. The PCA1 and PCA2 have eigenvalues of 2.80 and 1.09, respectively. The PCA1 accounts to 55.9% of variance and PCA2 accounts to 21.8% together making 77.7 % of total cumulative variance. PCA1 demonstrates noteworthy positive loadings of uranium (0.72), TDS (0.94), salinity (0.91) and conductivity (0.74). The elevated levels could stem from geological factors, industrial operations, or the application of phosphate fertilisers in the area. The high uranium levels reported in the area may be attributed to the interaction of groundwater with soils derived from the weathering of Malani granites and basement rocks [48]. Moreover, uranium discharges into groundwater at high salinity and TDS conditions as it is present in the form of soluble complexes in an oxidising state [16]. PCA2 exhibits a strong loading of pH (0.93) and negative loading of TDS and conductivity indicating alkaline groundwater. PCA2 predominantly reflects fluctuations associated with pH, TDS and conductivity exert contrasting effects on the PCA2 score. The statistical reliability of the PCA approach was confirmed by the Kaiser-Meyer-Olkin (KMO) with a value of 0.67 and Bartlett's test with a significance level, $p < 0.01$.

4.5 Conclusion

The enhanced uranium concentration is observed in groundwater samples of Mansa district, Punjab. The integrated methodology of using the biokinetic model and correlations of physico-chemical properties of water have led to the assessment of both

biological and ecological implications in the estimation of the population at risk. A high correlation is observed between uranium and TDS and between conductivity and salinity. The organ specific doses target organs and their bio markers. The kidneys are highly impacted by uranium ingestion based on dose as they act as storage sites. The uranium excretion pathways are constant through the years, whereas the cortical bone surface follows logarithmic growth with the highest storage over the years. Although biokinetic models connect scientific knowledge with real-world uses, providing advantages to society in terms of health and safety but they often presume that each of the compartment begin with no initial uranium load. Thus, disregarding existing uranium levels can impact the precision of forecasts. These models generally utilise mean parameters. Therefore, the absence of personalised data could restrict precision.

Table 4.1: Dataset of Mansa district, Punjab.

Uranium (μg/L)	**pH**	**TDS (ppm)**	**Salinity (ppm)**	**Conductivity (μS/cm)**
84.55	8.46	1190	1120	1110
43.43	8.26	400	560	827
67.23	8.48	560	650	2690
131.72	8.48	1380	1350	1910
234.2	7.8	1860	2360	3760
48.34	8.38	650	730	1250
264.92	8.75	1670	1320	2090
279.09	8.47	3070	3230	4890
235.65	8.69	1320	2320	2230
111.71	8.34	920	820	1990
91.28	8.3	1120	1020	3470
449.79	7.68	2450	2130	3320
104.8	8.04	1980	2460	3710
182.85	8.78	2230	2980	4550
98.17	8.25	1570	2150	4930
65.72	8.33	1310	1760	4260
133.45	8.44	1960	1990	970
239.99	8.53	1140	1370	2220
376.24	8.85	2180	2050	1900
135.68	8.57	1220	1830	2160
95.41	8.26	1270	2420	3100
116.63	8.14	1880	1250	3590
71.05	7.56	830	940	1380
147.11	7.99	2040	1450	3970
63.27	8.38	350	260	440
134.27	8.2	1407	1260	995

Table 4.2: Uranium retention in the different organs of the population under study based on Li *et al.* (2009) model.

Location	Uranium ingestion	Blood	Skeleton+				Kidney		Liver	OST
			†C-bone S$^{\Delta}$	C-bone V$^{\wedge}$	‡T-bone S	T-bone V	Retention	Conc.		
	μg L^{-1}	μg	μg	μg	μg	μg	ng g^{-1}	μg	μg	μg
Bir Khurd	84.55	0.05	0.62	116.1	0.77	29.66	1.45	4.7	4.54	50.21
Dhalewan	43.43	0.02	0.31	59.63	0.39	15.23	0.74	2.41	2.33	25.79
Bachonna	67.23	0.04	0.49	92.32	0.61	23.58	1.15	3.74	3.61	39.92
Datewas	131.72	0.08	0.96	180.88	1.21	46.2	2.27	7.32	7.07	78.22
Bareta	234.2	0.15	1.71	321.61	2.15	82.15	4.03	13.03	12.58	139.08
Kulrian	48.34	0.03	0.35	66.38	0.44	16.95	0.83	2.69	2.59	28.7
Bhakhrial	264.92	0.17	1.94	363.71	2.43	92.93	4.56	14.74	14.23	157.33
Boha	279.09	0.18	2.04	383.25	2.56	97.9	4.81	15.52	14.99	165.74
Bhaini Bagha	235.65	0.1	1.72	323.6	2.16	82.66	4.06	13.11	12.66	139.95
Khokhar Kalan	111.71	0.07	0.81	153.4	1.02	39.18	1.92	6.21	6	66.34
Moosa	91.28	0.06	0.66	125.34	0.83	32.02	1.57	5.07	4.9	54.21
Maujian	449.79	0.29	3.3	617.66	4.13	157.78	7.75	25.02	24.1	267.12
Raipur	104.8	0.06	0.76	143.91	0.96	36.76	1.8	5.83	5.63	62.23
Bajewala	182.85	0.12	1.34	250.95	1.67	64.11	3.15	10.16	9	108.53
Bhamma	98.17	0.06	0.72	134.81	0.9	34.43	1.69	5.46	5.27	58.3
Lakhmir Wala	65.72	0.04	0.48	90.24	0.6	23.05	1.13	3.65	3.53	39.03
Dalelwala	133.45	0.08	0.97	183.25	1.22	46.81	2.3	7.42	7.17	79.25
Jhunir	239.99	0.15	1.76	329.56	2.2	84.19	4.13	13.35	12.89	142.52
Fatta Maluka	376.24	0.25	2.76	516.66	3.45	131.98	6.48	20.9	20.21	223.44
Tibbi Hari Singh	135.68	0.09	0.99	186.32	1.24	47.59	2.34	7.55	7.29	80.57
Nangal Khurd	95.41	0.06	0.7	131.02	0.87	33.47	1.64	5.3	5.12	56.66
Mansa City	116.63	0.07	0.85	160.16	1.07	40.91	2.01	6.49	6.26	69.26
Khiala Kalan	71.05	0.04	0.52	97.56	0.65	24.92	1.22	3.95	3.81	42.19
Bhupal	147.11	0.09	1.07	202.01	1.35	51.6	2.53	8.18	7.9	87.36
Ralla	63.27	0.04	0.46	86.88	0.58	22.19	1.09	3.52	3.39	37.57
Khillan	134.27	0.08	0.98	184.15	1.23	47.04	2.31	7.46	7.14	79.64
Standard error		0.01	0.14	28.14	0.18	7.19	0.34	1.11	1.08	11.93

†C-bone=Cortical bone, ‡T-bone=Trabecular bone, ΔS=Surface, ^V=Volume, °OST=Other soft tissues

Table 4.3: Uranium retention in the different organs of the population under study based on Li et al. (2009) model. (continued)

Location	**$^{\Delta}$UB** μg	**Faeces** μg day^{-1}	**Urine** μg $^{-1}$	**Hair** μg $^{-1}$	**$\hat{}$ST cont** μg	**‡SI cont** μg	**• ULI cont** μg	**$\check{}$LLI cont** μg
Bir Khurd	0.02	117.66	0.24	0.45	4.93	19.6	65.36	117.66
Dhalewan	0.01	60.43	0.12	0.23	2.53	10.07	33.57	60.43
Bachonna	0.01	93.56	0.19	0.36	3.92	15.59	51.97	93.56
Datewas	0.03	183.3	0.38	0.71	7.68	30.55	101.83	183.3
Bareta	0.05	325.92	0.68	1.26	13.66	54.31	181.06	325.92
Kulrian	0.01	67.27	0.14	0.26	2.81	11.21	37.37	67.27
Bhakhrial	0.06	368.67	0.77	1.42	15.45	61.44	204.81	368.67
Boha	0.06	388.39	0.81	1.5	16.28	64.73	215.77	388.39
Bhaini Bagha	0.05	327.94	0.68	1.27	13.74	54.65	182.18	327.94
Khokhar Kalan	0.02	155.46	0.32	0.6	6.51	25.9	86.36	155.46
Moosa	0.02	127.02	0.26	0.49	5.32	21.17	70.57	127.02
Maujian	0.1	625.94	1.31	2.42	26.23	104.32	347.74	625.94
Raipur	0.02	145.84	0.3	0.56	6.11	24.3	81.02	145.84
Bajewala	0.04	254.32	0.53	0.98	10.66	42.38	141.29	254.32
Bhamma	0.02	136.61	0.28	0.52	5.72	22.76	75.89	136.61
Lakhmirwala	0.01	91.45	0.19	0.35	3.83	15.24	50.81	91.45
Dalelwala	0.03	185.71	0.39	0.71	7.78	30.95	103.17	185.71
Jhunir	0.05	333.98	0.7	1.29	13.99	55.66	185.54	333.98
Fatta Maluka	0.09	523.59	1.1	2.02	21.94	87.26	290.88	523.59
Tibbi Hari Singh	0.03	188.81	0.39	0.73	7.91	31.46	104.89	188.81
Nangal Khurd	0.02	132.77	0.27	0.51	5.56	22.12	73.76	132.77
Mansa City	0.02	162.3	0.34	0.62	6.8	27.05	90.17	162.3
Khiala Kalan	0.01	98.87	0.2	0.3	4.14	16.47	54.93	98.87
Bhupal	0.03	204.72	0.43	0.79	8.58	34.11	113.73	204.72
Ralla	0.01	88.04	0.18	0.34	3.69	14.67	48.91	88.04
Khillan	0.03	186.85	0.39	0.72	7.83	31.14	103.8	186.85
Standard error	0.00	27.97	0.05	0.10	1.17	4.66	15.53	27.97

ΔUB=Urinary bladder, †GI = Gastro intestinal, $\check{}$LLI=Lower large intestine, ‡SI=Small intestine, • ULI=Upper large intestine, $\hat{}$ST=Stomach

Table 4.4: Annual dose to different organs of the population of study region based on Li *et al.* (2009) model.

Location	**Adrenals**	**†BW**	**‡BS**	**Brain**	**Breasts**	**• ST wall**	**°SI wall**	**ΔULI wall**	**+LLI wall**	**Kidney**	**Liver**	**Lungs**
	μ Sv	μ Sv	μ Sv	μ Sv	μ Sv	μ Sv	μ Sv	μ Sv	μ Sv	μ Sv	μ Sv	μ Sv
Bir Khurd	6.36	6.36	183.2	6.36	6.36	7.44	8.95	22.6	55	65.8	24.8	6.36
Dhalewan	3.26	3.26	93.81	3.26	3.26	3.81	4.58	11.6	28.1	33.7	12.7	3.26
Bachonna	5.07	5.07	145.9	5.07	5.07	5.92	7.13	18	43.8	52.4	19.7	5.07
Datewas	9.92	9.92	285.8	9.92	9.92	11.6	14	35.3	85.7	100	38.7	9.92
Bareta	17.6	17.6	508.1	17.6	17.6	20.6	24.8	62.8	150	180	68.8	17.6
Kulrian	1.62	1.62	104.2	1.62	1.62	4.23	5.09	12.9	31.3	37.4	14.1	1.62
Bhakhrial	20	20	575.0	20	20	23.3	28.1	71	170	210	77.8	20
Boha	21	21	605.4	21	21	24.6	29.6	74.8	180	220	81.9	21
Bhaini Bagha	17.8	17.8	511.6	17.8	17.8	20.8	25	63.2	150	180	69.2	17.8
Khokhar Kalan	8.41	8.41	242.0	8.41	8.41	9.84	11.8	29.9	72.7	87	32.8	8.41
Moosa	6.87	6.87	198.0	6.87	6.87	8.04	9.67	24.5	59.4	71.1	26.8	6.87
Maujian	33.9	33.9	976.4	33.9	33.9	39.6	47.7	120	290	350	130	33.9
Raipur	7.84	7.84	225.8	7.84	7.84	9.17	11	27.9	67.8	81	30.6	7.84
Bajewala	13.7	13.7	396.1	13.7	13.7	16.1	19.3	48.9	120	140	53.6	13.7
Bhamma	7.39	7.39	212.8	7.39	7.39	8.64	10.4	26.3	63.8	76.4	28.8	7.39
Lakhimwala	4.94	4.94	142.4	4.94	4.94	5.78	6.96	17.6	42.7	51.1	19.3	4.94
Dalelwala	10	10	289.2	10	10	11.7	14.1	35.7	86.8	100	39.1	10
Jhunir	18.1	18.1	520.3	18.1	18.1	21.1	25.4	64.3	160	190	70.4	18.1
Fatta Maluka	28.3	28.3	816.5	28.3	28.3	33.1	39.9	100	240	290	130	28.3
Tibbi Hari Singh	10.2	10.2	294.4	10.2	10.2	12	14.4	36.4	88.3	110	39.8	10.2
Nangal Khurd	7.1	7.1	206.7	7.1	7.1	8.39	10.1	25.5	62	74.2	28	7.1
Mansa City	8.7	8.7	252.7	8.7	8.7	10.3	12.3	31.2	75.8	90.7	34.2	8.7
Khiala Kalan	5.3	5.3	153.7	5.3	5.3	6.24	7.51	19	46.1	55.2	20.8	5.3
Bhupal	11.1	11.1	318.8	11.1	11.1	12.9	15.6	39.4	95.6	110	43.1	11.1
Ralla	4.76	4.76	137.2	4.76	4.76	5.57	6.7	17	41.2	49.3	18.6	4.76
Khillan	10.1	10.1	291.0	10.1	10.1	11.8	14.2	35.9	87.3	100	39.4	10.1
Standard error	1.51	1.51	43.64	1.51	1.51	1.77	2.13	5.39	13.1	15.7	5.91	1.51

†BW=Bladder wall, ‡BS=Bone surface, • ST= Stomach, °SI=Small intestine, Δ ULI=Upper large intestine, +LLI=Lower large intestine

Table 4.5: Annual dose to different organs of the population of study region based on Li *et al.* (2009) model. (continued)

Location	**Muscle**	**Ovaries**	**Pancreas**	**RM †**	**Skin**	**Spleen**	**Testes**	**Thymus**	**Thyroid**	**Uterus**	**R ‡**
	μ Sv	μ Sv	μ Sv	μ Sv	μ Sv	μ Sv	μ Sv	μ Sv	μ Sv	μ Sv	μ Sv
Bir Khurd	6.36	6.36	6.36	19.4	6.36	6.36	6.25	6.36	6.36	6.36	7.01
Dhalewan	3.26	3.26	3.26	9.93	3.26	3.26	3.2	3.26	3.26	3.26	3.58
Bachonna	5.07	5.07	5.07	15.45	5.07	5.07	4.98	5.07	5.07	5.07	5.58
Datewas	9.92	9.92	9.92	30.26	9.92	9.92	9.75	9.92	9.92	9.92	10.93
Bareta	17.6	17.6	17.6	53.8	17.6	17.6	17.3	17.6	17.6	17.6	19.43
Kulrian	1.62	1.62	1.62	11.03	1.62	1.62	3.56	1.62	1.62	1.62	3.99
Bhakhrial	20	20	20	60.89	20	20	19.6	20	20	20	21.99
Boha	21	21	21	64.11	21	21	20.7	21	21	21	23.15
BhainiBagha	17.8	17.8	17.8	54.17	17.8	17.8	17.5	17.8	17.8	17.8	19.6
KhokharKala	8.41	8.41	8.41	25.66	8.41	8.41	8.27	8.41	8.41	8.41	9.2
Moosa	6.87	6.87	6.87	20.97	6.87	6.87	6.76	6.87	6.87	6.87	7.57
Maujian	33.9	33.9	33.9	103.4	33.9	33.9	33.3	33.9	33.9	33.9	37.3
Raipur	7.84	7.84	7.84	23.91	7.84	7.84	7.71	7.84	7.84	7.84	18.6
Bajewala	13.7	13.7	13.7	41.94	13.7	13.7	13.5	13.7	13.7	13.7	15.1
Bhamma	7.39	7.39	7.39	22.53	7.39	7.39	7.26	7.39	7.39	7.39	8.13
Lakhmirwala	4.94	4.94	4.94	15.08	4.94	4.94	4.86	4.94	4.94	4.94	5.44
Dalelwala	10	10	10	30.62	10	10	9.87	10	10	10	11.06
Jhunir	18.1	18.1	18.1	55.09	18.1	18.1	17.8	18.1	18.1	18.1	19.9
FattaMaluka	28.3	28.3	28.3	86.46	28.3	28.3	27.9	28.3	28.3	28.3	31.22
Tibbi Hari Singh	10.2	10.2	10.2	31.18	10.2	10.2	10	10.2	10.2	10.2	11.26
NangalKhurd	7.1	7.1	7.1	21.89	7.1	7.1	7.05	7.1	7.1	7.1	7.9
Mansa City	8.7	8.7	8.7	26.76	8.7	8.7	8.62	8.7	8.7	8.7	9.66
KhialaKalan	5.3	5.3	5.3	16.2	5.3	5.3	5.25	5.3	5.3	5.3	5.87
Bhupal	11.1	11.1	11.1	33.75	11.1	11.1	10.9	11.1	11.1	11.1	12.1
Ralla	4.76	4.76	4.76	14.5	4.76	4.76	4.6	4.76	4.76	4.76	5.24
Standard error	1.51	1.51	1.51	4.62	1.51	1.51	1.49	1.51	1.51	1.51	1.66

RM†= Red marrow, R‡=Remainder

Table 4.6: Descriptive analysis of dataset of the study region.

Parameter	**Min**	**Max**	**Mean**	**Median**	**Q1**	**Q3**
Uranium (µg L^{-1})	43.43	449.79	154.09	124.17	86.23	221.36
pH	7.56	8.85	8.32	8.36	8.25	8.48
TDS (ppm)	350	3070	1459.88	1350	1125	1940
Salinity (ppm)	260	3230	1606.92	1410	1045	2145
EC (µS cm^{-1})	440	4930	2604.3	2225	1510	3680

Table 4.7: Comparison of uranium concentration in groundwater in different parts of the world.

Location	**Uranium concentration (μg L^{-1})**	**References**
Punjab (Mansa), India	43.43-449.79	Present study
Punjab (Southwest)	0.48 - 645.22	[36]
West Bengal (Nadia district), India	0.21-20.9	[49]
Tamil Nadu (Tiruvannamalai district), India	0.2-25.8	[50]
Rajasthan (Northeast), India	0.89-166.89	[38]
Haryana, India		
Jhajjar, Haryana	14.4-57.43	[51]
Yamuna Nagar, Haryana	5-91	[52]
Yamuna Nagar, Haryana	7.12-29.94	[53]
Jaduguda, Jharkhand	0.03-11.6	[54]
Thailand	5.16-11.4	[55]
United States of America (Southeastern New Hampshire)	<1-270	[56]
Germany (Baden-Württemberg)	0.1-2.2	[47]
Saudi Arabia (Hail region)	3.2-44.4	[57]

Table 4.8: Pearson correlation between uranium and physico-chemical properties of water.

	Uranium	pH	TDS	Salinity	EC
Uranium	1				
pH	0.08	1			
TDS	0.68	-0.01	1		
Salinity	0.51	0.08	0.81	1	
EC	0.22	-0.14	0.61	0.66	1

Table 4.9: Principal component analysis for the dataset.

Initial Eigenvalues				Rotated Component Matrix		
	Total	**% of variance**	**Cumulative %**		**PCA 1**	**PCA 2**
1	2.80	55.9 %	55.9 %	Uranium	0.72	0.28
2	1.09	21.8 %	77.7 %	pH	0.04	0.93
3	0.73	14.6 %	92.3 %	TDS	0.94	-0.01
4	0.24	4.9 %	97.2 %	Salinity	0.91	-0.02
5	0.14	2.8 %	100 %	Conductivity	0.74	-0.39

4.6 References

1. Cotrovo, J.A. (2017). WHO Guidelines for Drinking Water Quality: First Addendum to the Fourth Edition.

2. Kurttio, P., Komulainen, H., Leino, A., Salonen, L., Auvinen, A., & Saha, H. (2005). Bone as a possible target of chemical toxicity of natural uranium in drinking water. *Environmental health perspectives*, *113*(1), 68-72.

3. Guéguen, Y., & Frerejacques, M. (2022). Review of knowledge of uranium-induced kidney toxicity for the development of an adverse outcome pathway to renal impairment. *International journal of molecular sciences*, *23*(8), 4397.

4. Pavlakis, N., Pollock, C. A., McLean, G., & Bartrop, R. (1996). Deliberate overdose of uranium: toxicity and treatment. *Nephron*, *72*(2), 313-317.

5. van Gerwen, M., Alpert, N., Lieberman-Cribbin, W., Cooke, P., Ziadkhanpour, K., Liu, B., & Genden, E. (2020). Association between uranium exposure and thyroid health: a national health and nutrition examination survey analysis and ecological study. *International journal of environmental research and public health*, *17*(3), 712.

6. McDiarmid, M. A., Gaitens, J. M., Hines, S., Cloeren, M., Breyer, R., Condon, M., ... & Streeten, E. (2021). Surveillance of depleted uranium-exposed Gulf War veterans: more evidence for bone effects. *Health physics*, *120*(6), 671-682.

7. Wang, S., Ran, Y., Lu, B., Li, J., Kuang, H., Gong, L., & Hao, Y. (2020). A review of uranium-induced reproductive toxicity. *Biological trace element research*, *196*, 204-213.

8. UNSCEAR (2000). Report to the general assembly with scientific annexes: sources and effects of ionizing radiation: Vol 1: Annuxure A.

9. Lin, M. *et al.* (2021). 70-year anthropogenic uranium imprints of nuclear activities in Baltic Sea sediments. *Environmental science & technology*, *55*(13), 8918-8927.

10. Mwalongo, D. A., Haneklaus, N. H., Lisuma, J. B., Kivevele, T. T., & Mtei, K. M. (2023). Uranium in phosphate rocks and mineral fertilizers applied to agricultural soils in East Africa. *Environmental science and pollution research*, *30*(12), 33898-33906.

11. UNSCEAR (2000). Report to the General Assembly, with Scientific Annexes: Sources and effects of ionizing radiation: Vol 1: Annuxure C and E.

12. Kaur, S., & Mehra, R. (2019). Toxicological risk assessment of protracted ingestion of uranium in groundwater. *Environmental geochemistry and health*, *41*, 681-698.

13. Smedley, P. L., Smith, B., Abesser, C., & Lapworth, D. (2006). Uranium occurrence and behaviour in British groundwater.

14. Bala, R., & Das, D. (2022). Occurrence and behaviour of uranium in the groundwater and potential health risk associated in semi-arid region of Punjab, India. *Groundwater for sustainable development*, *17*, 100731.

15. Vandenhove, H., Hurtgen, C., & Payne, T. E. (2010). Uranium. *Radionuclides in the environment*, 261-272.

16. Kumar, A. *et al.* (2011). Geochemical modelling of uranium speciation in the subsurface aquatic environment of Punjab state in India. *Journal of geology and mining research*, *3*(5), 137-146.

17. Grenthe, I., Drozdzynski, J., Fujino, T., Buck, E. C., Albrecht-Schmitt, T. E., & Wolf, S. F. (2006). Uranium: The chemistry of the actinide and transactinide elements, Vol. 1; Morss LR, Edelstein NM, Fuger J., Eds.

18. Acharya, S., Sharma, S. K., & Khandegar, V. (2018). Assessment of groundwater quality by water quality indices for irrigation and drinking in South West Delhi, India. *Data in brief*, *18*, 2019-2028.

19. Sahoo, P. K. *et al.* (2022). Meta-analysis of uranium contamination in groundwater of the alluvial plains of Punjab, northwest India: Status, health risk, and hydrogeochemical processes. *Science of the total environment*, *807*, 151753.

20. Wagner, S. E. *et al.* (2011). Groundwater uranium and cancer incidence in South Carolina. *Cancer causes & control*, *22*, 41-50.

21. Lipsztein, J. L. (1981). *An improved model for uranium metabolism in the primate.* New York University.

22. Fisher, D. R., Kathren, R. L., & Swint, M. J. (1991). Modified biokinetic model for uranium from analysis of acute exposure to UF6. *Health physics*, *60*(3), 335-342.

23. Wrenn, M. E., Durbin, P. W., Howard, B., Lipsztein, J., Rundo, J., Still, E. T., & Willis, D. L. (1985). Metabolism of ingested U and Ra. *Health physics*, *48*(5), 601-633.

24. Leggett, R. W., & Harrison, J. D. (1995). Fractional absorption of ingested uranium in humans. *Health physics*, *68*(4), 484-498.

25. Leggett, R. W., & Pellmar, T. C. (2003). The biokinetics of uranium migrating from embedded DU fragments. *Journal of environmental radioactivity*, *64*(2-3), 205-225.

26. ICRP (1995). Age-dependent doses to members of the public from intake of radionuclides: Part 3 ingestion dose coefficients (Pergoman Press: Oxford).

27. Li, W. B. *et al.* (2009). A compartmental model of uranium in human hair for protracted ingestion of natural uranium in drinking water. *Health physics*, *96*(6), 636-645.

28. WWAP (2012). World water assessment programme: The United Nations World Development Report 4: Managing water under uncertainty and risk.

29. CGWB (2021). National compilation on dynamic ground water resources of India, 2020. Ministry of Water Resources, River Development and Ganga Rejuvenation, Government of India.

30. WHO (2004). Guidelines for drinking water quality, vol 1, Geneva.

31. AERB (2004). Drinking water specifications in India. Department of atomic energy, Government of India.

32. FICCI (2022). Call for action: Making cancer care more accessible and affordable in India. FICCI, Government of India.

33. Blaurock-Busch, E., Busch, Y. M., Friedle, A., Buerner, H., Parkash, C., & Kaur, A. (2015). Comparing the metal concentration in the nails of healthy and cancer patients living in the Malwa region of Punjab, India with a random European group-a follow up study. *British journal of medicine and medical research*, *5*(4), 480.

34. Shrivastava, B. K. (2015). Elevated uranium and toxic elements concentration in groundwater in Punjab state of India: extent of the problem and risk due to consumption of unsafe drinking water. *Water quality, exposure and health*, *7*(3), 407-421.

35. Bjørklund, G., Christophersen, O. A., Chirumbolo, S., Selinus, O., & Aaseth, J. (2017). Recent aspects of uranium toxicology in medical geology. *Environmental research*, *156*, 526-533.

36. Saini, K., Singh, P., & Bajwa, B. S. (2016). Comparative statistical analysis of carcinogenic and non-carcinogenic effects of uranium in groundwater samples from different regions of Punjab, India. *Applied radiation and isotopes*, *118*, 196-202.

37. CGWB (2013). Ground water information booklet Mansa district, Punjab. Ministry of Water Resources, River Development & Ganga Rejuvenation, Government of India.

38. Mittal, S., Rani, A., Mehra, R., Balaram, V., Satyanarayanan, M., & Sawant, S. S. (2017). Assessment of uranium in correlation with physico-chemical properties of drinking water of Northern Rajasthan. *Journal of the geological society of India*, *90*, 233-238.

39. K. Eckerman, J. Harrison, H.G. Menzel, C.H. Clement ICRP publication 119: Compendium of dose coefficients based on ICRP publication 60. Annals of the ICRP 41:1-130 (2012).

40. Cooper, J. R., Stradling, G. N., Smith, H., & Ham, S. E. (1982). The behaviour of uranium-233 oxide and uranyl-233 nitrate in rats. *International journal of radiation biology and related studies in physics, chemistry and medicine*, *41*(4), 421-433.

41. Qiang, S. *et al.* (2023). The damage mechanism of uranium (VI) to HK-2 cells. *Journal of radioanalytical and nuclear chemistry*, *332*(4), 1277-1285.

42. Garry, S. (2022). *U.S. Nuclear regulatory guide 8.34, rev. 1: Monitoring criteria and methods to calculate occupational radiation doses.*

43. Omo-Irabor, O. O., Olobaniyi, S. B., Oduyemi, K., & Akunna, J. (2008). Surface and groundwater water quality assessment using multivariate analytical methods: a case study of the Western Niger Delta, Nigeria. *Physics and chemistry of the earth, parts A/B/C*, *33*(8-13), 666-673.

44. N. Subba Rao, B. Sunitha, N. Adimalla &. Chaudhary, M. (2020). Quality criteria for groundwater use from a rural part of Wanaparthy District, Telangana State, India, through ionic spatial distribution (ISD), entropy water quality index (EWQI) and principal component analysis (PCA). *Environmental geochemistry and health*, *42*, 579-599.

45. https://www.ibm.com/products/spss-statistics (assessed on Jan, 2024).

46. Moore, D. S., McCabe, G. P., & Craig, B. A. (2014).*Introduction to the practice of statistics.* Eighth edition. New York, W.H. Freeman and Company, a Macmillan Higher Education Company.

47. Liesch, T., Hinrichsen, S., & Goldscheider, N. (2015). Uranium in groundwater—fertilizers versus geogenic sources. *Science of the total environment*, *536*, 981-995.

48. Bajwa, B. S., Kumar, S., Singh, S., Sahoo, S. K., & Tripathi, R. M. (2017). Uranium and other heavy toxic elements distribution in the drinking water samples of SW-Punjab, India. *Journal of radiation research and applied sciences*, *10*(1), 13-19.

49. Das, A., Das, S. S., Chowdhury, N. R., Joardar, M., Ghosh, B., & Roychowdhury, T. (2020). Quality and health risk evaluation for groundwater in Nadia district, West Bengal: an approach on its suitability for drinking and domestic purpose. *Groundwater for sustainable development*, *10*, 100351.

50. Ganesh, D., Kumar, G. S., Najam, L. A., Raja, V., Neelakantan, M. A., & Ravisankar, R. (2020). Uranium quantification in groundwater and health risk from its ingestion in and around Tiruvannamalai, Tamil Nadu, India. *Radiation protection dosimetry*, *189*(2), 137-148.

51. Tanwer, N., Khyalia, P., Deswal, M., Laura, J. S., & Khosla, B. (2022). Spatial distribution of uranium in groundwater and its health risk assessment in Haryana, India. *Rasayan journal of chemistry*, *15*(1), 343-349.

52. Kumari, A., Panghal, A., Singh, B., Kataria, N., Dhiman, R., Rani, S., & Dalal, R. (2023). Analysis of Natural Uranium in Groundwater of Jhajjar District of Haryana, India using LED Fluorimeter. *Indian journal of pure & applied physics, 61*, 934-937.

53. Dhiman, R. *et al.* (2024). Investigation of radiation dose-dependent risk on individuals due to drinking water ingestion in Yamunanagar District, India. *Journal of radioanalytical and nuclear chemistry*, 1-11.

54. Patra, A. C., Mohapatra, S., Sahoo, S. K., Lenka, P., Dubey, J. S., Tripathi, R. M., & Puranik, V. D. (2013). Age-dependent dose and health risk due to

intake of uranium in drinking water from Jaduguda, India. *Radiation protection dosimetry*, *155*(2), 210-216.

55. O-Manee, A. *et al.* (2023). Assessment of natural radioactivity in industrial line production waters from major industrial cities of Thailand. *Journal of radioanalytical and nuclear chemistry*, *332*(3), 797-807.

56. Flanagan, S. M., Belaval, M., & Ayotte, J. D. (2014). *Arsenic, iron, lead, manganese, and uranium concentrations in private bedrock wells in southeastern New Hampshire, 2012-2013* (No. 2014-3042). US Geological Survey.

57. Fallatah, O., & Khattab, M. R. (2023). Determination of uranium concentrations and 234U/238U isotopic ratios in plants and the groundwater used in their cultivation in an area with high background radiation. *Sustainability*, *15*(2), 1590.

Chapter 5

Assessment of natural radionuclides in soil and wheat

Wheat is a vital staple grain for humans and it plays a crucial role in the nutritional cycle of human beings. The contamination in wheat due to heavy metals and naturally occurring radionuclides is a significant concern worldwide owing to their adverse health effects. This chapter commences with an introduction followed by the sampling procedure in section 5.2. The health indices are defined in section 5.3. In section 5.4, radiological risks stemming from radionuclides in soil and wheat grains collected from Mansa, Punjab are calculated. The radiological risk comparison of organic and conventional food samples is done in section 5.5, followed by the conclusion.

5.1 Introduction

Wheat, belonging to the Triticum genus, is a staple cereal grain that holds significant importance in the dietary patterns of humans throughout numerous countries globally. It has been produced on a worldwide scale in regions with moderate weather and extensive agricultural areas, ranking it third in terms of worldwide output [1]. In recent years, an increasing apprehension has emerged regarding the excessive buildup of metal contaminants in agricultural produce. This is mainly due to the pollution of agricultural soils with heavy metals, which has harmful effects on living creatures [2]. Heavy metals are widespread environmental toxins, especially in places with considerable human activity, due to their non-biodegradable and bio-accumulative nature [3]. Agricultural activity is a significant contributor to heavy metal pollution [4]. Mercury (Hg), cadmium (Cd), lead (Pb) and chromium (Cr) are extremely hazardous to living cells, even at extremely low concentrations [5]. Micronutrients like zinc (Zn), copper (Cu), nickel (Ni), iron (Fe) and manganese (Mn) have crucial functions in several metabolic pathways in plants and humans when present at an optimal concentration [6]. Ingestion is a primary pathway, apart from occupational exposure, by which humans are exposed to heavy metals [7]. Heavy metal pollutants provide a dual risk to agricultural product safety and the well-being of organisms by adversely affecting their immunological, reproductive

and nervous systems upon ingestion through food. Excessive consumption of heavy metals by humans can harm vital organs such as the thyroid, kidneys, liver, bones and heart. The buildup of these metals in human organs can lead to numerous disorders, including osteoporosis, emphysema, cardiovascular disease, and renal and hepatic dysfunction [8]. Heavy metals that infiltrate plant tissues can impede many physiological processes in plants [9]. Moreover, the presence of metal toxicity leads to oxidative stress, and alteration of pigment function, in addition to modification in protein activity. The excessive production of reactive oxygen species due to metal pressure can lead to significant harm to cellular structures in plants [10].

Natural radioactivity is present in a variety of matrices such as soil, minerals, air as well as water. Soil can serve as both a source and conduit for the movement of radionuclides [11]. The concentration of radionuclides in diverse soil classifications varies significantly and is influenced by factors such as regional geology, elevation, and climate, in addition to human activity in the region [12-13]. The soil-plant-man pathway is a significant environmental route through which radionuclides are ingested by humans. Various factors, including the characteristics of the soil, types of plants, competing ions, environmental variables, along with agricultural practices, affect the absorption of radionuclides by plant roots and their subsequent movement to edible plant parts [14]. Naturally occurring radionuclides are commonly found in food to varying extents influenced by variations in background radiation levels, the environment and agricultural settings [15].

Organic and conventional ways of agricultural produce are extensively practiced commercial farming techniques. Organic farming preserves the soil and plant nutrients by maintaining the salt ratio, thus impeding desertification by retaining moisture [16]. Organic farming is based on an environment-friendly approach using bovine, guano manure or vermicompost, whereas, conventional farming is done using chemical fertilizers and pesticides to increase the yield. The phosphate ores (rock phosphate) are present in sedimentary rocks, consequently, elevated levels of uranium, thorium and their progenies are found [17-18]. The concentrations of phosphoric anhydride (P_2O_5) and uranium in various fertilizers are correlated in a proportional manner [19]. The ternary fertilizers, characterized by their inclusion of nitrogen, phosphorus, and potassium (NPK), exhibit an elevated concentration of uranium [20]. Hence, the usage of these fertilizers impacts the radioactivity levels in the soil, which further affects the crops cultivated in the region. The radionuclides are absorbed by plants through two main mechanisms: via the leaves from the surrounding atmosphere and through the roots from the soil.[21]. Various plant species also adsorb uranium from polluted water [22-23]. The plants are reliant only on the chemical characteristics of an element for the uptake of essential nutrients. They cannot differentiate uptake on the basis of radioactive properties therefore, take radionuclides as well [24-25]. The consumption of staple foods that have high phosphate fertilizers can result in higher internal exposure to radiation [19]. The uranium ingestion through vegetables is 33% of the overall consumption by adults, and different studies have confirmed the presence of uranium in plants [26-28].

As wheat serves as the primary dietary staple for the population in Punjab, therefore impact of the accumulation of natural radionuclides in the human body and the health implications associated with the same should be taken into account. The primary goal of vegetation as well as soil monitoring programmes is to establish

suitable remediation strategies and long-term protective measures [29]. The available data is significantly restricted on the uptake of amounts of radioactive elements by plants through the soil, particularly in natural environments. The composition of the soil, including factors such as pH, levels of calcium and potassium, clay mineral content, organic matter, as well as the application of soil additives like fertilisers, have a significant impact on how radionuclides are absorbed, retained and distributed throughout plants [30]. The heavy metal analysis of wheat grains can serve as the guide for the contamination analysis of staple food of the region for further studies. The study aims to

a) analyse the natural radionuclides in both soil and wheat grains.

b) determine the transfer factor of radionuclides from soil to wheat grains.

c) the assessment of heavy metal contamination in wheat grains.

d) correlate radionuclides and heavy metals contamination of wheat grains.

e) analyse the difference in the concentration of radionuclides in conventional and organic staple food.

5.2 Materials and Methods

5.2.1 Sample collection and preparation

For analysing natural radioactivity in soil samples, a total of 31 soil samples were collected from various locations in Mansa district, Punjab as shown in figure 5.1. Similarly, for measuring natural radioactivity in wheat samples, 15 samples of wheat grains were collected from the field from same locations, transferred into a plastic bag and subsequently tagged. The in-depth sample collection and procedure is already discussed in chapter 2.

A cylindrical Atomtex Gamma-Beta spectrometer of 63mm×63 mm, with an energy resolution of less than 7.5% and an efficiency of around 20%, was utilised to ascertain the activity concentration of natural radionuclides in the soil as well as wheat samples. The energy scale stabilization of the gamma radiation line with the energy of 661.6 keV from the reference source of ^{137}Cs, 1170 keV and 1330 keV from ^{60}Co were carried out. ^{137}Cs was used as the reference source for detector efficiency. Each sample was assigned a counting period of 10,800 sec, which was necessary to yield reliable statistics and to limit the occurrence of counting errors. Furthermore, the background spectra were also computed under identical conditions as the reference materials and the samples. The specific activity is calculated using-

$$C_{\mathrm{n}} = \frac{N_{\mathrm{n}}}{\gamma_{\mathrm{d}} \times \eta_{\mathrm{E}} \times T \times W} \tag{5.1}$$

where C_n is the specific activity in Bq/kg, N_n is the net counts, γ_d is γ ray emission probability, η_E is the detection efficiency, T is the counting time (sec), and W is the dry mass of the sample (kg). The activity of ^{226}Ra, ^{232}Th and ^{40}K from soil and wheat samples collected from Mansa, ^{226}Ra, ^{232}Th and Punjab is listed in table 5.1 and 5.2. The minimum detectable concentration for ^{226}Ra and ^{232}Th is 1 Bq/kg and

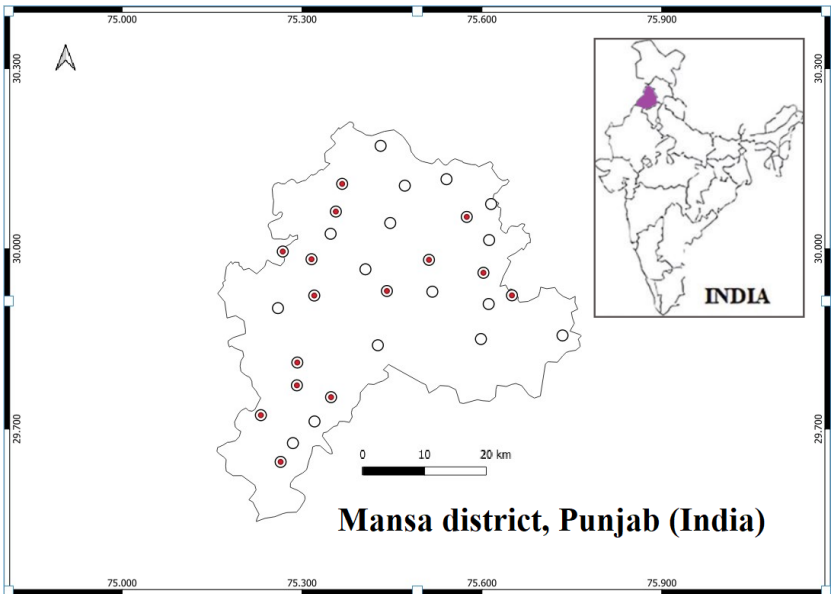

Figure 5.1: Sampling locations of soil (circled) and wheat samples (red dots) in Mansa district.

for ^{40}K is 50 Bq/kg. The Prodigy ICP-OES, manufactured by Teledyne Leeman labs was utilised for the measurement of heavy metals in wheat samples. The calibration process involves the use of standard solutions provided by LGC standards (VHG labs, England) with $R^2 = 0.99$. In order to ensure sustained accuracy and precision throughout the analysis of wheat samples, blank and spike recovery samples were conducted at regular intervals. Manganese (Mn), iron (Fe), arsenic (As), copper (Cu), lead (Pb), strontium (Sr), cadmium (Cd) and zinc (Zn) were detected in wheat grain, and their concentrations are listed in table 5.3. The calibration curves are shown in figure 5.2. The minimum detectable concentration for As, Mn, Fe, Zn, Cd, Cu and Pb are 0.005 mg L^{-1}, 0.0002 mg L^{-1}, 0.0003 mg L^{-1}, 0.0001 mg L^{-1}, 0.0004 mg/L, 0.0004 mg/L, 0.0014 mg/L, respectively .

Different samples of regular staple food, which includes wheat, rice and pulses were collected from the organic brands and local markets in Patiala, a city in the Punjab region (India). The activity of ^{226}Ra, ^{232}Th and ^{40}K for organic and regular wheat samples is listed in table 5.4.

5.3 Health risk indices

The assessment of the radiological danger posed by environmental radioactivity in soil and food is conducted for evaluating hazards. The radium equivalent activity is determined for materials containing a combination of ^{232}Th, ^{226}Ra or ^{238}U and ^{40}K as it results in a similar index of the gamma yield. The same gamma dose rate is achieved with an activity concentration of 259 Bq kg^{-1} of ^{232}Th, 370 Bq kg^{-1} of ^{238}U (can be Ra_C) or 4810 Bq kg^{-1} of ^{40}K [31-32]. It is calculated as -

$$Ra_{eq} = Ua_c + (1.43 \times Th_c) + (0.077 \times K_c) \tag{5.2}$$

where Ra_{eq} is the radium equivalent in Bq kg^{-1}, the activity of uranium, thorium

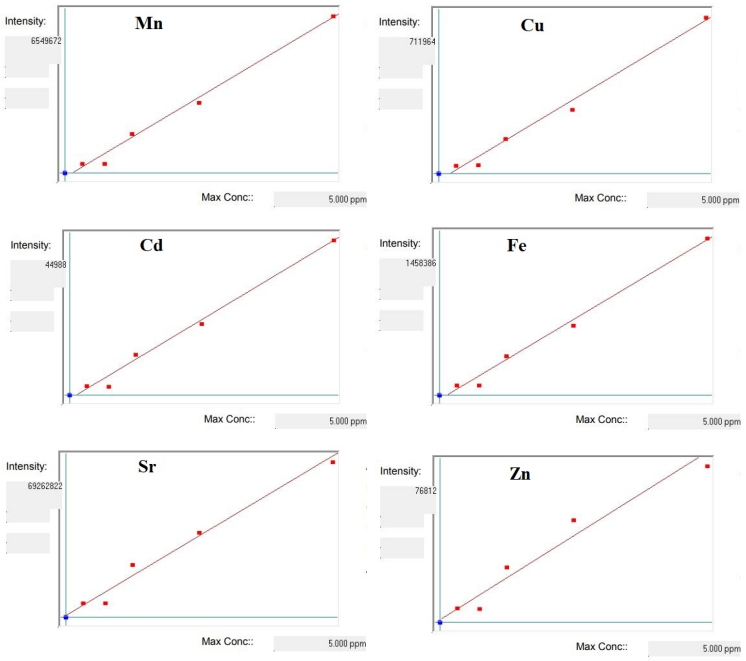

Figure 5.2: Calibration curves with $R^2 = 0.99$ in ICP-OES for different heavy metals.

and potassium is denoted by Ua_c, Th_c and K_c, respectively in Bq kg^{-1}.

The annual effective dose quantifies the cumulative radiation exposure an individual receives within a year, taking into account the specific type of radiation and the differing sensitivities of various organs or tissues to such exposure. It is calculated as [33]-

$$AED_{grain} = A \times DCF \times I \tag{5.3}$$

where AED_{grain} is the annual effective dose due to consumption of wheat grains in mSv $year^{-1}$, A represents the specific activity measured in Bq kg^{-1}, DCF refers to the dose conversion factor measured in mSv Bq^{-1} and I represent the yearly intake measured in kg $year^{-1}$. The DCF for different age groups given by ICRP [34] are listed in table 5.5. The yearly intake of cereals given by UNSCEAR for infants is 45 kg $year^{-1}$, for children is 90 kg $year^{-1}$ and for adults is 140 kg $year^{-1}$ [35]. The annual intake of cereals and pulses based on Indian standards is given in table 5.6 [36]. The age group of children is average values of two age groups 7-9 years and 10-12 years mentioned in NNMB (National Nutrition Monitoring Bureau) [36].

The annual effective dose for soil is given by [37]-

$$AED = G_a D_r \times t \times CF \times OF \times 10^{-6} \tag{5.4}$$

where

$$G_a D_r = (0.462 Ra_c + 0.621 Th_c + 0.0417 K_c) \tag{5.5}$$

where AED is the annual effective dose in mSv $year^{-1}$, G_aD_r is the outdoor absorbed dose rate in (nGy hr^{-1}), Ra_c is the activity of radium, Th_c is the activity of thorium

Table 5.1: Activity concentration (Bq kg^{-1}) of soil samples of Mansa, Punjab.

S.no.	^{226}Ra	^{232}Th	^{40}K
1	8.88±2.29	22.47±6.41	291.03±50.15
2	12.45±2.51	22.29±6.55	266.82±48.39
3	13.10±2.57	21.94±6.58	227.38±44.98
4	12.10±2.47	21.14±6.44	250.60±46.84
5	11.72±2.47	24.99±6.58	243.06±46.27
6	14.03±2.29	21.38±6.68	260.21±48.23
7	11.80±2.45	24.43±6.44	251.39±46.83
8	14.75±2.65	22.75±6.58	313.06±52.19
9	12.17±2.49	22.08±6.47	291.88±50.26
10	10.94±2.42	21.14±6.44	274.80±48.70
11	10.21±2.35	20.47±6.34	276.53±48.60
12	12.42±2.51	22.57±6.47	346.13±54.64
13	12.78±2.52	23.14±6.34	265.54±48.01
14	7.37±1.91	20.83±5.81	385.69±55.65
15	11.46±2.46	25.41±6.58	226.58±45.12
16	11.94±2.47	20.58±6.47	248.18±46.94
17	10.13±2.32	24.95±6.37	262.03±47.19
18	9.81±2.30	25.09±6.34	233.84±44.50
19	11.68±2.43	24.95±6.47	257.35±47.07
20	13.37±2.56	16.31±6.51	243.03±46.30
21	11.63±2.45	20.09±6.47	327.17±53.23
22	10.37±2.36	29.61±7.07	250.50±46.45
23	10.56±2.34	21.18±6.30	263.75±47.19
24	12.82±2.50	23.10±6.47	221.77±44.10
25	11.38±2.42	23.48±6.47	246.83±46.21
26	12.97±2.51	23.94±6.47	261.82±47.46
27	14.20±2.58	19.88±6.405	242.41±45.66
28	9.65±2.30	27.16±6.86	282.42±48.95
29	11.17±2.43	26.81±7	298.00±50.93
30	13.44±2.62	26.28±6.82	175.36±41.22
31	13.05±2.51	22.23±6.41	316.81±51.96

and K_c is the activity of ^{40}K in Bq kg^{-1}, t is the time taken as 8760 hr $year^{-1}$, CF is the conversion factor of 0.7 Sv Gy^{-1}, OF is the occupancy factor of 0.2.

The internal hazard index is calculated for wheat grains, and it quantifies the level of internal exposure of living cells to radon ^{222,220}Rn along with their daughter nuclei. It is given by [32] -

$$H_{in} = \frac{Ra_c}{185} + \frac{Th_c}{259} + \frac{K_c}{4810} \tag{5.6}$$

where H_{in} represents the internal hazard index. The activity concentrations of ^{226}Ra, ^{232}Th and ^{40}K are denoted as Ra_c, Th_c and K_c, respectively.

The external hazard index due to the presence of radionuclides in soil is calculated

as [38]-

$$H_{ex} = \frac{Ra_c}{370} + \frac{Th_c}{259} + \frac{K_c}{4810} \tag{5.7}$$

where the activity of ^{226}Ra, ^{232}Th and ^{40}K are denoted as Ra_c, Th_c and K_c, respectively in Bq kg^{-1}.

In order to maintain a negligible radiation threat, the value of the hazard index must be lower than one.

Table 5.2: Activity concentration (Bq kg^{-1}) of wheat grain samples of Mansa, Punjab.

S.no.	^{226}Ra	^{232}Th	^{40}K
1	7.91±2.07	22.86±6.17	414.83±58.51
2	10.02±2.20	23.52±6.29	437.71±60.39
3	7.84±2.07	26.27±6.73	434.70±60.17
4	6.56±1.91	24.45±6.51	387.14±55.81
5	7.23±1.91	23.56±6.14	390.43±55.97
6	8.70±2.09	17.94±6.06	395.74±56.56
7	5.67±1.32	23.34±6.12	418.12±58.39
8	6.23±1.81	25.53±6.30	436.02±60.42
9	6.11±2.5	20.32±6.10	425.05±59.40
10	5.89±1.99	29.08±6.99	441.31±61.23
11	5.72±1.43	18.64±6.18	398.55±55.80
12	6.74±1.90	22.2±6.10	369.04±54.20
13	7.56±1.94	27.45±6.77	418.10±58.67
14	5.98±1.53	19.67±6.09	383.01±54.70
15	8.42±2.12	24.71±6.32	442.82±61.12

5.4 Radiological risks due to soil and wheat samples of Mansa

The dataset comprising of mean, minimum, maximum, quartile 1 and 3 of activity levels, the annual effective dose of ^{226}Ra, ^{232}Th, and ^{40}K for soil and wheat are given in table 5.7 and 5.8, respectively. The radium equivalent and hazard indices are also listed in these tables. The radium equivalent of soil varied between 55.40 to 72.45 Bq kg^{-1} with an average of 65.24 Bq kg^{-1}, which is below the established threshold of 370 Bq kg^{-1}. The soil samples show modest levels of radium equivalent activity, indicating minimal radioactive risk associated with humans. The mean external hazard index for soil is 0.17. The activity of ^{226}Ra for soil samples varied between 7.37 to 14.75 Bq kg^{-1} with an average of 11.75 Bq kg^{-1}. Similarly, the activity of ^{232}Th varied between 16.31 to 29.61 Bq kg^{-1} with an average of 22.98 Bq kg^{-1}. The activity of ^{40}K varied between 175.36 to 267.81 Bq kg^{-1} with an average of 267.81 Bq kg^{-1}. The local geological variables, soil composition and evolution in addition to ambient conditions like temperature and moisture may influence the radioactivity [39-40]. Bandhan *et al.* reported the average activity in soils to be 28.58 Bq kg^{-1} for ^{238}U, 50.95 Bq kg^{-1} for ^{232}Th and 569.59 for ^{40}K in Ludhiana,

Punjab [41]. According to Kaintura *et al.*'s findings in the neutral terrain of Ropar (Punjab) [42], the activity concentration of ^{232}Th, ^{238}U and ^{40}K varied from 55.58 to 106.82 Bq kg^{-1}, 37.00 to 76.13 Bq kg^{-1} and 381.37 to 526.26 Bq kg^{-1}, respectively. The comparison of the present data of soil is done with different parts of India and the world in table 5.9. The activities of ^{226}Ra, ^{232}Th and ^{40}K in Mansa are below the permissible limits of 35, 45 and 420 Bq kg^{-1}, respectively [43].

Table 5.3: Heavy metal concentration in wheat grain samples in mg/L with adjusted uncertainties.

S.no.	Mn (mg/L)	Cd (mg/L)	Cu (mg/L)	Fe (mg/L)	Pb (mg/L)	Zn (mg/L)	As (mg/L)
1	0.1457 ± 0.0087	0.1333 ± 0.0067	0.2076 ± 0.0142	0.1981 ± 0.0099	0.2155 ± 0.0151	BDL	0.2092 ± 0.0103
2	0.2137 ± 0.0085	0.1284 ± 0.0051	0.2204 ± 0.0086	0.2880 ± 0.0058	0.2287 ± 0.0091	0.0310 ± 0.0022	0.2070 ± 0.0083
3	0.1466 ± 0.0088	0.1320 ± 0.0066	0.2076 ± 0.0145	0.2030 ± 0.0102	0.2246 ± 0.0157	BDL	0.2021 ± 0.0102
4	0.1677 ± 0.0101	0.1309 ± 0.0065	0.2129 ± 0.0149	0.2125 ± 0.0106	0.2646 ± 0.0185	0.0150 ± 0.0011	0.2101 ± 0.0105
5	0.2574 ± 0.0077	0.1282 ± 0.0064	0.2280 ± 0.0091	0.3135 ± 0.0063	0.2179 ± 0.0087	0.0448 ± 0.0031	0.0448 ± 0.0022
6	0.2325 ± 0.0070	0.1316 ± 0.0067	0.2197 ± 0.0085	0.2721 ± 0.0054	0.2310 ± 0.0092	0.0147 ± 0.0010	0.2032 ± 0.0081
7	0.1467 ± 0.0087	0.1350 ± 0.0068	0.2077 ± 0.0145	0.2015 ± 0.0101	0.2205 ± 0.0154	BDL	0.2111 ± 0.0106
8	0.2192 ± 0.0088	0.1302 ± 0.0062	0.2194 ± 0.0085	0.2701 ± 0.0054	0.2196 ± 0.0088	0.0103 ± 0.0007	0.2208 ± 0.0088
9	0.2431 ± 0.0073	0.1266 ± 0.0063	0.2245 ± 0.0090	0.3200 ± 0.0064	0.2413 ± 0.0097	0.0519 ± 0.0036	0.2100 ± 0.0084
10	0.1864 ± 0.0093	0.1292 ± 0.0065	0.2175 ± 0.0087	0.2303 ± 0.0046	0.2123 ± 0.0085	0.0030 ± 0.0002	0.1988 ± 0.0080
11	0.2507 ± 0.0075	0.1299 ± 0.0063	0.2206 ± 0.0084	0.3384 ± 0.0068	0.2126 ± 0.0082	0.0475 ± 0.0033	0.1999 ± 0.0083
12	0.1469 ± 0.0088	0.1307 ± 0.0065	0.2085 ± 0.0146	0.2005 ± 0.0100	0.1942 ± 0.0136	BDL	0.2085 ± 0.0104
13	0.1940 ± 0.0058	0.1294 ± 0.0066	0.2196 ± 0.0088	0.2480 ± 0.0050	0.2307 ± 0.0092	0.058 ± 0.0041	0.2129 ± 0.0085
14	0.1501 ± 0.0090	0.1308 ± 0.0067	0.2081 ± 0.0144	0.2080 ± 0.0104	0.2351 ± 0.0165	BDL	0.2029 ± 0.0103
15	0.2010 ± 0.0062	0.1286 ± 0.0064	0.2063 ± 0.0144	0.2560 ± 0.0051	0.1965 ± 0.0098	0.0148 ± 0.0013	0.2043 ± 0.0082

In Mansa, the activity of ^{226}Ra in wheat grains varied between 5.67 to 10.02 Bq kg^{-1} with an average of 7.10 Bq kg^{-1}. Likewise, the activity of ^{232}Th varied between 17.94 to 29.08 with an average of 23.30 Bq kg^{-1}. The activity of ^{40}K varied between 369.04 to 442.82 Bq kg^{-1} with an average of 412.82 Bq kg^{-1}. Soil naturally contains ^{40}K and the wheat plants actively absorb potassium from the soil. As wheat grows, it absorbs ^{40}K resulting in higher quantities in wheat grains as compared to the soil around it [44]. The mean internal hazard index for wheat grains is 0.19. Similarly, the radium equivalent for wheat grains varied between 59.79 to 71.63 Bq kg^{-1} with an average of 65.63 Bq kg^{-1}. The annual effective doses of ^{226}Ra and ^{232}Th for wheat grains are well below the reference value of 2.4 mSv year^{-1} [43] whereas for ^{40}K, it is higher than the reference dose for all three groups of infants, children and adults. The children have a higher annual effective dose of ^{40}K than the other two age groups because the body composition of children differs significantly from that of infants and adults. The children possess a greater proportion of body water, which enhances the distribution of ^{40}K, a radionuclide that is soluble in water [45].

5.4.1 Transfer factor from soil to wheat grains

Grains are the consumable part of the wheat crop that is directly ingested by humans. The contamination of the consumable portions of a plant occurs through a sequence of meticulously coordinated processes that begin with soil contamination. This is followed by the absorption of contaminants by the roots, their subsequent transport through the root system to the stem, and finally, the movement from the stem to the

Table 5.4: Activity concentration in various food samples collected from the market.

Sample type	Type	^{226}Ra (Bq kg^{-1})	^{232}Th (Bq kg^{-1})	^{40}K (Bq kg^{-1})
Wheat	Organic 1	17.86±3.23	6.37±1.01	465.25±32.42
	Organic 2	20.13±3.2	4.34±0.85	453.21±38.23
	Organic 3	15.13±2.85	3.22±0.36	432.29±38.09
	Conventional 1	20.83±3.01	6.39±0.96	469.28±36.23
	Conventional 2	22.21±3.89	5.32±0.89	427.82±37.36
Rice	Organic 1	19.43±4.21	6.89±0.95	473.22±28.34
	Organic 2	19.41±3.08	6.97±1.01	485.82±38.09
	Organic 3	18.73±3.25	6.06±0.98	455.81±36.23
	Conventional 1	19.72±3.45	7.01±0.87	472.82±31.28
	Conventional 2	19.52±3.28	7.60±0.66	465.42±32.21
Rajma	Organic 1	16.83±1.96	6.3±0.63	450.81±30.21
	Organic 2	18.81±2.09	5.59±0.12	470.82±32.25
	Organic 3	17.72±2.63	7.41±1.02	493.84±31.28
	Conventional 1	14.72±2.52	5.93±0.96	452.83±28.39
	Conventional 2	19.41±3.25	7.11±0.65	422.89±32.25
Chana Dal	Organic 1	15.62±2.58	8.13±1.02	479.82±31.25
	Organic 2	14.31±1.97	7.22±0.54	472.89±39.21
	Organic 3	11.39±2.32	8.19±0.96	435.4±31.24
	Conventional 1	16.32±3.01	9.13±0.56	480.81±34.12
	Conventional 2	14.32±3.25	8.28±0.85	489.29±31.28
Masoor Dal	Organic 1	13.42±3.65	7.82±0.78	480.22±28.39
	Organic 2	14.83±2.07	6.89±1.03	490.22±32.25
	Organic 3	16.82±2.92	7.93±1.01	432.29±37.24
	Conventional 1	16.89±2.98	8.08±0.98	472.21±38.09
	Conventional 2	19.83±3.52	8.92±0.91	481.89±36.23

Table 5.5: Dose conversion factors for annual effective dose in mSv Bq^{-1} given by ICRP [34].

Element	Infants	Children	Adult
^{226}Ra	9.60E-04	8.00E-04	2.80E-04
^{232}Th	4.50E-04	2.90E-04	2.30E-04
^{40}K	4.20E-05	1.30E-05	6.20E-05

leaves, which constitute the aerial parts of the plant [46]. The study of the dispersal of uranium and thorium within various sections of the wheat plant revealed a decreasing trend from root to grains [30]. The degree of contamination by radionuclides in wheat grains can serve as an indication of the amount of radiation exposure a person may experience through consumption [30]. The transfer of naturally occurring radioactive materials from the rhizospheric zone of soils to wheat grains was assessed using transfer factors. The transfer factor (TF) is the ratio of the activity concentration in a specific portion of a plant (measured in Bq kg^{-1} dry weight) to the activity concentration in the soil (measured in Bq kg^{-1} dry weight). The dry weight was chosen as an ideal measurement because the variability of radioactivity per kilogram of dry weight is significantly lower compared to the variability per unit of fresh

weight. It decreases ambiguities [39]. The equation is given as

$$TF = \frac{C_{plant}}{C_{soil}} \tag{5.8}$$

where TF is the transfer factor from soil to plant (wheat grain), C_{plant} is the activity concentration of a radionuclide in a plant (Bq kg^{-1}) and C_{soil} is the activity concentration of radionuclide in soil (Bq kg^{-1}).

Table 5.6: Average yearly consumption of cereals and pulses for different age groups (Indian standards) [36].

Sample type	Age group (years)	Average Consumption (kg $year^{-1}$)
Cereals	Infants	43.07
	Children	92.16
	Adults (Male)	141.62
Pulses	Infants	5.47
	Children	9.12
	Adults (Male)	12.41
	Adults (Female)	11.31

Table 5.7: The statistical analysis for soil samples.

Parameter	Mean	Minimum	Maximum	Q1	Q3	Radionuclide
Activity (Bq kg^{-1})	11.75	7.37	14.75	10.75	12.89	^{226}Ra
	22.98	16.31	29.61	21.16	24.95	^{232}Th
	267.81	175.36	385.69	244.95	286.73	^{40}K
Raeq (Bq kg^{-1})	65.24	55.40	72.45	62.62	67.01	
AED (mSv $year^{-1}$)	0.037	0.032	0.041	0.035	0.038	
H_{ex}	0.17	0.14	0.19	0.16	0.18	

The transfer factor of ^{226}Ra, ^{232}Th and ^{40}K from soil to wheat grains is given in table 5.10. The transfer factor values are greater than the acceptable values given by IAEA. The acceptable value of transfer factor for ^{226}Ra is 4×10^{-2}, ^{232}Th is 5×10^{-2} and ^{40}K is 1 [39]. The transfer factor for ^{226}Ra varied from 0.46 to 0.89 with an average of 0.59. For ^{232}Th, the transfer factor varied between 0.73 to 0.92 with an average of 0.81. The transfer factor for ^{40}K varied between 1.21 to 1.92 with an average of 1.52. Various factors that may influence the transfer of radionuclides from soil to plants encompass climatic factors such as weathering, humidity, etc., impact of competing species, plant physiology, soil traits such as texture, cation exchange, pH of soil in conjunction with the physico-chemical state of the radionuclides. Moreover, agricultural practices such as the usage of fertilizers can also impact the transfer factor [25]. Tufail et al. [47] reported the transfer factors for ^{40}K, ^{226}Ra and ^{232}Th from soil to wheat grain to be 0.118, 0.022 and 0.036, respectively, in Faisalabad, Pakistan. The transfer factors of natural radionuclides from soils to wheat grains grown in fertilised fields in Pakistan have been measured as 2×10^{-2} to 3×10^{-2} for ^{232}Th, 3×10^{-2} to 4×10^{-2} for ^{226}Ra and 17×10^{-2} to 20×10^{-2} for ^{40}K [48]. The transfer factors of the radionuclides ^{226}Ra, ^{232}Th and ^{40}K from soil to wheat flour of Kars, Turkiye were found to range from 0.30 to 1.29, 0.15 to 0.86, and 0.45 to 0.83, respectively [49].

Table 5.8: The statistical analysis for wheat samples.

Parameter	Mean	Minimum	Maximum	Q1	Q3	Radionuclide
Activity (Bq kg^{-1})	7.10	5.67	10.02	6.04	7.87	^{226}Ra
	23.30	17.94	29.08	21.26	25.12	^{232}Th
	412.82	369.04	442.82	393.08	435.35	^{40}K
Raeq (Bq kg^{-1})	65.63	59.79	71.63	63.25	68.38	
AED (mSv $year^{-1}$)	0.29	0.23	0.41	0.24	0.32	^{226}Ra (Infant)
	0.29	0.23	0.41	0.25	0.33	^{226}Ra (Child)
	0.04	0.03	0.05	0.03	0.04	^{226}Ra (Adult)
	0.64	0.52	0.72	0.60	0.68	^{232}Th (Infant)
	0.47	0.49	0.56	0.47	0.03	^{232}Th (Child)
	0.03	0.03	0.02	0.03	0.03	^{232}Th (Adult)
	4.97	4.45	5.34	4.74	5.25	^{40}K (Infant)
	8.75	7.82	9.38	8.33	3.45	^{40}K (Child)
	3.62	3.24	3.88	3.45	3.88	^{40}K (Adult)
H_{in}	0.19	0.17	0.22	0.18	0.20	

5.5 Heavy metal analysis of wheat grains

The interaction of plant with metals is contingent upon soil characteristics such as organic matter, pH as well as clay absorption [50]. These metals accumulate in soil and permeate the food chain resulting in health problems. Plants can be harmed by the presence of high amounts of heavy metals, which can disrupt the permeability of their membranes, hinder the activity of enzymes and deactivate photosystems [51]. Heavy metal concentration in the wheat grain samples is listed in table 5.11. Mn, Cd, Ar, Cu, Cr, Pb, Mo, Bi and Sr were measured in wheat grain samples of the study region. The average concentration of Mn in wheat grains is 0.193 ppm, with minimum and maximum values varying between 0.145 and 0.257, respectively. The results demonstrate that the measurements are beneath the allowable limit of Mn in wheat grains i.e. 46 ppm [52]. The cadmium concentration varied between 0.126 to 0.135 ppm with an average of 0.130 which is higher than the permissible limit of 0.1 ppm for cereals set by Kent [52] but below the Indian permissible limit of 1.5 ppm [53]. The reason for the high cadmium concentration in wheat grains can be various types of fertilisers based on sulphur, nitrogen and potassium, which increase the concentration of Cd in wheat grains [54-56]. The copper concentration in wheat grains varied between 0.206 to 0.228 ppm with an average of 0.215 which is beneath the allowable threshold of 30 ppm [53]. The arsenic concentration in wheat grains varied between 0.044 to 0.220 ppm with an average of 0.196 ppm, which is below the permissible limit of 0.5 ppm. The concentration of lead in wheat grains varied from 0.194 to 0.264 ppm with an average of 0.223 ppm, which falls below the acceptable limit of 2.5 ppm [53]. The average concentration of Zn in wheat grains is 0.013 ppm which is far below the permissible limit of 50 ppm [53]. The average concentration of iron is 0.250 ppm and varied between 0.198 ppm to 0.338 ppm, which falls below the acceptable limit of 46 ppm [52]. Strontium was below the detection limit. The sequence of heavy metals in increasing order of concentration for the present study is: strontium, zinc, cadmium, manganese, arsenic, copper, lead and iron. Similarly, the heavy metal concentration is decreasing in wheat grains in Kunschan, China was: zinc, copper, lead, chromium, nickel, cadmium, arsenic, and mercury [57]. Wang *et*

al. [58] found the accumulation of heavy metals in wheat grains as (in ascending order): Zn, Pb, Cr, Cu, As, Hg, and Cd. Furthermore, the study found that wheat has a higher tendency to accumulate heavy metals compared to maize.

Table 5.9: Comparison of the concentration of radionuclides of soil in Mansa, Punjab with various studies.

Location	**^{226}Ra** (Bq kg^{-1})	**^{232}Th** (Bq kg^{-1})	**^{40}K** (Bq kg^{-1})	**References**
Mansa, Punjab, India	11.75	22.98	267.81	
Algeria	53	50	311	[59]
China	40	59.6	751.2	[60]
Pakistan	27.7	45.5	525	[61]
Turkey	8.93	11.39	281.94	[62]
World average	33	45	420	[63]

Table 5.10: The transfer factor from soil to wheat grains for ^{226}Ra, ^{232}Th and ^{40}K.

Radionuclide	**Mean**	**Minimum**	**Maximum**	**Q1**	**Q3**
^{226}Ra	0.59	0.46	0.89	0.51	0.65
^{232}Th	0.81	0.73	0.92	0.77	0.85
^{40}K	1.52	1.21	1.92	1.32	1.72

Table 5.11: Heavy metal concentration (ppm) in wheat grain samples of Mansa, Punjab.

Element	**Average**	**Minimum**	**Maximum**	**Q1**	**Q3**
Mn	0.193	0.145	0.257	0.148	0.225
Cd	0.130	0.126	0.135	0.128	0.131
Cu	0.215	0.206	0.228	0.207	0.220
As	0.196	0.044	0.220	0.202	0.220
Pb	0.223	0.194	0.264	0.214	0.230
Zn	0.013	BDL*	0.058	BDL*	0.037
Fe	0.250	0.198	0.338	0.205	0.280
Sr	BDL*				

*BDL-Below detection limit

5.5.1 Correlation between radionuclides and heavy metals

The Pearson correlation between radionuclides and heavy metals for wheat grains at a confidence level of 95% is listed in table 5.12. These correlations offer a comprehensive understanding of the relationship between heavy metal concentrations and radionuclide levels in wheat grains from the Mansa district. It is essential to comprehend these relationships in order to evaluate the potential causes for contamination or natural variability in the radionuclide and heavy metal content of agricultural products, which is essential for environmental monitoring and food safety. A strong correlation of Mn with Cu, Fe and Zn is found. Stepien *et al.* [64] observed that the content of Cu and Zn in grain was increased when mineral NPK

fertilisation was combined with micronutrients (Cu, Zn, and Mn) justifying the strong correlation among them. Cu has a strong correlation with Fe and Zn. As cadmium competes with zinc, copper and iron for absorption and transportation within plants therefore, Cd has a strong negative correlation with zinc, copper and iron [65]. Radionuclides have no relation among themselves as well as with heavy metals.

Table 5.12: Pearson correlation between radionuclides and heavy metals found in wheat grains.

	Mn	**Cd**	**Cu**	**Fe**	**Pb**	**Zn**	**As**	**^{226}Ra**	**^{232}Th**
Cd	-0.683*								
Cu	0.878*	-0.649*							
Fe	0.969*	-0.692*	0.838*						
Pb	0.035	-0.028	0.241	0.016					
Zn	0.866*	-0.746*	0.833*	0.839*	0.242				
As	-0.424	0.274	-0.471	-0.363	0.105	-0.259			
^{226}Ra	0.095	-0.122	0.014	0.063	-0.056	0.125	-0.034		
^{232}Th	-0.116	-0.306	0.012	-0.047	-0.199	-0.083	0.132	0.133	
^{40}K	0.104	-0.191	0.027	0.112	-0.139	0.182	0.266	0.258	0.059

5.6 Radiological risk comparison of organic and conventional food

The average activity of ^{226}Ra is 17.70 Bq kg^{-1},^{232}Th is 4.64 Bq kg^{-1} and ^{40}K and 450.25 Bq kg^{-1}, respectively in organic wheat samples, whereas in conventional samples, the values are 21.52 Bq kg^{-1} for ^{226}Ra , 5.85 Bq kg^{-1} for ^{232}Th and 448.55 Bq kg^{-1} for ^{40}K, respectively. In organic rice, the average activities of ^{226}Ra, ^{232}Th and ^{40}K are 19.19 Bq kg^{-1}, 6.64 Bq kg^{-1} and 471.61 Bq kg^{-1}, respectively. The average activities of ^{226}Ra, ^{232}Th and ^{40}K in market samples of rice are 19.62 Bq kg$^{-1,}$ 7.30 Bq kg^{-1} and 469.12 Bq kg^{-1}, respectively. For pulses, the ^{226}Ra, ^{232}Th and ^{40}K activity concentrations in organic rajma are 17.78 Bq kg^{-1}, 6.43 Bq kg^{-1} and 471.82 Bq kg^{-1}, respectively. In conventional market bought rajma, the activity concentrations of ^{226}Ra, ^{232}Th and ^{40}K are 17.06 Bq kg^{-1}, 6.52 Bq kg^{-1} and 437.86 Bq kg^{-1}, respectively. In organic channa dal, the average activity concentrations of ^{226}Ra, ^{232}Th and ^{40}K are 13.77 Bq kg^{-1}, 7.84 Bq kg^{-1} and 462.70 Bq kg^{-1}, respectively. Similarly, for the conventional samples, the average activity concentrations of ^{226}Ra, ^{232}Th and ^{40}K for channa dal are 15.32 Bq kg^{-1}, 8.70 Bq kg^{-1} and 485.05 Bq kg^{-1}, respectively. The activity concentrations of ^{226}Ra, ^{232}Th and ^{40}K in organic masoor dal are 15.02 Bq kg^{-1}, 7.54 Bq kg^{-1} and 467.57 Bq kg^{-1}, respectively. The average activity concentrations of ^{226}Ra, ^{232}Th and ^{40}K in conventional market samples of masoor dal are 18.36 Bq kg^{-1}, 8.5 Bq kg^{-1} and 477.05 Bq kg^{-1}, respectively. The bar graph in figure 5.3 shows the activity concentration in different samples. Although the values of ^{40}K are higher than the reference value of 420 Bq kg^{-1}, but the hemostatic balance of the human body keeps the concentration of ^{40}K in control despite the intake variations [66]. The radium equivalent and internal hazard index are listed in table 5.13.

The calculated ^{226}Ra average annual effective dose of organic and conventional wheat and rice for children is the highest among all age groups ranging between 1.30 and 1.58 mSv year^{-1}. For all age groups, the values are below the reference value of 2.4 mSv year^{-1} given by UNSEAR [35]. The annual effective dose is highest for rice samples among all samples and can be attributed to their high transfer coefficient and leaching of water into the soil [67]. A lower annual effective dose is observed for pulses due to less consumption as compared to cereals in India. The calculated values are listed in table 5.14 and 5.15. Both the UNSCEAR and Indian standards gave similar values for cereals [32].

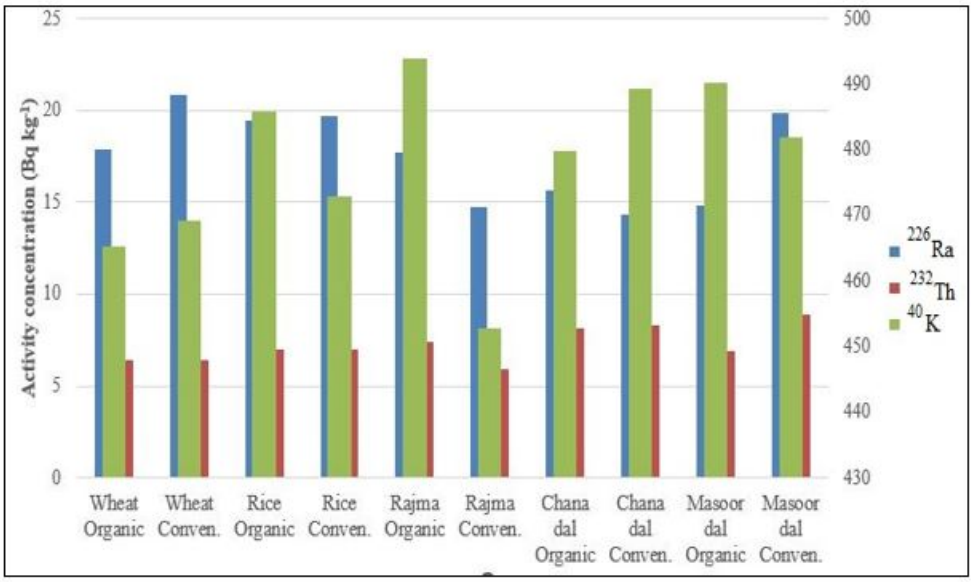

Figure 5.3: Activity concentration of ^{226}Ra, ^{232}Th and ^{40}K in different organic and conventional market bought staple food samples.

5.7 Conclusion

The risk analysis is carried out for samples of soil, wheat, organic and conventional samples. The activity of ^{40}K in few wheat samples of Mansa is higher than the permissible limit of 420 Bq kg^{-1}. The radium equivalent for both soil and wheat is well below 370 Bq kg^{-1}. The annual effective dose for both soil and wheat grains of Mansa is below the recommended limits. The hazard indices are lower than 1 for both wheat and soil samples of Mansa. The heavy metal analysis of wheat samples of Mansa is conducted, and the sequence of heavy metals in increasing order for the present study is: Sr, Zn, Cd, Mn, As, Cu, Pb and Fe. It is found that cadmium is in higher amounts than the permissible limits of 0.1 ppm but well below Indian permissible limits. The organic food shows low activity concentration as compared to conventional food samples. Moreover, there is a need to further investigate the effects of fertilizers as the concentration of radionuclides was somewhat higher in that case. Although organic food is much costlier than regular market food, there is not much difference in naturally occurring radionuclides concentration in organic and regular market samples. From the samples collected of organic and conventional staple food, both categories are safe for consumption as far as radionuclide concentrations are

concerned.

Table 5.13: Average radium equivalent and hazard indices for different samples taken from market.

Sample type	**Ra_{eq} (Bq kg^{-1})**	**H_{in}**
Wheat Organic	59.01	0.20
Wheat Conventional	64.43	0.23
Rice Organic	64.99	0.22
Rice Conventional	66.18	0.23
Rajma Organic	63.31	0.21
Rajma Conventional	60.10	0.20
Channa Dal Organic	60.62	0.20
Channa Dal Conventional	65.11	0.21
Masoor Dal Organic	61.81	0.20
Masoor Dal Conventional	67.24	0.23

Table 5.14: Comparison of average annual effective dose in mSv $year^{-1}$ due to cereals for consumption for different age groups for Indian and the world population.

Sample type	**Age group**	**^{226}Ra (India)**	**^{226}Ra (World)**	**^{232}Th (India)**	**^{232}Th (World)**	**^{40}K (India)**	**^{40}K (World)**
Wheat Organic	Infant	0.73	0.76	0.08	0.09	0.81	0.85
	Children	1.30	1.27	0.12	0.12	0.53	0.52
	Adults	0.70	0.69	0.15	0.14	3.95	3.90

Sample type	Age group	^{226}Ra (India)	^{226}Ra (World)	^{232}Th (India)	^{232}Th (World)	^{40}K (India)	^{40}K (World)
Wheat Conventional	Infants	0.88	0.92	0.11	0.11	0.81	0.84
	Children	1.58	1.54	0.15	0.15	0.53	0.52
	Adults	0.85	0.84	0.19	0.18	3.93	3.89
Rice Organic	Infants	0.79	0.82	0.12	0.13	0.85	0.89
	Children	1.41	1.38	0.17	0.17	0.56	0.55
	Adults	0.76	0.75	0.21	0.21	4.14	4.09
Rice Conventional	Infants	0.81	0.84	0.14	0.14	0.84	0.88
	Children	1.44	1.41	0.19	0.19	0.56	0.54
	Adults	0.77	0.76	0.23	0.03	4.11	4.07

Table 5.15: Average annual effective dose in mSv year^{-1} due to pulses consumption for different age groups for Indian population.

Sample type	Age group	^{226}Ra	^{232}Th	^{40}K
Channa Dal Organic	Infant	0.07	0.01	0.10
	Children	0.10	0.02	0.05
	Adult (Male)	0.04	0.02	0.03
	Adult (Female)	0.04	0.02	0.03
Channa Dal Conventional	Infant	0.08	0.02	0.11
	Children	0.11	0.02	0.05
	Adult (Male)	0.05	0.02	0.03
	Adult (Female)	0.04	0.02	0.03
Rajma Organic	Infants	0.09	0.01	0.10
	Children	0.13	0.01	0.05
	Adult (Male)	0.06	0.01	0.03

Sample type	**Age group**	**^{226}Ra**	**^{232}Th**	**^{40}K**
	Adult (Female)	0.05	0.01	0.03
Rajma Conventional	Infants	0.08	0.01	0.10
	Children	0.12	0.01	0.05
	Adult (Male)	0.05	0.01	0.03
	Adult (Female)	0.05	0.01	0.03
Masoor Dal Organic	Infant	0.07	0.01	0.10
	Children	0.11	0.02	0.05
	Adult (Male)	0.05	0.02	0.03
	Adult (Female)	0.04	0.01	0.03
Masoor Dal Conventional	Infant	0.09	0.02	0.10
	Children	0.13	0.02	0.05
	Adult (Male)	0.06	0.02	0.03
	Adult (Female)	0.05	0.02	0.03

5.8 References

1. Thabit, T. M., Shokr, S. A., Elgeddawy, D. I., & El-Naggar, M. A. (2020). Determination of heavy metals in wheat and barley grains using ICP-MS/MS. *Journal of AOAC international*, *103*(5), 1277-1281.

2. Tong, S., Yang, L., Gong, H., Wang, L., Li, H., Yu, J & Men, Z. (2022). Bioaccumulation characteristics, transfer model of heavy metals in soil-crop system and health assessment in plateau region, China. *Ecotoxicology and environmental Safety*, *241*, 113733.

3. Christou, A., Eliadou, E., Michael, C., Hapeshi, E., & Fatta-Kassinos, D. (2014). Assessment of long-term wastewater irrigation impacts on the soil geochemical properties and the bioaccumulation of heavy metals to the agricultural products. *Environmental monitoring and assessment*, *186*, 4857-4870.

4. Qi, X. B., Kamran, M., Yasin, G., Cheng, H. F., Rehim, A., Riaz, L., & Alyemeni, M. N. (2021). Silicon elevated cadmium tolerance in wheat (Triticum aestivum L.) by endorsing nutrients uptake and antioxidative defense mechanisms in the leaves.

5. Huang, S., Tu, J., Liu, H., Hua, M., Liao, Q., Feng, J. & Huang, G. (2009). Multivariate analysis of trace element concentrations in atmospheric deposition in the Yangtze River Delta, East China. *Atmospheric environment*, *43*(36), 5781-5790.

6. Sharma, R. K., Agrawal, M., & Marshall, F. (2007). Heavy metal contamination of soil and vegetables in suburban areas of Varanasi, India. *Ecotoxicology and environmental safety*, *66*(2), 258-266.

7. Zhou, M., & Zheng, S. (2022). Multi-omics uncover the mechanism of wheat under heavy metal stress. *International journal of molecular sciences*, *23*(24), 15968.

8. Singh, S., Parihar, P., Singh, R., Singh, V. P., & Prasad, S. M. (2016). Heavy metal tolerance in plants: role of transcriptomics, proteomics, metabolomics, and ionomics. *Frontiers in plant science*, *6*, 1143.

9. Rastgoo, L., Alemzadeh, A., Tale, A. M., Tazangi, S. E., & Eslamzadeh, T. (2014). Effects of copper, nickel and zinc on biochemical parameters and metal accumulation in Gouan,'Aeluropus littoralis'. *Plant knowledge journal*, *3*(1), 42-49.

10. Wang, Q. R., Cui, Y. S., Liu, X. M., Dong, Y. T., & Christie, P. (2003). Soil contamination and plant uptake of heavy metals at polluted sites in China. *Journal of Environmental science and health, Part A*, *38*(5), 823-838.

11. Hanfi, M. Y., Emad, B. M., Sayyed, M. I., Khandaker, M. U., & Bradley, D. A. (2021). Natural radioactivity in the prospecting tunnel in Egypt: Dose rate and risk assessment. *Radiation physics and chemistry*, *187*, 109555.

12. Daulta, R., Garg, V. K., & Singh, B. (2019). Natural radioactivity in soil, associated radiation exposure and cancer risk to population of Eastern Haryana, India. *Journal of the geological society of India*, *94*, 525-532.

13. Radhakrishna, A. P., Somashekarappa, H. M., Narayana, Y., & Siddappa, K. (1993). A new natural background radiation area on the southwest coast of India. *Health physics*, *65*(4), 390-395.

14. Omoniyi, I. M., Oludare, S. M., & Oluwaseyi, O. M. (2013). Determination of radionuclides and elemental composition of clay soils by gamma-and X-ray spectrometry. *Springerplus*, *2*, 1-11.

15. Yang, B., Zhou, Q., Zhang, J., Li, Z., & Tuo, F. (2021). Evaluation of the natural radioactivity in food and soil around uranium mining region. *Journal of radioanalytical and nuclear chemistry*, *329*, 127-133.

16. Mehmet Bakım and Aysun Ugur Gorgun.(2015). Radioactivity in soils and some terrestrial foodstuffs from organic and conventional farming areas in Izmir, Turkey. *Journal of Radioanalytical and Nuclear Chemistry*, *306*(1): 237-242.

17. Edward J Bouwer, John W McKlveen, and WJ McDowell (1978). Uranium assay of phosphate fertilizers and other phosphatic materials. *Health Physics*, 34.4: 345-352.

18. W. Eberhard Falck and Denis Wymer.(2006). *Uranium in phosphate fertilizer production.* Springer Berlin Heidelberg, Berlin, Heidelberg: 857-866.

19. M Tufail, Nasim Akhtar, and M Waqas.(2006). Radioactive rock phosphate: the feed stock of phosphate fertilizers used in Pakistan. *Health physics*, *90.4*: 361-370.

20. Wassila Boukhenfouf and Ahmed Boucenna. (2012). Uranium content and dose assessment for phosphate fertiliser and soil samples: comparison of uranium concentration between virgin soil and fertilised soil. *Radiation protection dosimetry*, *148*(2) : 263–267.

21. RK Rattan, SP Datta, PK Chhonkar, K Suribabu, and AK Singh. (2005). Long-term impact of irrigation with sewage effluents on heavy metal content in soils, crops and groundwater-a case study. *Agriculture, ecosystems & environment*, *109* 3-4: 310-322.

22. MS Al-Masri, Y Amin, B Al-Akel, and T AlNaama. (2010). Biosorption of cadmium, lead, and uranium by powder of poplar leaves and branches. *Applied biochemistry and biotechnology*, *1*60(4): 976–987.

23. HBL Pettersson, G Hancock, A Johnston, and AS Murray. (1993). Uptake of uranium and thorium series radionuclides by the waterlily, Nymphaea violacea. *Journal of Environmental Radioactivity*, *19.2* : 85–108.

24. F Carini. (2001). Radionuclide transfer from soil to fruit. *Journal of Environmental Radioactivity*, *52*(2-3):237-279.

25. Poonam Yadav, Balvinder Singh, VK Garg, Suman Mor, and Vandana Pulhani. (2017). Bioaccumulation and health risks of heavy metals associated with consumption of rice grains from croplands in Northern India. *Human and ecological risk assessment: an international journal*, *23(1)*:14–27.

26. N Karunakara, Chetan Rao, P Ujwal, I Yashodhara, Sudeep Kumara, and PM Ravi. (2013). Soil to rice transfer factors for ^{226}Ra, ^{228}Ra, ^{210}Pb, ^{40}K and ^{137}Cs: a study on rice grown in India. *Journal of environmental radioactivity*, *118*: 80–92.

27. M Anke, O Seeber, R Muller, U Sch¨ afer, and¨ J Zerull. (2009). Uranium transfer in the food chain from soil to plants, animals and man. *Geochemistry*, *69*:75-90.

28. Fredrick Oghenebrorie Ugbede and Okhuomaruyi David Osahon. (2021). Soil-to-plant transfer factors of ^{238}U and ^{232}Th in rice from Ezillo paddy fields, Ebonyi State, Nigeria. *Journal of Environmental Radioactivity*, 233:106606.

29. IAEA. guidelines on soil and vegetation sampling for radiological monitoring: technical report series 486.

30. Pulhani, V. A., Dafauti, S., Hegde, A. G., Sharma, R. M., & Mishra, U. C. (2005). Uptake and distribution of natural radioactivity in wheat plants from soil. *Journal of environmental radioactivity*, *79*(3), 331-346.

31. Tufail, M. (2012). Radium equivalent activity in the light of UNSCEAR report. *Environment monitoring and assessment 184*, 5663-5667.

32. Guron, B. K., Kalkal, S., & Mehra, R. (2023). A Comparison of the Concentration of Naturally Occurring Radionuclides in Organic and Conventional Staple Food. *Indian journal of pure & applied physics (IJPAP)*, *61*(6), 455-460.

33. Yadav, P., Garg, V. K., Singh, B., Pulhani, V., & Mor, S. (2018). Transfer factors and effective dose evaluation due to natural radioactivity in staple food grains from the vicinity of proposed nuclear power plant. *Exposure and health*, *10*, 27-39.

34. Eckerman, K., Harrison, J., Menzel, H. G., & Clement, C. H. (2012). ICRP publication 119: compendium of dose coefficients based on ICRP publication 60. *Annals of the ICRP*, *41*, 1-130.

35. United Nations Scientific Committee on the Effects of Atomic Radiation. (2000). *Sources and effects of ionizing radiation, United Nations Scientific Committee on the Effects of Atomic Radiation (UNSCEAR) 2000 Report, Volume I: Report to the general assembly, with scientific annexes-Sources*. United Nations.

36. NNMB (2012). Diet and nutritional status of rural population, prevalence of hypertension & diabetes among adults and infant & young child feeding practices: NNMB Technical Report No. 26.

37. Srinivasa, E., Rangaswamy, D. R., Suresh, S., & Sannappa, J. (2022). Natural radioactivity levels and associated radiation hazards in soil samples of Chikkamagaluru district, Karnataka, India. *Journal of radioanalytical and nuclear chemistry*, 1-8.

38. Janković, M., Todorović, D., & Savanović, M. (2008). Radioactivity measurements in soil samples collected in the Republic of Srpska. *Radiation measurements*, *43*(8), 1448-1452.

39. International Union of Radioecologists. (1994). *Handbook of parameter values for the prediction of radionuclide transfer in temperate environments* (Vol. 364). International Atomic Energy Agency.

40. Rizvi, A., Zaidi, A., Ameen, F., Ahmed, B., AlKahtani, M. D., & Khan, M. S. (2020). Heavy metal induced stress on wheat: phytotoxicity and microbiological management. *Royal society of chemistry advances,* 10(63), 38379-38403

41. Badhan K, Mehra R (2012). Primordial radioactivity (^{238}U, ^{232}Th and ^{40}K) measurements for soils of Ludhiana district of Punjab, India. *Radiation protection dosimetry 152*(1- 3):29-32.

42. Kaintura, S. S., Thakur, S., Kaur, S., Devi, S., Tiwari, K., Sharma, A., & Singh, P. P. (2024). Investigating radioactivity in soil samples from neutral and vegetation land of Punjab/India. *arXiv preprint arXiv:2403.15414*.

43. Charles, M. (2001). UNSCEAR Report 2000: sources and effects of ionizing radiation.

44. Sead, S. M., Uzorka, A., & Olaniyan, A. O. (2024). Investigation into radioactivity levels in soil samples from wheat cultivation sites in Kapchorwa district Uganda. *Discover environment*, *2*(1), 55.

45. He, Q., Heo, M., Heshka, S., Wang, J., Pierson Jr, R. N., Albu, J., & Gallagher, D. (2003). Total body potassium differs by sex and race across the adult age span. *The American journal of clinical nutrition*, *78*(1), 72-77.

46. Al-Alawy, I. T., Mhana, W. J., & Ebraheem, R. M. (2020). Radiation hazards and transfer factors of radionuclides from soil to plant and cancer risk at Al-Taji city-Iraq. In *IOP Conference Series: Materials science and engineering* (Vol. 928, No. 7, p. 072139). IOP Publishing.

47. Tufail, M., Akhtar, N., & Akhter, J. (2010). Assessment of annual effective dose from natural radioactivity intake through wheat grain produced in Faisalabad, Pakistan. *Journal of radioanalytical and nuclear chemistry*, *283*, 585-590.

48. Akhtar, N., & Tufail, M. (2007). Natural radioactivity intake into wheat grown on fertilized farms in two districts of Pakistan. *Radiation protection dosimetry*, *123*(1), 103- 112.

49. Bilgici Cengiz (eker), G., Çağlar, İ., & Çağlar, A. (2020). Determination of transfer factors of natural radionuclides from soil-to-wheat flour consumed by Kars people. *Caucasian journal of science*, *7*(2), 140-152.

50. Rizvi, A., Zaidi, A., Ameen, F., Ahmed, B., AlKahtani, M. D., & Khan, M. S. (2020). Heavy metal induced stress on wheat: phytotoxicity and microbiological management. *Royal society of chemistry advances, 10*(63), 38379-38403.

51. Al-Othman, Z. A., Ali, R., Al-Othman, A. M., Ali, J., & Habila, M. A. (2016). Assessment of toxic metals in wheat crops grown on selected soils, irrigated by different water sources. *Arabian journal of chemistry*, *9*, S1555-S1562.

52. Kent, N. L. (1994). *Kent's Technology of Cereals: An introduction for students of food science and agriculture*. Elsevier.

53. Singh, A. K., Sathya, M., Verma, S., & Jayakumar, S. (2018). Health risk assessment of heavy metals in crop grains grown on open soils of Kanwar wetland, India. *Euro-Mediterranean Journal for Environmental Integration, 3,* 1-7.

54. Zhou, M., & Li, Z. (2022). Recent advances in minimizing cadmium accumulation in wheat. *Toxics*, *10*(4), 187.

55. Özkutlu, F. (2024). Effects of Applying Different N Sources on Cd Accumulation, Mineral Micronutrients, and Grain Yield of Durum Wheat. *Journal of soil science and plant nutrition*, 1-8.

56. Wang, K., Fu, G., Yu, Y., Wan, Y., Liu, Z., Wang, Q. & Li, H. (2019). Effects of different potassium fertilizers on cadmium uptake by three crops. *Environmental science and pollution research*, *26*, 27014-27022.

57. Huang, M., Zhou, S., Sun, B., & Zhao, Q. (2008). Heavy metals in wheat grain: assessment of potential health risk for inhabitants in Kunshan, China. *Science of the total environment*, *405*(1-3), 54-6.

58. Wang ShiYu, W. S., Wu WenYong, W. W., Liu Fei, L. F., Liao RenKuan, L. R., & Hu YaQi, H. Y. (2017). Accumulation of heavy metals in soil-crop systems: a review for wheat and corn.

59. Boukhenfouf, W., & Boucenna, A. (2011). The radioactivity measurements in soils and fertilizers using gamma spectrometry technique. *Journal of environmental radioactivity*, *102*(4), 336-339.

60. Lu, X., Li, X., Yun, P., Luo, D., Wang, L., Ren, C., & Chen, C. (2012). Measurement of natural radioactivity and assessment of associated radiation hazards in soil around Baoji second coal-fired thermal power plant, China. *Radiation protection dosimetry*, *148*(2), 219-226.

61. Akhtar, N., Tufail, M., Ashraf, M., & Iqbal, M. M. (2005). Measurement of environmental radioactivity for estimation of radiation exposure from saline soil of Lahore, Pakistan. *Radiation measurements*, *39*(1), 11-14.

62. Yalcin, P. A. Ş. A., Taskin, H., Kam, E., Taskin, H., Terzi, M., Varinlioglu, A., & Tasdelen, B. (2012). Investigation of radioactivity level in soil and drinking water samples collected from the city of Erzincan, Turkey. *Journal of radioanalytical and nuclear chemistry*, *292*(3), 999-1006.

63. IAEA/RCA (1989). *Health Physics Division, regional work on environmental sampling and measurement of radioactivity for monitoring purposes.* BARC, Kalpakkam.

64. Stepien, A., & Wojtkowiak, K. (2016). Effect of foliar application of Cu, Zn, and Mn on yield and quality indicators of winter wheat grain. *Chilean journal of agricultural research*, *76*(2), 220-227.

65. Ma, W., Li, Y., Ge, C., Wang, M., & Zhou, D. (2024). Effect of genotype on cadmium and trace element accumulation in wheat from weakly alkaline cadmium-contaminated soil. *Bulletin of environmental contamination and toxicology, 113(1),* 9.

66. Pintilie-Nicolov, V., Georgescu, P. L., Iticescu, C., Moraru, D. I., & Pintilie, A. G. (2021). The assessment of the annual effective dose due to ingestion of radionuclides from drinking water consumption: calculation methods. *Journal of radioanalytical and nuclear chemistry*, *327*, 49-58.

67. Barescut, J. C., Gariel, J. C., Péres, J. M., Uchida, S., Tagami, K., Hirai, I., & Komamura, M. (2005). Transfer factors of radionuclides and stable elements from soil to rice and wheat. *Radioprotection*, *40*(S1), S129-S134.

Chapter 6

Conclusion

The Mansa district, located in the southwestern region of Punjab, India, has as become a prominent area of research, primarily due to escalating concerns regarding environmental pollution. This thesis aims to evaluate the adverse effects on human health due to naturally occurring radionuclides and heavy metals found in the water, soil and food sources of Mansa. Additionally, it seeks to quantify the concentrations of these radionuclides in both organic and conventional staple foods. The results of these objectives contribute to a deeper comprehension of the environmental and health challenges faced by the residents of Mansa district, providing important insights for future mitigation efforts.

The health risks associated with groundwater through both deterministic and probabilistic methodologies is calculated. The research underscored alarming concentrations of uranium, cadmium and chromium present in the groundwater of Mansa district. The findings offered an extensive risk assessment, demonstrating that the local population is exposed to considerable health hazards, primarily stemming from the ingestion of polluted water. The assessed cancer and non-cancer risks surpassed acceptable thresholds, underscoring an urgent requirement for intervention and remediation strategies. The results of this study highlight the critical importance of regular monitoring of groundwater quality of the region. The use of advanced modelling tools such as MATLAB and Argo have proved effective in predicting health risks based on probabilistic assessment. It has been found that the probabilistic analysis should be used to estimate groundwater quality or associated contamination risk in order to better depict the actual scenario by taking into account variability as the deterministic approach can underestimate or overestimate the assessment. The evaluation of health risks indicated that children exhibit a greater susceptibility to health hazards compared to adults due to their lower body weight. The sensitivity analysis is also conducted and it revealed that the concentration of heavy metal is the dominant factor impacting the non-carcinogenic health risk assessment followed by exposure duration.

The broader toxic effects of contaminated uranium on human health using biokinetic modelling of uranium are also investigated. The in-depth toxicological risk assessment provided a comprehensive analysis of the mechanisms of uranium exposure and potential health effects on the population. Long-term exposure to uranium contaminated groundwater can lead to serious health conditions. The kidneys are highly impacted by uranium contaminated groundwater ingestion based on dose as

they act as storage sites. The excretion pathways remain consistent through the years whereas the cortical bone surface follow logarithmic growth with highest storage over the years. The correlations of physico-chemical properties of water showed high correlation between uranium concentration and TDS and between conductivity and salinity. The study calls for immediate public health interventions, including educating communities about the risks of uranium exposure and promoting safety measures to reduce exposure.

In addition to groundwater contamination, the investigation of naturally occurring radionuclides in soil and wheat grains collected from Mansa district is performed. The activity of ^{40}K in few wheat samples is exceeding the permissible limit of 420 Bq kg^{-1}. The annual effective dose and hazard indices for both soil and wheat grains are below the recommended limits. The heavy metal analysis of wheat grains is also conducted. It is found that cadmium is in higher amount than the permissible limit of 0.1 ppm however, is under Indian permissible limit.

A comparative study of organic and conventional staple food from the market revealed that organic foods tend to have lower levels of radionuclides compared to their conventional counterparts. This finding is important because the samples analysed show that both categories are considered safe for consumption in terms of radionuclide concentrations. The study indicates that more comprehensive research is necessary to analyse the effects of fertilizers as the concentration levels are somewhat elevated.

In this thesis, a comprehensive evaluation of the environmental and health issues encountered by the inhabitants of Mansa district as a result of uranium contamination in groundwater and the presence of naturally occurring radionuclides in food and soil is conducted. In summary, the work cohesively integrates all dimensions of the assessment of natural radionuclides across water, food and soil. The findings underscore the need for immediate and sustained interventions to reduce the health risks associated with contaminants. In addition, emphasizes has been given to the role of advanced analytical tools and toxicological studies in the complex interaction between environmental pollutants and human health. The findings derived from this research can offer a framework for subsequent investigations and the formulation of policies designed to safeguard the health and welfare of communities in Mansa and other regions.

FUTURE SCOPE OF THE WORK

Exploring the below mentioned prospective research avenues can enhance existing studies, thereby contributing to the advancement of knowledge, refining risk management strategies and safeguarding the public.

- The execution of extensive epidemiological studies in the area may facilitate the identification of particular health outcomes and enhance the precision of risk assessment models.
- Examining and assessing feasible groundwater remediation technologies to determine their efficacy in lowering uranium concentrations of the region. This analysis may encompass research on the implementation of sophisticated filtration techniques, bioremediation strategies and chemical treatment options.

- Analysing the seasonal fluctuations of groundwater, soil and food resources can enhance our comprehension of the dynamics within the study area.
- The bioaccumulation factor, which quantifies the transfer of heavy metals from soil to food can be assessed to enhance our comprehension of the movement of these contaminants from soil to plants.

Journal Publications

- Kaur Guron, B., Kalkal, S., & Mehra, R. (2024). Health risk assessment due to uranium contamination in groundwater: MATLAB based Monte-Carlo simulations. *International Journal of Environmental Analytical Chemistry*, 1-16.
- Kaur Guron, B., Kalkal, S., & Mehra, R. (2024). The impact of uranium contamination in groundwater on human health: a toxicological risk assessment. *International Journal of Environmental Analytical Chemistry*, 1-15.
- Kaur Guron, B., Kalkal, S., & Mehra, R. (2023). A Comparison of the Concentration of Naturally Occurring Radionuclides in Organic and Conventional Staple Food. *Indian Journal of Pure & Applied Physics*, Vol. 61, 455-460.
- Kaur Guron, B., Kalkal, S., & Mehra, R. Carcinogenic and non-carcinogenic risk assessment due to heavy metals in groundwater using probabilistic approach (Submitted).
- Kaur Guron, B., Kalkal, S., & Mehra, R. Comprehensive radiological assessment and transfer factor analysis of soil to wheat samples (to be submitted).

Poster Presentations

- Poster on 'A Comparison of the Concentration of Naturally Occurring Radionuclides in Organic and Conventional Staple Food' in 22nd National conference on nuclear track detectors and their applications (2022).
- Presentation on 'Health risk assessment of uranium in groundwater using Monte-Carlo simulations: A case study of Mansa district, Punjab' in 28th International conference in nuclear tracks and radiation measurements (2023).
- Poster presentation on 'Comprehensive radiological assessment and transfer factor analysis of soil to wheat samples' in RADNET-V (2024).